

# Spatiotemporally Controlled Photoresponsive Hydrogels: Design and Predictive Modeling from Processing through Application

Hongyuan Zhu, Haiqian Yang, Yufei Ma, Tian Jian Lu, Feng Xu, Guy M. Genin,\* and Min Lin\*

Photoresponsive hydrogels (PRHs) are soft materials whose mechanical and chemical properties can be tuned spatially and temporally with relative ease. Both photo-crosslinkable and photodegradable hydrogels find utility in a range of biomedical applications that require tissue-like properties or programmable responses. Progress in engineering with PRHs is facilitated by the development of theoretical tools that enable optimization of their photochemistry, polymer matrices, nanofillers, and architecture. This review brings together models and design principles that enable key applications of PRHs in tissue engineering, drug delivery, and soft robotics, and highlights ongoing challenges in both modeling and application.

interest because of their potential in applications such as tissue engineering,<sup>[1]</sup> drug delivery,<sup>[2]</sup> and soft robotics<sup>[3]</sup> (Figure 1). These soft, stretchable materials have high water storage capacity (up to 99% by volume), are often biocompatible, and can be made with tunable mechanical and chemical properties.<sup>[4]</sup> Their hydrophilic properties enable storage and transport of a range of small molecules, ions, and biomacromolecules. Of particular value of hydrogels is the ability to incorporating components that endow them with responsiveness to stimuli such as stretch,<sup>[5]</sup> pH,<sup>[6]</sup>

## 1. Introduction

Photoresponsive hydrogels (PRHs) with mechanical properties that change when illuminated with light are of technological

temperature,<sup>[7]</sup> electric fields,<sup>[8]</sup> magnetic field,<sup>[9]</sup> or, of course, light.<sup>[10]</sup> Light is particularly attractive because of its high spatial and temporal controllability and because it can act noninvasively and at a distance.

Four aspects of PRHs can be tuned to tailor their mechanical properties: their photochemistry, their polymer matrix, their filler, and their architecture (Figure 1). A range of photochemical reactions can be used to develop PRHs, including photo-crosslinking, photodegradation, photoisomerization, photocaging, and phototuned molecular crosslinking.<sup>[11]</sup> Among these, photo-crosslinking, and photodegradation are the most studied because they directly increase or decrease the crosslink density in polymer matrices through light irradiation through the inclusion of specific photosensitive compounds (PSCs). Polymer matrices can be chosen to tune the mechanical properties, biocompatibility, biodegradability, and hydrophilicity of a PRH. Nanoscale filler materials can enhance the stiffness and toughness of PRHs. The architecture of PRHs, especially at the microscale, can be adjusted to tune the heterogeneity and mechanics of PRHs.

Recent progress in controlling and utilizing the mechanical properties of PRHs for engineering purposes has been possible in large part due to the development of theoretical tools. Progress in understanding the photochemical processes underlying the synthesis of these polymers has led to a rapid growth in the field, as summarized in.<sup>[12]</sup> With this understanding now mature, theoretical tools have begun to be brought to bear. These tools enable optimization of the photochemistry, polymer matrices, nanofillers, and architecture of PRHs for specific applications. This review brings together a broad range of such models and the associated design principles for PRHs, as well as successes and challenges associated with key applications of PRHs such as tissue engineering, drug delivery, and soft robotics. The review begins in Section 2 with a summary of

H. Zhu, Y. Ma, Prof. F. Xu, Prof. G. M. Genin, Prof. M. Lin  
The Key Laboratory of Biomedical Information Engineering  
of Ministry of Education  
School of Life Science and Technology  
Xi'an Jiaotong University  
Xi'an 710049, P. R. China  
E-mail: minlin@mail.xjtu.edu.cn


H. Zhu, H. Yang, Y. Ma, Prof. F. Xu, Prof. G. M. Genin, Prof. M. Lin  
Bioinspired Engineering & Biomechanics Center (BEBC)  
Xi'an Jiaotong University  
Xi'an 710049, P. R. China

Prof. T. J. Lu  
State Key Laboratory of Mechanics and Control of Mechanical Structures  
Nanjing University of Aeronautics and Astronautics  
Nanjing 210016, P. R. China

Prof. T. J. Lu  
MOE Key Laboratory for Multifunctional Materials and Structures  
Xi'an Jiaotong University  
Xi'an 710049, P. R. China

Prof. G. M. Genin  
Department of Mechanical Engineering & Materials Science  
Washington University in St. Louis  
St. Louis, MO 63130, USA  
E-mail: genin@wustl.edu

Prof. G. M. Genin  
NSF Science and Technology Center for Engineering Mechanobiology  
Washington University in St. Louis  
St. Louis, MO 63130, USA

 The ORCID identification number(s) for the author(s) of this article can be found under <https://doi.org/10.1002/adfm.202000639>.

DOI: 10.1002/adfm.202000639

design principles for PRHs, including principles for choosing photochemistry, monomers and macromers, composite materials, and architecture. Section 2 further highlights trends in PRH design, including near infrared (NIR) induced photochemistry, nanocomposites, and 3D printing. Existing theories and models for predicting the mechanics of photo-crosslinkable, photodegradable hydrogels, and PRH-based composites are summarized in Section 3. In Section 4, applications of PRHs in three frontier fields (tissue engineering, drug delivery, and soft devices) are summarized. The review concludes in Section 5, with perspective on challenges in the mechanics of PRHs, and on novel technologies that are on the horizon.

## 2. Design Principles for Tuning the Mechanical Properties of PRHs

The mechanical properties of PRHs can be controlled by tuning 1) PSCs, 2) prescribing polymer matrices, 3) adding nanofillers, and 4) altering their architecture. PSCs enable temporal control over the mechanical properties of PRHs through light irradiation-determined addition or elimination of covalent bonds. Tuning the composition of polymer matrices and nanofillers extends the stiffness and toughness ranges of PRHs. Advanced fabrication techniques enable spatial control of the architecture and mechanics of PRHs. This section describes how these factors constitute design variables for PRHs, and the principles underlying design choices.

### 2.1. Photochemistry of PSCs in PRHs

PSCs in PRHs translate light energy into initiation energy for downward crosslinking or cleavage reactions, a process called photochemical transformation, with the aim of further altering network connections and tuning mechanical properties.<sup>[13]</sup> A rich diversity of PSCs exist, but the vast majority are not useful to many biological applications because they are excited by ultraviolet light, which may be harmful to cells and has low tissue penetrability.<sup>[14]</sup> Therefore, there is growing interest in new PSCs excited in the NIR range (Figure 2A). In this section, we introduce conventional single-photon-excited PSCs that have found utility for photo-crosslinking and photodegradation, then discuss two promising NIR technologies that can modify the excitation wavelength of PRHs to the NIR region will be discussed.

#### 2.1.1. Photo-Crosslinking

Photo-crosslinking is the light-driven generation of polymer branches based on one of two photopolymerization mechanisms: chain growth radical propagation reactions, and step growth radical propagation reactions.<sup>[10a]</sup> Both of these can be controlled through the addition of photoinitiators into the reaction systems.<sup>[15]</sup> The chain growth reaction involves the growth of radical species by radical addition to a carbon-carbon double bond, generating a new radical at the end of a polymer chain.<sup>[16]</sup> The most widely used monomers for chain growth are (meth)



**Hongyuan Zhu** is currently a Ph.D. student in the School of Life Science and Technology at Xi'an Jiaotong University. He received his B.S. and M.S. from Xi'an Jiaotong University in 2014 and 2016, both in biomedical engineering. His research focuses on developing theoretical tools for modeling the mechanics of biomaterials and cells,

and on investigating cross-interdisciplinary topics across mechanics, biology, and medicine, with emphasis on stimulus-responsive hydrogels and cell mechanobiology.



**Guy M. Genin** is Faught Professor of Mechanical Engineering at Washington University, Thousand Talents Professor at Xi'an Jiaotong University, and a fellow of ASME and AIMBE. He is co-director of the NSF Science and Technology Center for Engineering Mechanobiology. His research focuses on interfaces and adhesion in nature and engineering. He holds B.S.C.E. and M.S.

degrees from Case, S.M. and Ph.D. degrees from Harvard, and postdoctoral training from Cambridge and Brown.



**Min Lin** earned a B.S. degree in material science and engineering from Hefei University of Technology, China, and an M.S. degree in materials science and engineering from Xi'an Jiaotong University, China. After completing his Ph.D. in biomechanics at the Bioinspired Engineering and Biomechanics Center at Xi'an Jiaotong University,

he joined the faculty of Xi'an Jiaotong University. He is currently a full professor in the School of Life Science and Technology, Xi'an Jiaotong University. His current research is focused on biomechanics and mechanobiology of cells, and on bio and nanomaterial synthesis for simulating cell microenvironments.

acrylates. This reaction system can be easily implemented, and the composition of precursors is commercially available. However, it suffers some inefficiencies, such as oxygen inhibition and messy networks.<sup>[17]</sup> In contrast to chain growth working on repeated single steps, step growth involves two alternate steps.

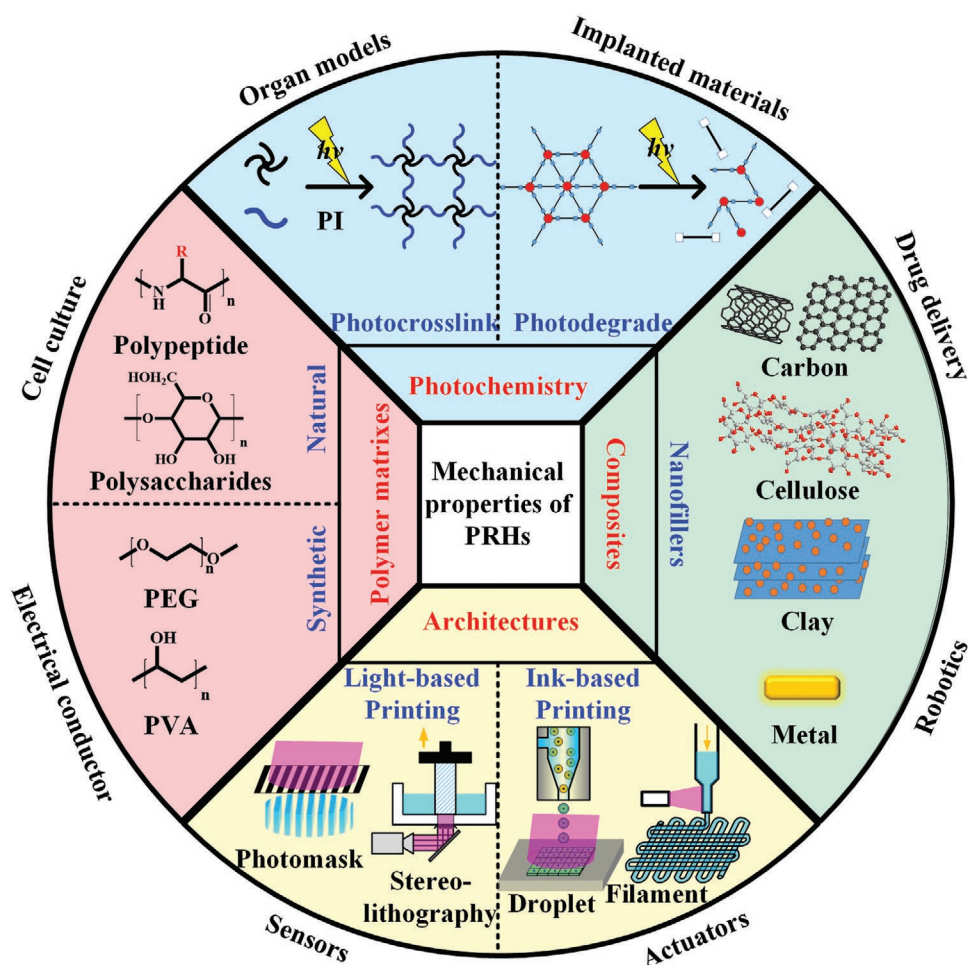


**Figure 1.** Basic design principles and promising applications of PRHs with tuned mechanical properties.

For example, the thiol-ene reaction is an alternation between thiyl radical propagation across the ene functional group and the abstraction of a hydrogen radical from thiol by the carbon-centered radical.<sup>[17a]</sup> Step growth reaction is considered free of oxygen inhibition and more controllable and biocompatible than chain growth.<sup>[17a]</sup> Chain growth and step growth are often considered in separated reaction systems. However, thiol-acylate polymerization is a mix-mode process of step growth and chain growth, where thiols could serve as co-initiators and chain-transfer agents simultaneously.<sup>[18]</sup>

Both chain growth and step growth polymerizations do not respond to light exposure without photoinitiators, which absorb photons from light and then generate radicals to initiate the subsequent radical polymerization processes. Meanwhile, a high concentration of photoinitiators could be harmful to cells. Thus, the photoinitiator is the key factor determining both the absorption wavelength and cytocompatibility in photopolymerization systems. Generally, photoinitiators can be divided into two types according to their reaction mechanisms, namely, “cleavage” type (type I) or hydrogen abstraction type (type II).<sup>[13,19]</sup> Type I photoinitiators usually have only one molecular component, which is capable of forming initiating radicals upon intramolecular bond cleavage on absorption of

light. Type II photoinitiators are composed of two molecular compounds, and radicals are generated by hydrogen abstraction from hydrogen donors to a molecule in triplet states excited by light.<sup>[13]</sup> Next, widely accepted biocompatible photoinitiators (Figure 2B) grouped into these two types will be briefly introduced respectively. For more details regarding the design, reaction mechanisms, and applications of other photoinitiators, readers are referred to other excellent reviews.<sup>[13,15a,19,20]</sup>

I2959 (2-hydroxy-1-[4-(hydroxyethoxy)phenyl]-2-methyl-1-propanone) is the most widely used type I initiator, and possesses the best cytocompatibility among UV initiators (cytocompatible at concentration  $<18 \text{ mmol L}^{-1}$ ).<sup>[21]</sup> Its absorption spectrum is 250–370 nm, and it has a very low initiating efficiency at 365 nm excitations.<sup>[21a]</sup> There are other water soluble type I photoinitiators applied in cell culture, such as I651 (2,2-dimethoxy-2-phenylacetophenone, DMPA) and I184 (1-hydroxycyclohexyl phenyl ketone).<sup>[21a,22]</sup> However, they show much more cytotoxicity than I2959. Recently, lithium acylphosphinate (LAP) has been proposed as a promising alternative, which has a broader absorbance spectrum up to the visible region (270–405 nm) with a reasonable cytocompatibility ( $<2.2 \text{ mmol L}^{-1}$ ).<sup>[23]</sup>

Compared with type I, type II photoinitiators can be considered advantageous because they require lower excitation energy

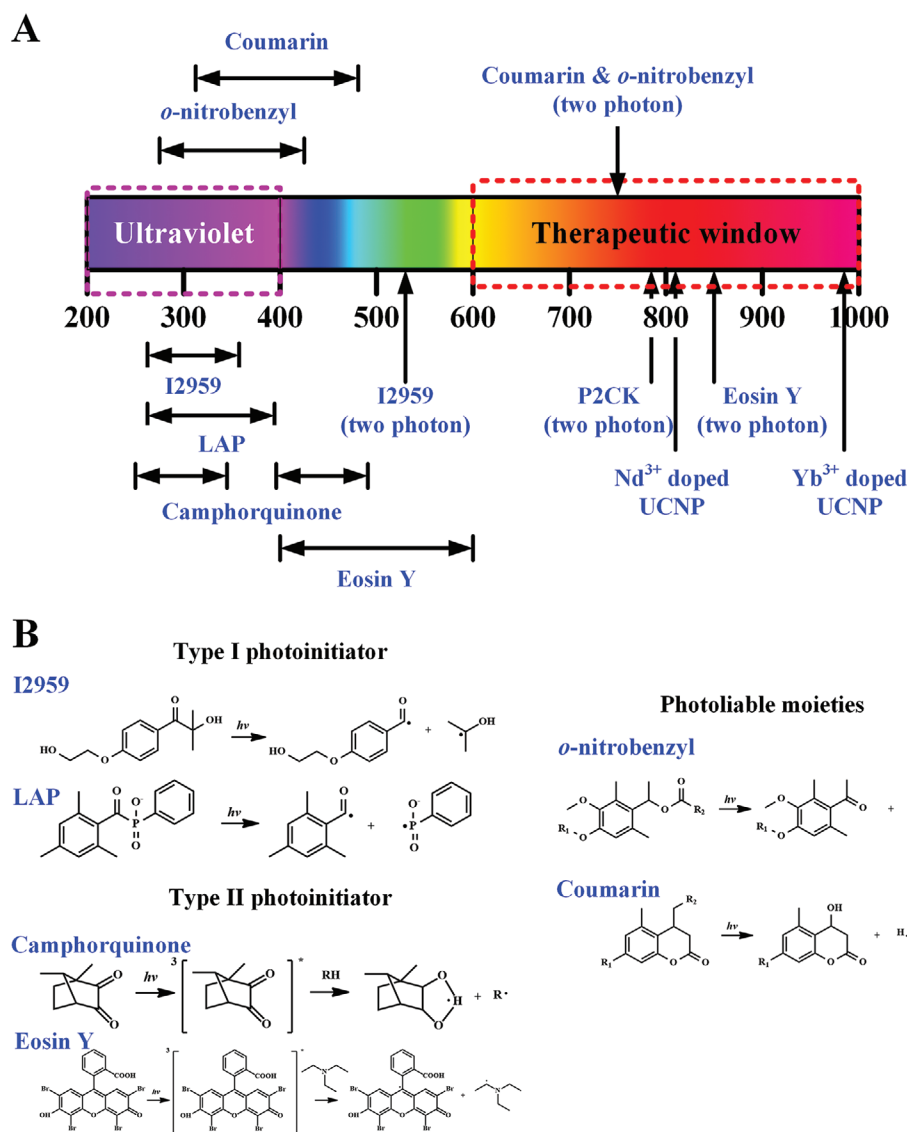


**Figure 2.** A) Absorption wavelength distribution and B) reaction schemes of widely used biocompatible photosensitive compounds. When photo-responsive hydrogels are irradiated with light, photoinitiators can trigger photo-crosslinking, while photolabile moieties can trigger photodegradation. The absorption wavelengths of these photosensitive compounds are located mainly in the ultraviolet and visible regions. To achieve light control in biologically benign regions (600–1000 nm), NIR excitation techniques based on two-photon absorption and upconversion nanoparticles have been developed.

(i.e., longer excitation wavelength) than type I photoinitiators.<sup>[19]</sup> The most popular type II initiator is eosin Y, which belongs to the family of xanthene dyes and has a wide visible absorption spectrum from 400 to 600 nm.<sup>[24]</sup> Eosin Y usually couples with amines or thiols to initiate radical polymerization.<sup>[24b,25]</sup> Camphorquinone (CQ) is another widely used type II initiator, which is cyto-compatible at a concentration of  $<0.6 \text{ mmol L}^{-1}$ .<sup>[26]</sup> It absorbs both UV region (250–350 nm) and visible region (400–500 nm) light.<sup>[27]</sup> Camphorquinone itself can initiate photopolymerization, but only at a low rate. Therefore, like eosin Y, co-initiators (e.g., amines and cyclic acetals) are also added to accelerate the initiation.<sup>[26a,28]</sup>

Besides these commonly used initiators, there are other potential initiators being explored for biomedical applications

(e.g., VA-086<sup>[29]</sup> and HABI<sup>[30]</sup>) and novel higher initiation efficient photoinitiation systems are continuously being developed.<sup>[13,15a]</sup> In addition to tuning the mechanical properties of hydrogels, photopolymerization based on these biocompatible photoinitiators could also be used to conjugate biomolecules on polymer networks, which could provide attachment points for bioactive molecules and cells.<sup>[31]</sup>

### 2.1.2. Photodegradation

In contrast to photo-crosslinking, photodegradation is a reverse process to decrease the stiffness of PRHs. At the molecular level, hydrogels can be rendered photodegradable through

the incorporation of specific photolabile moieties into the macromolecular precursors that comprise the gel network.<sup>[32]</sup> After gelation by addition reactions (e.g., radical polymerization, Michael-type conjugations, and click reactions), these photoactive moieties reside in the network backbone and can be cleaved irreversibly upon light (with appropriate wavelength) exposure.<sup>[32a,33]</sup> Through this process, light is employed to cleave bonds within the hydrogel, ultimately resulting in reduced elasticity and even erosion of hydrogels. Such systems afford opportunities for innovative experiments to better understand how hydrogel degradation influences the desired material properties, as well as offering unprecedented spatiotemporal control of the network structure in real time.<sup>[34]</sup>

Due to versatile modifications and the well-known photolysis mechanism, *ortho*-nitrobenzyl (ONB) and its derivatives are the most intensively studied photolabile functionalities.<sup>[34b]</sup> Upon exposure to UV light, the ONB group will degrade via a photo-induced intramolecular hydrogen extraction to produce an aldehyde and a carboxylic acid (Figure 2B).<sup>[34b]</sup> Substituent modifications on the aromatic ring or at the benzyl position are widely utilized to redshift the photocleavage wavelength and improve photocleavage efficiency.<sup>[34b]</sup> The most commonly used ONB derivative is dimethoxy nitrobenzyl, in which two methoxyl groups are introduced to the aromatic ring. It has a longer absorption wavelength ( $\lambda_{\text{max}} \approx 350$  nm) than the ONB parent ( $\lambda_{\text{max}} < 300$  nm) and provides reasonable absorbance even at 420 nm.<sup>[34a]</sup>

Besides ONB, coumarin and its derivatives have also been investigated (Figure 2B).<sup>[34c]</sup> Compared to the ONB system, coumarin systems are more bioinert. Cleaving product of coumarin is alcohol which is less reactive than aldehyde or ketone produced from cleaving ONB.<sup>[33a,34c,35]</sup> In addition to good biocompatibility, coumarin has much larger one-photon and two-photon absorption (TPA) cross sections than ONB.<sup>[36]</sup> The library of coumarin derivatives has been expanded to over 1000 different chemical structures.<sup>[34c]</sup> Impressively, its absorption wavelength could be shifted to 470–500 nm by specific chemical modifications.<sup>[37]</sup> Despite wide applications in photodegradable hydrogel design, photolabile moieties have also been explored for application in the photocaged gelation of hydrogels.<sup>[34a,38]</sup>

### 2.1.3. NIR-Induced Photochemistry

As discussed above, most photosensitive moieties work in the UV region (170–400 nm) by a single-photon absorption process. However, UV light is problematic for biomedical applications due to its limited tissue penetration capability and potential damage to cells. Compared to UV light, NIR light is better suited to biomedical applications, especially for transdermal applications.<sup>[18c,39]</sup> The spectrum of NIR falls within a region called the “therapeutic window” (i.e., 600–1000 nm), which facilitates deep tissue penetration and minimizes photo damage.<sup>[40]</sup> Another limitation of all single-photon excitation is the optical attenuation in the PRHs, which leads to limited thickness and nonuniformity of the crosslinked/degraded layer.<sup>[41]</sup> Therefore, replacing UV light by NIR is attractive for fabrication of biomimetic extra cellular matrix (ECM).<sup>[42]</sup> Currently, there are two main technologies to realize NIR-induced

photochemical reactions, namely TPA,<sup>[43]</sup> and rare earth material-based up conversion (UC),<sup>[14,44]</sup> both of which have aroused wide interest in PRH engineering.

**TPA:** One approach to realize NIR-sensitivity of hydrogels is based on TPA technologies. The excitation wavelength of PSCs mentioned above is measured under single-photon excitation. Besides, these PSCs can also be excited by absorbing a pair of photons with energy half of the single photon instantaneously at the high intensity excitation of a focused laser (Figure 3A).<sup>[43,45]</sup> The energy difference between the ground state and excited state of a molecule is covered by the sum of the pair of photons; thus, the excitation wavelength of TPA is nearly double that of single photon absorption.<sup>[45]</sup> Based upon this excitation mechanism, TPA has a square dependence on light intensity, while single-photon absorption is usually linear to light intensity.<sup>[45]</sup> PSCs in both photopolymerization<sup>[43,46]</sup> and photodegradation<sup>[32a]</sup> could be excited at the NIR region by TPA. A typical experimental setup for the fabrication of PRHs based on TPA is presented in Figure 3B. It is mainly composed of i) an ultrafast pulsed laser, ii) a scanning system, iii) beam focusing optics, iv) a beam intensity control with a beam shutter, and v) a computer with control software.<sup>[47]</sup>

To achieve two-photon photopolymerization (TPP), an initiator should have enough TPA cross section, high initiation efficiency, low cytotoxicity, and sufficient water solubility.<sup>[47,48]</sup> A few of the aforementioned initiators have been proved suitable for TPP. For example, I2959 has been demonstrated suitable for TPP at around 515 nm.<sup>[49]</sup> Xanthene dyes (e.g., eosin Y) can initiate radical polymerization at 860 and 1028 nm by two-photon absorption.<sup>[25a,50]</sup> However, due to the small TPA cross section of these initiators, the efficiency of TPP based on these initiators is limited. Therefore, there is an urgent need to explore novel initiators that suitable for TPP with good water solubility and biocompatibility. So far, cycloketone-based initiators (e.g., P2CK, E2CK, G2CK) have been explored to meet these requirements, and they have been proved to possess comparable cytocompatibility to I2959 and high initiation efficiency, which are suitable for both hydrogel fabrication and biomolecule conjugation.<sup>[48,51]</sup> Based on TPP technologies, 3D hydrogels could be constructed into complex microstructures at a sub-micrometer resolution, and they could allow cells to adhere and migrate into the microstructures (Figure 3C).<sup>[51a]</sup>

Regarding two-photon-induced photodegradation, both the PSCs mentioned above (*o*-nitrobenzyl and coumarin) can be stimulated by two-photon excitation, which are often explored simultaneously with single-photon-excited photodegradation. For example, Anseth and co-workers developed a nitrobenzyl-based photodegradable hydrogel that was found to be two-photon susceptible at 740 nm. This could be used to construct arbitrary 3D features on the micrometer scale.<sup>[25a,32a,52]</sup> The eroded and arginine-glycine-aspartic acid (RGD) functionalized channels in hydrogels allowed guidance of axon growth and cell migration (Figure 3D). A coumarin-based photodegradable hydrogel also has been found to be two-photon excitable from 720 to 860 nm, with the highest degradation at 740 nm by TPA.<sup>[33a]</sup>

Two-photon technology can not only substitute the UV or visible excitation by NIR, but also provide the spatial control that is needed for 3D patterning with high spatial resolution

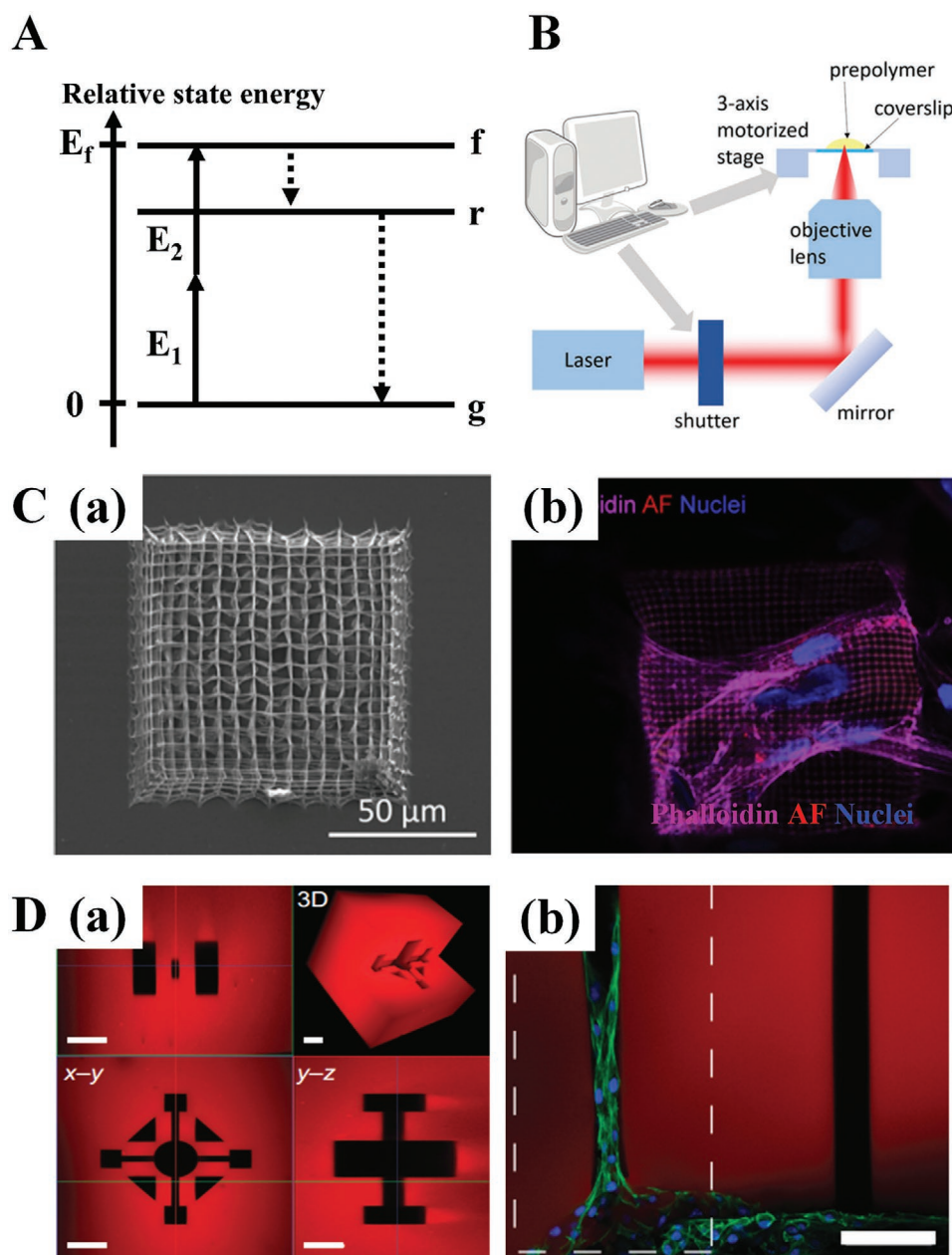


**Figure 3.** Two-photon absorption (TPA) techniques for NIR-engineering PRHs. A) Schematic energy-level diagram of TPA. A molecule at ground state ( $g$ ) could be excited to excited state ( $f$ ) by simultaneously absorbing two photons with energy  $E_1$ ,  $E_2$ , ( $E_1$  could equal to  $E_2$ ). After excitation, the molecule relaxes to lowest vibronic level ( $r$ ), and then returns to the ground state by radiative or irradiative pathways. B) Typical setup for two-photon PRH fabrication. Reproduced with permission.<sup>[47]</sup> Copyright 2018, Royal Society of Chemistry. C) Woodpile scaffold fabricated by two-photon photopolymerization. Reproduced with permission.<sup>[51a]</sup> Copyright 2017, Elsevier. a) Scanning-electron microscopy images of a scaffold. b) Fluorescence image of the scaffold and seeded cells. D) 3D channels for cell culture fabricated by two-photon degradation. Reproduced with permission.<sup>[25a]</sup> Copyright 2011, Nature Publishing Group. a) Confocal images of a 3D structure (scale bar: 100  $\mu\text{m}$ ). b) Fluorescence image of a channel with seeded cells (scale bar: 100  $\mu\text{m}$ ).

on a nanoscale.<sup>[53]</sup> However, there are several limitations of two-photon absorption technology: i) it requires a focused laser beam with high intensity, ii) most two-photon initiators are hydrophobic, iii) time-consuming spot-by-spot curing process. These limitations restrict its broader application and fabrication size (typically under 1  $\text{mm}^3$ ).<sup>[54]</sup>

**UC Nanoparticles:** Another method for fabricating PRHs by NIR light is based on lanthanide-doped upconversion

nanoparticles (UCNPs). UCNPs could transfer NIR light into UV-vis light and thus control the aforementioned photochemical reactions.<sup>[55]</sup> Compared to the virtual intermediate state (lifetime  $<1$  ps) in two-photon absorption, UCNPs have abundant real excited states (lifetime  $\approx 1 \mu\text{s}$ – $1$  ms), which make molecule excitation from lower energy photons much more efficient than TPA.<sup>[56]</sup> The excitation light intensity required by UCNP-assisted photochemistry is several orders of magnitude lower

than that for simultaneous two-photon absorption.<sup>[57]</sup> Thus, continuous-wave NIR laser diodes with a large beam diameter (e.g., several cm) can trigger photoreactions on macroscopic samples, while TPA can only be accomplished within a few micrometers by a pulse laser.

The excitation wavelength of UCNPs is determined by the sensitizer incorporated in them. Among various rare earth ions, Yb<sup>3+</sup> ion is a commonly used sensitizer in UCNPs due to its narrow absorption band and broad absorption cross section around 980 nm.<sup>[58]</sup> For example, a Yb<sup>3+</sup>/Tm<sup>3+</sup> ion pair is usually used to generate ultraviolet to blue light, while a Yb<sup>3+</sup>/Er<sup>3+</sup> ion pair is used to generate green to red light.<sup>[59]</sup> A schematic energy level diagram of a Yb<sup>3+</sup>/Er<sup>3+</sup> ion pair is shown in **Figure 4A**, where the high energy states of Er<sup>3+</sup> ions are excited by energy transfer from excited Yb<sup>3+</sup> ions.<sup>[60]</sup> Recently, Nd<sup>3+</sup> ions have been proposed as an alternative sensitizer for Yb<sup>3+</sup>. Using Nd<sup>3+</sup> ions as a sensitizer can maintain upconversion emission intensity while generating much less heat due to three factors: the higher absorption cross section of Nd<sup>3+</sup> at 808 nm compared to that of Yb<sup>3+</sup> at 980 nm; the high Nd<sup>3+</sup>-Yb<sup>3+</sup> energy transfer efficiency; and the low absorption of water at 808 nm.<sup>[61]</sup>

There have been a few well-established examples of UCNP-assisted NIR-induced photochemistry for PRH engineering (e.g., photopolymerization,<sup>[41,62]</sup> photocleavage,<sup>[63]</sup> photoisomerization<sup>[64]</sup>) (**Figure 4B**). In these applications, UCNPs could be used to tune the physicochemical properties of hydrogels by either 3D encapsulation or planar lithography as a secondary light source. Their advantages in terms of penetration depth and cytocompatibility have been demonstrated. For the 3D encapsulation of UCNPs in resin precursors, there has been evidence of ultradeep curing applications, which could realize hydrogel gelation beyond 13.7 cm.<sup>[41]</sup> Recently, Li et al. grafted photoinitiators on surface of UCNPs, which could initiate both thiolene and acrylate photopolymerization at a relatively low NIR intensity (around 20 W cm<sup>-2</sup>) within limited time (30 min).<sup>[65]</sup> Moreover, a 3D resin fabrication method with sub-micrometer resolution has been proposed recently based on focus laser-excited UCNPs, which demonstrated that UCNPs could be used for 3D fabrication at a micrometer scale similar to the two-photon excitation method (**Figure 4C**).<sup>[54a]</sup> For planar lithography, NIR-triggered photocleaving strategies have been used to release cells and proteins and adhere them to substrates. These techniques show advantages in terms of tissue penetration in comparison to traditional single-photon excitation strategies (**Figure 4D**).<sup>[66]</sup> Recently, Yan et al. demonstrated a method for the NIR-controlled differentiation of mesenchymal stem cells (MSCs) on an upconversion substrate by detachment of UV-cleavable polymers on the substrate. They showed that MSCs could be differentiated into adipocytes or osteoblasts by adjustment of the NIR irradiation. This provided a new way to produce NIR-controlled cell behaviors (**Figure 4E**).<sup>[67]</sup>

However, in comparison to widely accepted single-photon excitation methods, the use of UCNP-based NIR sensitive materials to engineer the mechanics of PRHs is still rare. This is likely due to low conversion efficiency and requirement of high NIR irradiation dose, which leads to a long tuning time or high heat generation. For example, cleavage of an Ru complex using an UCNP-assisted method requires a 25 W cm<sup>-2</sup> 974 nm

laser, whereas analogous cleavage at an excitation of 520 nm requires only a thousandth lower power (2–6 mW cm<sup>-2</sup>).<sup>[63b]</sup> Thus, highly efficient UCNPs, which could be excited by a low-power laser and produce less heat might be more suitable for achieving NIR-controlled hydrogels.

## 2.2. Polymer Matrices of PRHs

Polymer matrices of hydrogels are crosslinked hydrophilic polymer networks. These networks, especially their type, cross-link density, molecular weight, and concentration, are the main determinant of PRH mechanics. Polymers in PRHs can be natural or synthetic.<sup>[68]</sup> Natural polymers have the advantages of inherent biocompatibility and abundant sites for chemical modifications, whereas synthetic polymers have the advantages of bio-inert properties and highly designable physicochemical properties.<sup>[68]</sup> Chemically grafted (meth)acrylates, norbornene, thiols, or other functionalities could provide these polymers with photo-crosslinkable sites, and chemically incorporated photolabile sites on these polymers could provide photodegradability for PRHs. Hence, this section provides a brief introduction of the properties and chemical modification of these polymers for corresponding photochemical reactions. A statistical plot of the Young's modulus against the polymer concentration for various polymer matrices mentioned in the literature (**Figure 5**) shows that Young's moduli of PRHs generally increase with polymer concentration, and that existing polymer matrices could cover a large stiffness range from 1 to 100 kPa below a limited concentration (e.g., 30 wt%).

### 2.2.1. Natural Polymer Derivatives for PRHs

Natural polymers extracted from animal tissues are attractive for biological applications because many are inherently biocompatible. Specifically desirable natural polymers include polypeptides such as fibrin,<sup>[69]</sup> collagen,<sup>[70]</sup> gelatin,<sup>[71]</sup> Matrigel,<sup>[72]</sup> and silk fibroin;<sup>[73]</sup> and polysaccharides such as hyaluronic acid (HA),<sup>[74]</sup> alginate,<sup>[75]</sup> chitosan,<sup>[76]</sup> cellulose,<sup>[77]</sup> and chondroitin sulfate.<sup>[78]</sup> However, these natural polymers lack specific functional groups for photo-crosslinking and photodegradation, and therefore must be modified chemically for use in PRHs. Suitable chemical modifications include grafting of thiols, carbon double bonds, or photolabile moieties to endow them with photosensitivity. Additional modification is needed for PRHs that are to be used as cell scaffolds to ensure adequate cell binding sites. In this section, we discuss two natural polymers that have been modified successfully for use as PRH cell scaffolds: gelatin, which is a polypeptide, and HA, which is a polysaccharide.

Gelatin, a hydrogel “generally recognized as safe” by the US food and drug administration (FDA),<sup>[71]</sup> is a polypeptide mixture hydrolyzed from collagen, the most abundant protein of mammalian ECM.<sup>[68]</sup> It is particularly attractive for cell culture and tissue engineering because of its accessible functional polypeptides, including the RGD sequence for cell attachment, and its biodegradability by matrix metalloproteinases (MMPs).<sup>[79]</sup> However, for use as a PRH, gelatin must be modified with by

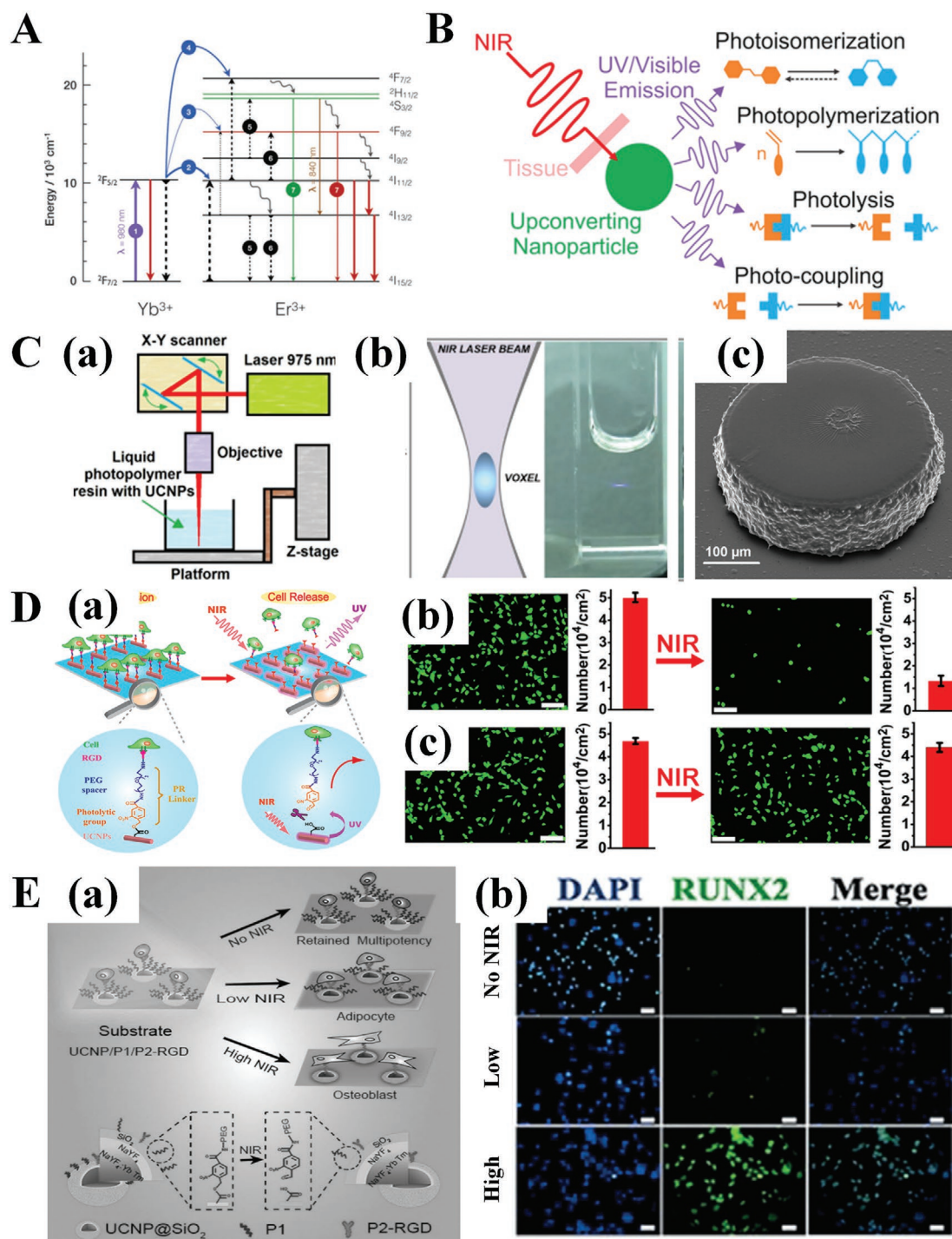


**Figure 4.** Upconversion nanoparticle (UCNP)-assisted NIR-engineering of PRHs. A) Schematic energy-level diagram of an  $\text{Yb}^{3+}/\text{Er}^{3+}$  ion pair. Reproduced with permission.<sup>[59]</sup> Copyright 2015, Royal Society of Chemistry. B) Schematic of UCNP-assisted NIR-induced photochemistry. Reproduced with permission.<sup>[55]</sup> Copyright 2017, Royal Society of Chemistry. C) UCNP-assisted 3D fabrication. Reproduced under the terms of the CC-BY License.<sup>[54a]</sup> Copyright 2018, the Authors. Published by Nature Publishing Group. a) Schematic of the experimental setup. b) Luminescent voxel formation in resin-contained UCNPs under CW NIR light illumination. c) Scanning electron microscopy image of a 3D polymer microstructure obtained by UCNP-assisted 3D fabrication. D) NIR-controlled cell adhesion using UCNPs. Reproduced with permission.<sup>[66a]</sup> Copyright 2014, American Chemical Society. a) Schematic illustration. b,c) Fluorescence images of NIR light-induced cells released on substrate with b) and without c) UCNPs (scale bar: 100  $\mu\text{m}$ ). E. NIR-controlled differentiation of MSCs using UCNPs. Reproduced with permission.<sup>[67]</sup> Copyright 2018, Wiley-VCH. a) The matrix was modified by two distinct polymers: P1, which is (ONB-PEG), and P2, which is (RGD-PEG). P1 is photocleavable and can block interaction between cells and the substrate, while P2 can anchor the cells. NIR irradiation could trigger UCNP-assisted detachment of P1, and change cell–matrix interactions. b) Immunofluorescence imaging of markers for osteogenic (RUNX2, green) differentiation under matrix with various NIR irradiation doses (scale bar: 50  $\mu\text{m}$ ).



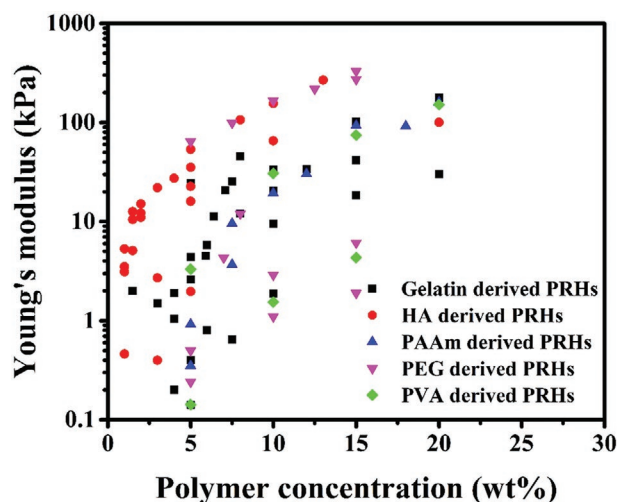


**Figure 5.** Polymer concentration-dependent Young's modulus plot for PRHs with a range of polymer matrices. Data are from reports on gelatin-derived,<sup>[23c,d,80a,c-e,g-i,81]</sup> hyaluronic acid (HA)-derived,<sup>[85a-e,g,h,86-88]</sup> polyacrylamide (PAAm)-derived,<sup>[94]</sup> poly ethylene glycol (PEG)-derived,<sup>[25c,97b,98b,d,f]</sup> and poly vinyl alcohol (PVA)-derived<sup>[51b,c]</sup> PRHs. The measured shear modulus ( $G$ ) in these references is transformed into Young's modulus ( $E$ ) by  $E = 2(1+\nu)G$ , where  $\nu$  is Poisson's ratio, which was assumed to be 0.5.

covalent grafting of photo-crosslinkable functional groups such as methacryloyl, acrylamide, norbornene, and styrene groups.<sup>[71]</sup>

Gelatin methacryloyl (GelMA) is the most investigated gelatin derived photo-crosslinkable monomer.<sup>[80]</sup> The degree of functionalization, polymer concentration (usually 5–20 wt%), photoinitiators, and light exposure are designable variables that can be varied to obtain a desired modulus of elasticity of GelMA-based PRHs.<sup>[71]</sup> Beside acrylates, thiol and ene functionalities can also be added to gelatin to form photoclick hydrogels.<sup>[23c,d,81]</sup> For example, Lin and co-workers prepared norbornene functionalized gelatin (GelNor), which could be photo-crosslinked with thiol-containing linkers (dithiothreitol, or PEG-tetra-thiol).<sup>[81]</sup> In another work, they prepared a norbornene and heparin dual-functionalized gelatin (GelNor-Hep) scaffold for investigating behaviors of hepatocellular carcinoma cells.<sup>[23c]</sup> Recently, Tytgat et al. grafted norbornene and thiols onto gelatin (GelNor and GelSH) to form a photoclick cell scaffold, which has similar biocompatibility but better adipogenic differentiation potential than GelMA.<sup>[82]</sup> Apart from photo-crosslinkability, gelatin derivatives have also been endowed with photodegradability either by introducing photocleavable crosslinkers<sup>[35]</sup> or by directly incorporation of photolabile moieties in their strands.<sup>[83]</sup>

HA, a polysaccharide in animal ECM that is composed of alternating units of  $[\beta(1,4)\text{-D-glucuronic acid-}\beta(1,3)\text{-N-acetyl-D-glucosamine}]_n$ , plays an important role in cellular signaling, wound repair, morphologies, and matrix organization.<sup>[68,84]</sup> HA is a biocompatible substance that can degraded within days by hyaluronidase in the body.<sup>[74]</sup> Similar to gelatin, HA must be modified to endow it with photo-crosslinkability. This has been achieved through the grafting of methacrylate (MeHA),<sup>[85]</sup> glycidyl methacrylate (GMHA),<sup>[86]</sup> maleimide (MAHA),<sup>[87]</sup> norbornene (NorHA),<sup>[88]</sup> and thiol groups (HASH).<sup>[89]</sup> All of these hyaluronic acid-based hydrogels show good cytocompatibility. However, in comparison with gelatin, HA lacks adhesion sites;

thus, adhesion polypeptides, such as RGD, need to be grafted onto HA for it to be effective for cell culture.<sup>[68]</sup>

Hydrogels based on these natural polymers show the advantages of biodegradability and abundant sites for chemical modifications. However, they also have limitations, such as large batch-to-batch variations. Reducing these batch-to-batch variations is essential for expanding the use of these natural polymer based PRHs.

### 2.2.2. Synthetic Polymers Derivatives for PRHs

Although natural polymers are attractive for supporting cell activities such as migration, proliferation and differentiation, they are limited because of batch-to-batch variation, immunogenic risk, and weak mechanical properties.<sup>[31a]</sup> Instead, synthetic polymers can provide hydrogels with better-defined mechanical properties, bioactive factors, and degradation kinetics.<sup>[90]</sup> Synthetic polymers, such as polyacrylamide (PAAm), poly ethylene glycol (PEG), poly vinyl alcohol (PVA) are frequently investigated polymers for constructing photo-crosslinkable or photodegradable hydrogels.<sup>[3d,68,91]</sup>

PAAm hydrogel is a crosslinked network consisting of acrylamide monomers and small amounts of crosslinkers (e.g., bis-acrylamide, ethylene glycol dimethacrylate).<sup>[92]</sup> Both the acrylamide monomers and crosslinkers could be involved in free radical polymerization, which could be controlled by exciting photoinitiators. Thus, PAAm hydrogel is a typical photo-crosslinkable hydrogel.<sup>[93]</sup> Initiator ammonium persulfate (AP) and accelerator tetramethylethylenediamine (TEMED) is a commonly used initiation system for crosslinking PAAm. This initiation system could also slowly trigger polymerization without light irradiation, while UV irradiation would accelerate its initiation process.<sup>[94]</sup> The abundant amide groups on PAAm could be further chemically modified for specific functions (e.g., collagen for cell adhesion).<sup>[93]</sup> PAAm hydrogels have advantages such as high stretchability, good biocompatibility, and simple synthesis.

PEG, referred to as poly ethylene oxide (PEO) when it has a high molecular weight above 20 000, is a commonly used synthetic polymer for biomedical applications owing to its simple and clear chemical structure, good hydrophilicity, bio-inertness, and programmable biochemical and biophysical properties.<sup>[95]</sup> The traditional PEG monomer has only two hydroxyl groups at its two ends, and the internal chemical component is  $-\text{[CH}_2\text{-CH}_2\text{-O]}_n\text{-}$ , which contains neither biological recognition sites nor active sites for chemical modification.<sup>[96]</sup> Thus, traditional PEG hydrogels are usually constructed by chain-growth of di-(meth)acrylated monomers (i.e., PEGDA, PEGDMA).<sup>[25c,97]</sup> Recently, PEG with four or more arms has been developed, which could not only be crosslinked by the modification of (meth)acrylates for chain growth and the modification of thiolene groups for step growth.<sup>[25b,90,98]</sup>

Besides photo-crosslinkable hydrogels, PEG-based macromers can also be used to construct photodegradable hydrogels. For example, Kloxin et al. grafted a nitrobenzyl ether-derived acrylated moiety onto PEG-bis-amine to form a photocleavable macromer (PEGdiPDA), which could be further used to form photolabile networks by redox-initiated free

radical polymerization.<sup>[32a]</sup> In a similar case, Yanagawa et al. designed a photocleavable crosslinker (NHS-PC-4armPEG) for the construction of photodegradable hydrogels, which could form photodegradable networks by activated ester reactions with amino-4arm PEG or gelatin.<sup>[33b]</sup> Tamura et al. constructed photodegradable hydrogels by a click reaction, strain-promoted azide-alkyne cycloaddition (SPAAC), where photocleavable crosslinker DBCO-PC-4armPEG could react with azide-modified gelatin to form a gel.<sup>[33c]</sup> Besides modifying the small groups at the end of PEG chains, biomacromolecules can also graft onto PEG to form hydrogels with much more complex functionalities. For example, Du and co-workers photocrosslinked a DNA grafted PEG acrylate and formed self-assembling microhydrogels with high shape programmability and controllability.<sup>[99]</sup> These studies demonstrate the great potential of PEG for designing diverse PRHs.

PVA is another widely studied synthetic polymer with excellent biocompatibility and water solubility. Pure PVA can be used to form hydrogels crosslinked by physical entanglements through freezing and thawing methods.<sup>[100]</sup> However, these hydrogels are mechanically weak and do not respond to light. To realize light controllability and covalent crosslinking, special functional groups need to be modified on PVA, such as methacrylate,<sup>[78,101]</sup> glycidyl methacrylate,<sup>[102]</sup> and thiol-ene functionalities.<sup>[51b,c,103]</sup> PVA could surpass PEG due to its hundreds of hydroxyl groups, which could be chemical modified by photocrosslinkable functionalities and adhesive ligands, while PEG can only provide less than eight moieties for substitution.<sup>[51c]</sup>

### 2.3. PRH-Based Nanocomposites

Although the photochemistry, structure, and composition of a polymer matrix can be tuned to alter the mechanical properties of PRHs, the ranges of stiffness and toughness achievable by these methods are still limited. A favored approach to developing properties beyond this range, seen throughout nature in materials such as wood, bone, and nacre<sup>[104]</sup> and seen in stiffening and strengthening of engineering polymers,<sup>[105]</sup> is the addition of a stiff and strong nanoscale phase to the polymer matrix. The resulting nanoparticle–polymer composites can show greatly enhanced stiffness, maximum elongation, and toughness.

Reinforcement phases added to PRH's that have at least one dimension in the nanoscale are termed “nanofillers.” These include “0D” nanoparticles, 1D nanofibers, and 2D nanosheets. Nanofillers are incorporated into PRHs either covalently or noncovalently<sup>[106]</sup> through dispersal in precursor solution of the matrix before gelation. The nanofillers themselves do not contribute to the photosensitivity while the matrix hydrogel enables photosensitivity. Property enhancement can be tuned by the type, concentration, and surface properties of reinforcement and fillers. Besides changing the mechanical properties of PRHs, nanofillers can also affect the viscosity of pre-gel precursors and the optical properties of PRHs, and endow PRHs with conductivity.<sup>[107]</sup> The nanofillers have effects on the optical properties and photosensitivity of the matrix hydrogel that are not yet well characterized and that are typically overcome through empirical experimentation.<sup>[108]</sup>

In addition, nanofillers can inadvertently endow PRHs with biotoxicity. This section thus begins with a short section on the biotoxicity concerns that surrounding nanoparticles. It then continues to describe successes and challenges associated with reinforcement of PRHs, including photo-crosslinkable hydrogels, by four different types of nanofillers: carbon, cellulose, clay, and metallic. A broad range of PRH-based nanocomposites has been developed (Table 1).

#### 2.3.1. Biotoxicity

Nanofillers must be biocompatible in biomedical applications because biodegradation of PRH-based nanocomposites through hydrolysis, enzymatic action, and other PRH aging processes can lead to release of these nanofillers into the body. Many natural hydrogels are stiffened by fully biocompatible nanofillers. For example, cellulose nanofibers are biocompatible nanofillers for pectin hydrogels in plant cell walls with no known biotoxicity,<sup>[109]</sup> and isolated cellulose fibers and nanocrystals have no established biotoxicity except through inhalation.<sup>[110]</sup> Clay nanoparticles (CNPs), similarly, have minimal toxicity in vivo but can be toxic in powder form when handled for processing.<sup>[111]</sup>

However, several nanofillers, especially carbon-based nanofillers, can have surface energy sufficiently high to serve as the cores of so-called biocoronas and can thus serve as the cores of relatively stable accumulations of biomolecules with physicochemical characteristics that are hard to predict and that can become toxic.<sup>[112]</sup> The particles themselves can be toxic to cells and tissues both near the site or a PRH and far from it.<sup>[113]</sup> Exposed nanofillers can become toxic when internalized into cells via passive transport or active endocytosis<sup>[114]</sup> and when delivered into tissues through blood circulation.<sup>[115]</sup> Although a science of understanding and predicting these effects is developing,<sup>[112]</sup> doses that are safe for humans are not established clearly and evaluation must be done on a case by case basis.

For the case of metal nanoparticles, biotoxicity varies strongly with composition, shape, size, and structure.<sup>[116]</sup> The gold and silver nanoparticles discussed below do show cellular toxicity at sufficiently high concentration and duration of exposure.<sup>[117]</sup>

However, despite much progress in understanding fundamental mechanisms of biotoxicity by nanoparticles,<sup>[118]</sup> FDA approvals of nanoparticles continue to be issued on an ad hoc basis. The FDA's own center for devices and radiological health has an office of science and engineering laboratories, with researchers who weigh the benefits of a new material against the risks associated with nanoparticles interacting with human cells.<sup>[119]</sup> Thus, the choices and concentrations of all nanofillers need to be carefully selected and tested for in vivo biosafety when used for developing PRH-based nanocomposites for bioapplications.

#### 2.3.2. Carbon/PRH Nanocomposites

Carbon nanomaterials (e.g., graphene, carbon nanotube, CNT) are promising reinforcement fillers for polymer due to their stiffness, toughness, density, conductivity, biocompatibility,

**Table 1.** Summary of data for PRH-based nanocomposites.

Filler <sup>a)</sup>	Polymer matrix	Young's modulus	Fractured strength	Ref.
<b>Carbon</b>				
GO (0.4 mg mL <sup>-1</sup> )	PAAm (6–15 wt%)	8–127 kPa	–	[121]
GO (0–4 mg mL <sup>-1</sup> )	PEGDA (6–12 wt%)	8–38 kPa	–	[121]
GO (0–5 mg mL <sup>-1</sup> )	PAAm (35 wt%) + gelatin (5%)	75–187 kPa	260–330 kPa	[126]
GO (0–2 mg mL <sup>-1</sup> )	GelMA (5 wt%)	8–24 kPa	–	[124a]
GO (0–0.5 mg mL <sup>-1</sup> )	GelMA (20 wt%) + PEGDA (15 wt%)	105–137 kPa	–	[124c]
GO (0–4 wt%)	PEGDA (70 wt%)	10–400 MPa	1–10 MPa	[127]
rGO (0–5 mg mL <sup>-1</sup> )	GelMA (7 wt%)	1.8–22.5 kPa	–	[108c]
GO/rGO (0–6 mg mL <sup>-1</sup> )	PAAm (8 vol%)	18–54 kPa	–	[124b]
GO/MeGO (0–3 mg mL <sup>-1</sup> )	GelMA (8 wt%)	1.9–6.5 kPa	11–116 kPa	[108a]
Ca <sup>2+</sup> induced GO network	PAAm	5.3–31.6 kPa	100–510 kPa	[128]
CNT (0–5 mg mL <sup>-1</sup> )	GelMA (5 wt%)	9–32 kPa	–	[108b]
CNT (0–1 mg mL <sup>-1</sup> )	GelMA (5 wt%)	12–24 kPa	–	[129d]
CNT (0–1 mg mL <sup>-1</sup> )	GelMA (5 wt%)	14–59 kPa	–	[129b]
<b>Cellulose</b>				
CNC (0–5 wt%)	PEGDA (50 wt%)+DiGlyDA (50 wt%)	52–133 MPa	6–7.5 MPa	[108d]
CNC (0–1.27 wt%)	PEGDA (70 wt%)	8–12 MPa	5.5–6.8 MPa	[139c]
CNC (0–0.7 vol%)	PEGDMA (10 wt%)	32–61 kPa	–	[138]
NFC (0–0.5 vol%)	PEGDMA (10 wt%)	43–157 kPa	–	[300a]
NFC (0–0.7 vol%)	PEGDMA (10 wt%)	150–300 kPa	219–633 kPa	[137]
CNC (0–1.4 vol%)	PEGDA (30 vol%)	8–31 kPa	65–375	[136]
<b>Clay</b>				
MMT (0–10 wt%)	PAAm (20 wt%)	133–208 kPa	101–176 kPa	[146]
MMT (0–0.5 wt%)	PAAm (50 wt%)	200–500 kPa	37–95 kPa	[145]
Laptonite (1–4 wt%)	PAAm (10 wt%)	2–9 kPa	4–110 kPa	[144]
Laponite (0–7 wt%)	PNAGA (10–30 wt%)	33–182 kPa	67–1166 kPa	[149]
Laptonite (0–10 wt%)	PEGDA (10 wt%)	24–38 kPa	0.14–3.7 MPa	[148]
<b>Metal</b>				
AgNP (0–100 × 10 <sup>-3</sup> μm)	PHEMA (60 vol%)	28–38 kPa	–	[152a]
AuNR (0–0.5 mg mL <sup>-1</sup> )	GelMA (7 wt%)	3.8–4.7 kPa	–	[108e]
AuNR (0–1 mg mL <sup>-1</sup> )	GelMA (10 wt%)	2.7–3.5 kPa	–	[152b]
AuNR (0–1.5 mg mL <sup>-1</sup> )	GelMA (5 wt%)	0.4–1.2 kPa	–	[152c]

<sup>a)</sup>GO: graphene oxide, rGO: reduced graphene oxide, MeGO: methacrylated graphene oxide, CNT: carbon nanotube CNC: cellulose nanocrystal, NFC: nanofibrillated cellulose, MMT: montmorillonite, AgNP: silver nanoparticle, AuNR: gold nanorod, GelMA: gelatin methacryloyl, PAAm: polyacrylamide, PEGDA: poly ethylene glycol di-acrylate, PEGDMA: poly ethylene glycol di-methacrylate, PNAGA: poly N-acryloyl glycinamide, PHEMA: poly hydroxyethyl methacrylate.

and commercial availability. For example, monolayer graphene has a Young's modulus near 1 TPa, an intrinsic strength of 130 GPa, a density of only 2 g cm<sup>-3</sup>, and good electrical conduction and biocompatibility.<sup>[120]</sup> Because of surface energy factors described in detail in Section 3.3, addition of very small quantities of nanofillers can increase stiffness by amounts that would seem to be outside of thermodynamic limits for conventional engineering composite materials. For example, incorporating only 4 mg mL<sup>-1</sup> of carbon nanomaterials into hydrogels can increase the stiffness of up to 16-fold.<sup>[121]</sup>

Graphene is a 2D atomic-layered sheet that consists of a hexagonal honeycomb lattice of strong C–C bonds<sup>[105b,122]</sup>. It can be obtained by either top-down techniques (e.g., Hummers'

method, chemical vapor deposition) or bottom-up approaches (e.g., surface-assisted polymerization and cyclodehydrogenation).<sup>[122a]</sup> Graphene-derived functional nanomaterials, including mono/multilayered graphene, graphene oxides (GO), reduced graphene oxides (rGO), show advantages such as large surface area, abundant functional chemical groups, controllable conductivity, and good mechanical properties.<sup>[122a]</sup> However, graphene is difficult to disperse in water due to high surface energy,<sup>[123]</sup> which hinders its utilization in hydrogels.

In contrast, GO, with abundant oxygen-containing functional groups (e.g., –OH, –COOH), can be distributed at 5 mg mL<sup>-1</sup> in water.<sup>[108a,c,124]</sup> PRHs doped with GO at or below this safe concentration have been shown to be noncytotoxic to

fibroblasts,<sup>[108a,124a]</sup> cardiac cells,<sup>[108c]</sup> myoblasts,<sup>[124b]</sup> and stem cells.<sup>[124c]</sup> Therefore, GO has been used much more than graphene as a hydrogel nanofiller.<sup>[125]</sup>

Examples include that of Cha et al., who explored the incorporation of GO and methacrylated graphene oxides (MeGO) into GelMA and found that GO would aggregate at high concentration (3 mg mL<sup>-1</sup>), while MeGO remains stably dispersed, which results in higher stiffness and fracture strength of MeGO/GelMA at a high doping content.<sup>[108a]</sup> A similar GO/GelMA hybrid hydrogel was synthesized by Shin et al., and was demonstrated to support cellular spreading and alignment in a 3D environment.<sup>[124a]</sup> In another work, Shin et al. directly incorporated rGO into GelMA and found a significant improvement in electrical conductivity and mechanical properties.<sup>[108c]</sup> They found that cardiomyocytes on an rGO/GelMA matrix show better biological activities (e.g., viability, proliferation, maturation, and spontaneous beating rate) in comparison to pristine GelMA hydrogels.<sup>[108c]</sup> Unlike Shin et al., Jo et al. proposed to reduce GO in a prepared GO/PRH composite through a mild chemical reduction to avoid aggregation of rGO in aqueous solutions.<sup>[124b]</sup> They found that a small addition (6 mg mL<sup>-1</sup>) of GO into PAAm could increase its Young's modulus from 18 to 54 kPa, and reduction of GO in the GO/PAAm did not change the Young's modulus significantly.<sup>[124b]</sup> Yan et al. used GO to enhance the mechanical properties of gelatin/PAAm double network hydrogels and showed that the composite hydrogels are not only stiffer and stronger, but also show a large hysteresis loop, softening phenomenon, and self-recovery properties.<sup>[126]</sup> Through systematic experiments, Jang et al. demonstrated that different types of polymer matrix (PAAm or PEGDA), polymer concentration, and different fillers (GO or MeGO) could significantly affect the mechanical properties of the resulting composite hydrogels.<sup>[121]</sup> Shin et al. incorporated GO into UV-curable PEGDA hydrogels, and showed that GO could significantly improve the mechanical strength and reduce the gas permeability of the hydrogel.<sup>[127]</sup> Cong et al. demonstrated that the mechanical properties of GO/PRHs could be further improved by Ca<sup>2+</sup>-induced crosslinks of GOs.<sup>[128]</sup> The increasing concentration of Ca<sup>2+</sup> would gradually improve the maximum elongation of the hybrid hydrogels (from 160% to 1100% of original length), while the fracture strength would be maximum at an optimum calcium content (**Figure 6A**).<sup>[128]</sup> GO/PRHs nanocomposites have also been used as bioinks for 3D bio printing.<sup>[124c]</sup>

CNTs are 1D nanomaterials, which are effectively rolled-up graphene sheets. CNTs have either a single- or multiple-layer structure, namely, single-walled nanotubes (SWNTs) and multi-walled nanotubes (MWNTs).<sup>[95a,105b,120b]</sup> The outer diameter of SWNTs ranges from 0.6 to 2.4 nm, while that of MWNTs ranges from 2.5 to 100 nm.<sup>[95a]</sup> Similar to GO, CNTs have a strong effect on the stiffness of a hydrogel, have good water dispersibility at 5 mg mL<sup>-1</sup>, and additionally have electrical conductivity.<sup>[108b,129]</sup> PRHs doped with CNTs below 5 mg mL<sup>-1</sup> are noncytotoxic for fibroblasts,<sup>[129b]</sup> cardiac cells,<sup>[108b]</sup> and myoblasts.<sup>[129c,d]</sup>

Examples of application of CNTs include that of Shin et al., who developed photo-crosslinkable CNT/GelMA composite hydrogels, and demonstrated stiffness enhancement while maintaining the porosity, biocompatibility, and biodegradability are maintained of the PRH.<sup>[129b]</sup> Only 0.5 mg mL<sup>-1</sup> of

CNTs increased the compressive modulus of GelMA hydrogels from 10 to 30 kPa.<sup>[129b]</sup> In a later work, it was demonstrated that stiffening by CNTs was maximum at 3 mg mL<sup>-1</sup>, and that further addition of CNTs decreased the stiffness of the hydrogel composite due to reduction of UV light penetration by the CNTs.<sup>[108b]</sup> Moreover, the CNT/GelMA composite could significantly improve the electrophysiological functions of myocardial tissues due to its excellent mechanical integrity and electrical conductivity.<sup>[108b]</sup> Ramón-Azcón et al. and Ahadian et al. proposed a dielectrophoretic method to align CNTs within GelMA hydrogels.<sup>[129c,d]</sup> The GelMA with aligned CNTs maintains a higher Young's modulus and electrical conductivity than that with random CNTs.<sup>[129c,d]</sup> Further, engineered myofibers on aligned CNT/GelMA showed more maturation and contractility than myofibers on random CNT/GelMA and pristine GelMA, especially after electrical stimulation.<sup>[129c,d]</sup>

We note, however, that while CNTs are not cytotoxic in the *in vitro* studies reported above, they and other fullerenes have been shown to be cytotoxic in a range of other studies, and can be deadly to an organism.<sup>[130]</sup> Although certain cells can withstand interaction with CNTs, pathological processes that can be initiated that affect how cells interact with their microenvironments,<sup>[131]</sup> and protein biocoronas can lead to pathological interactions between CNTs and human blood platelets.<sup>[132]</sup> We reiterate that because of such issues associated with the unknown fate of nanofillers as these nanofilled PRHs degrade, no carbon nanofilled PRHs are currently FDA approved, and much work needs to be done before their safety can be ensured. This is an important, ongoing direction for future investigation.

### 2.3.3. Cellulose/PRH Nanocomposites

Cellulose is a naturally 1D, stiff (tensile modulus  $\approx$  58–220 GPa) and strong (tensile strength  $\approx$  75–77 GPa) material, which is formed through multiscale structures.<sup>[104c,133]</sup> Long chains of  $\beta$ -1,4-linked D-glucose rings gather into microfibrils, and microfibrils stack into cellulose through H-bond and van der Waals interactions.<sup>[134]</sup> Cellulose is easy to access due to its many sources, such as plants, bacteria, and sea animals (e.g., tunicates).<sup>[134a,135]</sup> Nanoscale cellulose fibers (diameter <100 nm) can be obtained by biosynthesis (e.g., bacterial cellulose, BC), acid hydrolysis from cellulosic fibers (e.g., cellulose nanocrystal, CNC), or mechanical peeling from plant materials (e.g., nanofibrillated cellulose, NFC).<sup>[104c,125,134a]</sup> Nanocellulose has advantages, such as low density (around 1.5 g mL<sup>-1</sup>), highly dispersible content (up to 1.4 vol%) in water, good biodegradability, renewability, and high optical transparency, which is becoming an increasing utilized nanofiller for PRHs.<sup>[104c,134a]</sup>

For example, Yang et al. prepared added CNCs into I2959-initiated PEGDA (**Figure 6B**).<sup>[136]</sup> Compared to neat PEGDA hydrogel, the CNC/PEGDA composite hydrogel exhibited a significant improvement in the Young's modulus (from 75 to 31 kPa), fracture strength (from 99 to 375 kPa), and fracture strain (from 650% to 1300%) with a CNC loading of 1.4 vol%.<sup>[136]</sup> In a similar work, Khoushabi et al. incorporated NFC into I2959-initiated PEGDMA.<sup>[137]</sup> They showed that 0.7 vol% NFC could increase the hydrogel's stiffness from 40 to 150 kPa and

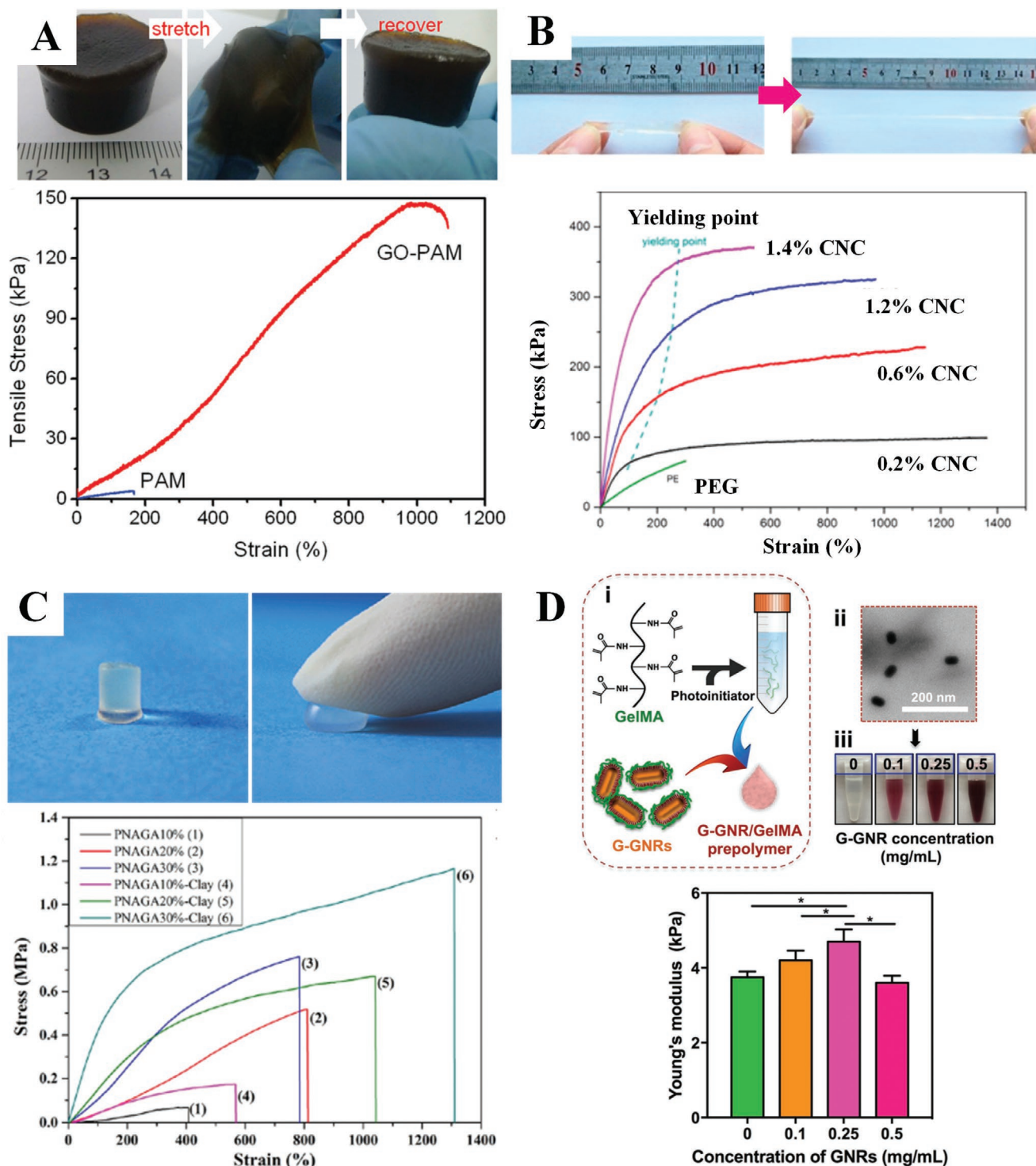


**Figure 6.** Reinforcement of PRHs by nanoparticle fillers. A) Photographs and tensile stress–strain curves of a graphene oxide (GO)-doped polyacrylamide (PAAm) hydrogel, where  $\text{Ca}^{2+}$  is used as the crosslinker of GO sheets. The composite hydrogel is much more ductile and stiff than an undoped PAAm hydrogel. Reproduced with permission.<sup>[128]</sup> Copyright 2013, Wiley-VCH. B) Photographs and tensile stress–strain curves of a cellulose nanocrystal (CNC)-doped PAAm hydrogel. With increasing CNC nanofiller content, the composite hydrogels increased in Young's modulus and fracture strength. Reproduced with permission.<sup>[136]</sup> Copyright 2013, American Chemical Society. C) Photographs and compressive stress–strain curves of a clay nanoparticle-doped poly N-acryloyl glycinamide (PNAGA) hydrogel. The clay nanofiller increased the compressive modulus and strength of the hydrogel. Reproduced with permission.<sup>[149]</sup> Copyright 2017, American Chemical Society. D) Preparation of GelMA-coated gold nanorods (G-GNRs)/GelMA hydrogels. TEM image and photographs of G-GNRs in solution, and Young's moduli of G-GNRs/GelMA hydrogels at various concentrations of G-GNRs. Reproduced with permission.<sup>[108e]</sup> Copyright 2017, Wiley-VCH.

the fracture strain from 62% to 72% in compression experiments.<sup>[137]</sup> Moreover, the swelling ratio and crosslinking kinetics would also change after doping with NFC.<sup>[137]</sup> This work also showed that the degree of enhancement varies with the molecular weight of PEGDA.<sup>[137]</sup> Through 10 million compression cycles, Khoushabi et al. showed that NFC/PEGDMA-based PRHs are softened in the first cycle and then remain constant while the modulus of neat PEGDMA hydrogel is maintained throughout cyclic loading.<sup>[138]</sup> They also claimed that the extent of softening could be tuned by the swelling degree of the matrix.<sup>[138]</sup> Based on CNC/PRH nanocomposites, inks for 3D printing have also been developed.<sup>[108d,139]</sup> For example, Palaganas et al. developed a photocurable CNC/PEGDA ink for stereolithography (SL), and the printed nanocomposite hydrogel structures showed a high degree of repeatability, fidelity, and mechanical integrity of complex design.<sup>[139a]</sup> Utilizing the local and anisotropic swelling behavior of directionally oriented cellulose fibrils, Gladman designed an NFC/clay/PAAm composited photocurable ink for direct ink writing.<sup>[139b]</sup> Combined with a theoretical framework, the curvature of the printed bilayer structure in swelling could be precisely controlled, and dynamic architectures responding to hydration could be designed.<sup>[139b]</sup>

#### 2.3.4. Clay/PRH Nanocomposites

Clays are hydrous aluminum silicates, often with substantial iron and magnesium, and have been used to reinforce hydrogels.<sup>[140]</sup> Clay minerals can be exfoliated into 2D CNPs through treatments such as ion exchange and the use of polymeric exfoliating agents.<sup>[141]</sup> Common clay nanofillers included natural montmorillonite and synthetic hectorite.<sup>[141]</sup> These CNPs are efficient reinforced fillers for hydrogels, not only due to their excellent mechanical properties (e.g., Young's modulus of montmorillonite could be 5–250 GPa<sup>[142]</sup>), but also due to their multiple strong physical and chemical interactions with polymers (e.g., covalent bond, hydrogen bonding, electrostatic interactions, coordination bonds, and hydrophobic interaction).<sup>[121]</sup> CNPs are also highly hydrophilic and disperse well in water well at relatively high concentration (e.g., at 13 wt% Laponite XLS ( $\text{Na}_{0.7}[\text{Si}_8\text{Mg}_{5.5}\text{Li}_{0.3}\text{O}_{20}(\text{OH})_4]$ ) in water).<sup>[143]</sup>

The most widely investigated photo-crosslinkable hydrogel reinforced by CNP is PAAm. Xiong et al. investigated mechanical enhancement by two kinds of hectorite CNPs, laponite RDS and laponite RD, on PAAm gels and found that the resulting nanocomposites to have high extensibility at breakage, exceeding 4000%, with laponite RD having better gelation than laponite RDS.<sup>[144]</sup> Helvacioğlu et al. investigated the mechanical properties of PAAm-based composites nanofilled with two kinds of montmorillonite, namely sodium montmorillonite (NaMMT) and organically modified montmorillonite (OrgMMT).<sup>[145]</sup> The optimal composite hydrogel with the highest equilibrium swelling ratio and compressive modulus is that with 0.5 wt% OrgMMT loading.<sup>[145]</sup> Gao et al. synthesized a montmorillonite (MMT)/PAAm composite hydrogel with self-healing ability, high toughness, and high fracture elongation (up to 11 800%).<sup>[146]</sup> However, these clay/hydrogel nanocomposites showed remarkable hysteresis, which implies decreasing mechanical properties of hydrogel under cyclic loading. Thus,

Su et al. proposed grafting chitosan onto MMT to enhance MMT-PAAm interaction and achieve lower hysteresis.<sup>[147]</sup> The chitosan-treated MMT/PAAm composite showed 237%, 102%, and 389% improvement of tensile strength, fracture elongation, and energy at breaking in comparison to a composite without chitosan.<sup>[147]</sup> Other polymer matrices (e.g., PEGDA) could also be reinforced by CNPs.<sup>[148]</sup> Some researchers are also designing inks for 3D printing using clay/PRH composites. For example, Zhai et al. developed a UV-curable laponite XLG doped poly N-acryloyl glycinamide (PNAGA) hydrogel (Figure 6C). They showed that laponite XLG can significantly improve the viscosity of the pre-gel solution and the mechanical properties of PNAGA when the addition content is more than 7 wt%.<sup>[149]</sup> The composite hydrogel is a suitable ink for extrusion printing and constructing bioscaffolds for bone defects.<sup>[149]</sup>

#### 2.3.5. Metal/PRH Nanocomposites

Noble metal (e.g., Au, Ag) nanoparticles are attractive nanofillers for hydrogels because of their good mechanical properties (e.g., Young's modulus and yield strength of Au nanowires are around 70 and 3.5–5.6 GPa<sup>[150]</sup>), biocompatibility, high electronic conductivity, resistance against electrochemical degradation, unique optical properties, and bioactivities (e.g., antibacterial, antiinflammatory).<sup>[106,151]</sup> Compared to the aforementioned filler materials, metals have much higher density (Au 19.3 g cm<sup>-3</sup>, Ag 10.5 g cm<sup>-3</sup>). Thus, the upper volume limit (usually less than 0.1 vol%) for metal nanoparticles suspended in aqueous solution is much lower than those of the aforementioned nanofillers.

However, even minimal addition of metal nanoparticles could improve mechanical properties and functionalities of PRHs.<sup>[108e,152]</sup> For example, Xu et al. developed an Ag nanoparticle-loaded porous PHEMA hydrogel by a photocuring reaction and found that the compressive modulus of the porous hydrogels increases from 28 to 38 kPa with  $100 \times 10^{-3} \text{ M}$  ( $\approx 0.1 \text{ vol}\%$ ) of Ag nanoparticles as nanofiller.<sup>[152a]</sup> This Ag nanofiller further endowed the PRHs with antibacterial properties and resistance to foreign-body reactions. Zhu et al. incorporated Au nanorods (34 nm long and 25 nm wide) into GelMA and found that Au nanoparticles increase the hydrogels stiffness from 3.7 to 4.7 kPa at a content below 0.5 mg mL<sup>-1</sup> ( $\approx 0.0026 \text{ vol}\%$ ), and further provided it with the ability to be printed.<sup>[108e]</sup> The Au nanofiller furthermore endowed the GelMA with electrical conductivity sufficient to enable culture of cardiac cells (Figure 6D).

#### 2.4. Architectural Design Techniques for PRHs

Material architecture, including micro and nanoscale structural features such as pores,<sup>[153]</sup> fibers,<sup>[154]</sup> cellular structures,<sup>[155]</sup> and stiffness gradients,<sup>[156]</sup> can be tuned to govern the macroscale properties of a structure. Architected materials are observed in nature in structures such as honeycomb,<sup>[157]</sup> vascular tissues,<sup>[158]</sup> and the tendon-to-bone attachment.<sup>[159]</sup> These strategies have also been widely used to construct metamaterials.<sup>[155,160]</sup> To realize these complex structural features in PRHs, various manufacturing methods have been developed, such as

templating,<sup>[153,161]</sup> electrospinning,<sup>[162]</sup> phase separation,<sup>[163]</sup> and printing.<sup>[164]</sup> Templating by salt, porogens, or emulsion is a simple and efficient method of constructing porous structures in hydrogels; however, it has some limitations. It is difficult to control the pore size and shape or to completely remove the templates. Moreover, it is hard to form a multiscale structure in one sample.<sup>[161]</sup> Electrospinning is a feasible approach to form fibers with diameters down to several hundred nanometers from polymeric solution or melts, but it is difficult to form stable 3D structures and control the spacing between fibers.<sup>[162,165]</sup>

Printing of PRHs has emerged as an effective way of forming more complex structures than is possible by templating, electrospinning, or phase separation. Compared to other fabrication methods, it has the advantages of large scalability (from tens of nanometer to several centimeter), high resolution, fast fabrication, and relatively little labor.<sup>[3b,165,166]</sup> Among the broad range of printing techniques and inks available for PRH-based materials (Table 2), two classes of printing methods have been adopted widely: light-based printing, and ink-based printing.<sup>[167]</sup> Light-based printing methods include photomask-, laser-, and projection-based lithography. These techniques directly pattern a photo-crosslinkable hydrogel or photodegradation hydrogels using specified light dosages on different positions of the samples. Ink-based printing techniques include inkjet and extrusion based printing. In these approaches, photo-crosslinkable hydrogels are used in the form of printable inks. Details of light-based printing and ink-based printing are elaborated upon in the following two subsections.

#### 2.4.1. Light-Based Printing

In light-based printing, PRHs can form specific structures or elastic heterogeneities by selectively crosslinking or degrading through precisely patterned light exposures.<sup>[3b,168]</sup> Light-based printing methods are categorized according to the manner of forming patterns; they include photomask-based lithography, laser-based lithography, and projection-based lithography. These techniques can be used to create 3D structures in a layer-by-layer manner, which is also known as SL.

In photomask-based lithography, light passes a photomask with patterned transparency<sup>[169]</sup> or a moving photomask,<sup>[170]</sup> which determines the irradiation doses on PRHs and thus controls hydrogel elasticity. Patterning PRHs by photomask-based lithography is the most widely used method for designing a 2D substrate with spatial mechanical heterogeneities due to its simple and low-cost preparation process.<sup>[171]</sup> Thus, diverse PRHs based on different photochemistry have been fabricated through photomask-based lithography for a range of applications. For example, Gramlich et al. showed that elasticity and various peptides could be sequentially patterned on a same substrate by orthogonal thiol-ene chemistry.<sup>[88]</sup> Mehta et al. created a composite hydrogel with stiff, sinusoidal-patterns by using photomasks, which displayed more tissue-like mechanical properties than uniform hydrogels.<sup>[172]</sup> Samorezov et al. created mechanical patterns on dual ionic- and photo-crosslinkable hydrogels by photomasking, which could spatially control the cell attachment and proliferation.<sup>[173]</sup> In addition,

photodegradation and uncaged gelation chemistry could also be applied to create spatial elasticity patterns by using a simple photomask.<sup>[170c,174]</sup> Furthermore, taking advantage of wavelength-dependent photo-crosslinking and photocleavage reactions, Radl et al. showed that switchable patterns on polymer networks could also be prepared by using photomasks.<sup>[175]</sup> Despite its wide application, photomask-based lithography also has limitations, such as the requirement of additional labor and time cost for the preparation of photomasks, and the complex processes for creating multilayer structures.

Alternatively, laser-based lithography is a mask-free strategy in which a computer-aided design (CAD)-controlled focal laser beam scans the PRHs and then selectively crosslinks or degrades the beam-scanned position.<sup>[176]</sup> The spot size, power, and scanning speed of lasers are key factors that determine the resolution. Scott et al. developed a two-color irradiation scheme for laser-based lithography in which one wavelength could initiate photopolymerization, and the other independent wavelength inhibited the photopolymerization by trapping radicals instantly.<sup>[176b]</sup> This approach could enhance the spatial control over the photopolymerization.<sup>[176b]</sup> Despite the advantages at high resolution and controllability of photopolymerization, laser-based lithography is a highly time-consuming method for large-area patterns due to its point-by-point fabrication process.

Projection-based lithography employs a virtual mask sequence (created by either a digital micromirror device (DMD)<sup>[170d,177]</sup> or a liquid-crystal display<sup>[33b,178]</sup>) to create light exposure patterns. Compared to traditional liquid-crystal display-based projection, DMD-based projection offers much more fabrication flexibility and higher process speed, which has attracted wide interest recently.<sup>[179]</sup> The DMD chip consists of millions of micro-mirrors that can modulate light beams to generate optical patterns that are the same as computer-designed patterns.<sup>[179]</sup> The size and resolution of projected light patterns can be tuned by a lens.<sup>[180]</sup>

Based on the aforementioned light-based printing techniques, SL holds potential for developing 3D structures and elastic heterogeneities. The strategy is to stack 2D printed patterns in a layer-by-layer manner using techniques such as photomask-based SL,<sup>[181]</sup> laser-based SL,<sup>[139a,182]</sup> and projection-based SL<sup>[80i,179,180,183]</sup> (Figure 7A). To control the thickness of each printed layer, the light penetration depth of bioinks is always a critical consideration in SL, which may be controlled through tuning the light absorbance of hydrogel precursors (e.g., adding pigments, nanofiller or tuning concentration of initiators).<sup>[54b,184]</sup> To optimize patterning resolution, curing kinetics are usually tuned by radical quenchers, such as TEMPO.<sup>[177c]</sup>

Efforts to improve resolution and printing speed focus on improvements to SL devices and techniques. Tumbleston et al. developed a technique called continuous liquid interface production (CLIP) that used projection-based SL printing.<sup>[185]</sup> In this technique, oxygen inhibition is cleverly utilized to create a “dead zone” (persistent liquid interface) that can realize synchronous ink renewal, light exposure, and platform movement instead of the discrete steps in traditional methods, which improved printing efficiency to enable printing of hundreds of millimeters in height per hour.<sup>[185]</sup> Zheng et al. developed large-area projection microstereolithography (LAPμSL), which

**Table 2.** Summary of bioinks and printing parameters for designing PRHs.

Printing method <sup>a)</sup>	Bioink properties				Printing parameters				
	PSCs	Polymer matrices	Additives	Young's modulus	Excitation wavelength	Light intensity	Fabrication time	Minimal feature size	Ref.
2D photomask	I2959 (0.05 wt%)	MeHA(3 wt%)	–	2.3–100 kPa	320–500 nm	10 mW cm <sup>-2</sup>	120–240 s	25–500 μm	[291–292]
	I2959 (0.05 wt%)	PAAm (8.5–16 wt%)	–	1–240 kPa	365 nm	3.9 mW cm <sup>-2</sup>	270 s	–	[170a]
	SCQ (0.9 wt%)	StG (30 wt%)	–	50–500 kPa	488 nm	100–400 mW cm <sup>-2</sup>	300–500 s	20 μm	[26]
	Eosin Y (9.7 × 10 <sup>-4</sup> wt%), TEOA (0.97 wt%)	MeHA (5 wt%)	–	0.5–1.5 kPa	Visible light	–	1500 s	21 μm	[169a]
	ONB	PEGdiPDA(2.5–8.2 wt%), PEGA(6.8–10 wt%)	–	2–32 kPa	365 nm	10 mW cm <sup>-2</sup>	300–720s	2 μm	[32a,170c,174b]
	ONB	NHS-PC-4armPEG (12–22 wt%), Amino-4armPEG (0–9.6 wt%), Gelatin (0–5 wt%)	–	0–10 kPa	365 nm	30 mW cm <sup>-2</sup>	300 s	20 μm	[33b]
	I819 (0.5–4 wt%), ONB	PETMP/TMPMP/HDT; vinyl-NBE	–	–	Cure:420–450 nm, Degradate:250–470 nm	3.63 mW cm <sup>-2</sup> 82.1 mW cm <sup>-2</sup>	800 s	4 μm	[175]
2D projection	ONB	PEGdiPDA (4.3–10 wt%), PEGDA (2.9–35 wt%)	–	13.9–220.8 kPa	UV	–	720 s	0.25 μm	[177b]
	ONB	NHS-PC-4armPEG (1.2–10.8 wt%), NHS-4armPEG (0.96–8.6 wt%), Amino-4armPEG (10 wt%)	–	3.5–23 kPa	365 nm	125 mW cm <sup>-2</sup>	7.2 s	1.4 μm	[178b]
	ONB	DBCO-PC-4armPEG Matrigel (0–0.05 wt%) azide-gelatin (2.5 wt%)	–	0–1 kPa	365 nm	156 mW cm <sup>-2</sup>	30 s	10 μm	[33c]
SL photomask	I2959 (0.5 wt%)	GelMA (5 wt%)	–	–	UV	2.9–6.9 mW cm <sup>-2</sup>	20 s	xy: 100 μm z: 150 μm	[181]
SL laser	I2959 (0.5 wt%)	PEGDA (20 wt%)	–	4.73–503 kPa	325 nm	–	–	xy: – z: 100 μm	[182a]
	I2959 (0.5 wt%)	PEGDMA (20 wt%)	–	12 kPa	325 nm	–	–	xy: – z: 100 μm	[182b]
	I2959 (0.3 wt%)	Pluronic F127DA (1 wt%)	–	165 kPa	355 nm	200 mW cm <sup>-2</sup>	1 s mm <sup>-1</sup>	xy: 135 μm z: 50 μm	[176c]
	LAP (0.75 wt%)	PEGDA (75 wt%)	Cellulose (0–1.2 wt%)	26 MPa	405 nm	250 mW cm <sup>-2</sup>	–	xy: 140 μm z: 50 μm	[139a]
	SL projection	I2959 (1 wt%)	GelMA (10–15 wt%)	HMBS (0.1 wt%) CaCO <sub>3</sub>	0–800 kPa	UV	50 mW cm <sup>-2</sup>	20 s per layer	xy: 200 μm z: –
SL projection	I2959 (1 wt%)	PEGDA (20–100 wt%), GelMA (0–15 wt%)	HMBS (0.1 wt%) CaCO <sub>3</sub>	–	–	–	12 s per layer	xy: 200 μm z: –	[179]
	LAP (0.5 wt%)	PEGDA (20 wt%)	–	–	UV	2.7 mW cm <sup>-2</sup>	2.6 s per layer	xy 10.8 μm z: 500 μm	[180]
	LAP (0.3–0.45 wt%)	GelMA (2.5–10 wt%), GMHA (0–2 wt%)	–	3–5 kPa	365 nm	88 mW cm <sup>-2</sup>	–	xy – z: 200 μm	[183]
	Eosin Y (7–28 × 10 <sup>-4</sup> wt%), TEOA (0.1–0.4 wt%)	GelMA (10–20 wt%)	–	4.4–14 kPa	Vis	48.6 mW cm <sup>-2</sup>	120 s per layer	xy 50 μm z: 200 μm	[80i]
	Inkjet	I2959 (0.05 wt%)	PEGDMA (10–20 wt%)	–	36–396 kPa	UV	4.5 mW cm <sup>-2</sup>	600s	xy: – z: 18 μm
I2959 (0.05 wt%)		PEGDMA (10 wt%), GelMA (1.5 wt%)	–	30–70 kPa	UV	4.5 mW cm <sup>-2</sup>	600s	xy: – z: 18 μm	[191c]



**Table 2.** Continued.

Printing method <sup>a)</sup>	Bioink properties				Printing parameters				Ref.
	PSCs	Polymer matrices	Additives	Young's modulus	Excitation wavelength	Light intensity	Fabrication time	Minimal feature size	
Extrusion	Eosin Y TEOA	Pluronic F127DA (20 wt%), PEGDA (10 wt%)	–	–	460 nm	–	–	xy: 117 μm z: 24 μm	[192]
	I2959 (0.097 wt%)	di-MAAm (0–7.8 wt%), NIAAm (0–7.8 wt%)	Cellulose (0.73 wt%), Clay (9.7 wt%)	20–1200 kPa	UV	–	–	xyz: 150 μm	[139b]
	I2959 (0.1 wt%)	GelMA (10 wt%)	Gellan Gum (1 wt%), PLA (0–5 wt%)	25–50 kPa	320–500 nm	6 mW cm <sup>-2</sup>	0.13 s mm <sup>-1</sup>	xyz: 500 μm	[196b]
	I2959 (0.1–0.2 wt%)	PEGDA (10–30 wt%)	Alginate (10–15 wt%)	5.3–74.6 kPa	365 nm	245 mW cm <sup>-2</sup>	0.17–0.33 s mm <sup>-1</sup>	xy: 800 μm z: 600 μm	[196a]
	I2959 (0.05 wt%)	MeHA (2–6 wt%) GelMA (6–12 wt%)	–	4.2–13 kPa	365 nm	2 mW cm <sup>-2</sup>	–	–	[297]
	I2959 (0.3 wt%)	GelMA (15 wt%)	Pluronic F127 (40 wt%)	–	UV	5 mW cm <sup>-2</sup>	0.1–1 s mm <sup>-1</sup>	xyz: 30 μm	[91b]
	I2959 (0.5 wt%)	GelMA (15 wt%)	–	1.5–2.6 kPa	UV	3.95 mW cm <sup>-2</sup>	0.15 s mm <sup>-1</sup>	xyz: 500 μm	[80e]
	I2959 (0–0.05 wt%) or LAP (0–0.05 wt%)	MeHA (0–5 wt%), or GelMA (0–5 wt%), or PEGDA (0–5 wt%), or NorHA (0–2 wt%)	–	3–4 kPa	320–390 nm 400–500 nm	10 mW cm <sup>-2</sup> 15 mW cm <sup>-2</sup>	9000 s mL <sup>-1</sup>	xyz: 60 μm	[197]
	LAP (0.05 wt%)	MeHA (2 wt%), CSMA (5 wt%), HA-pNIPAAm (10–20 wt%)	–	0.134–4.45 kPa	365 nm	6.09 mW cm <sup>-2</sup>	0.12 s mm <sup>-1</sup>	xy: 620 μm z: 200 μm	[195b]
	LAP (0.05 wt%)	Pluronic F127DA (0–20 wt%), MeHA (0.1–0.5 wt%)	Pluronic F127 (0–20 wt%)	1.42–24.1 kPa	365 nm	6.09 mW cm <sup>-2</sup>	0.6 s mm <sup>-1</sup>	xy: 700 μm z: 110 μm	[195a]
	VA-086	GelMA (5–20 wt%)	–	3–14 kPa	365 nm	4 mW cm <sup>-2</sup>	0.08–0.2 s mm <sup>-1</sup>	xyz: 150 μm	[80b]

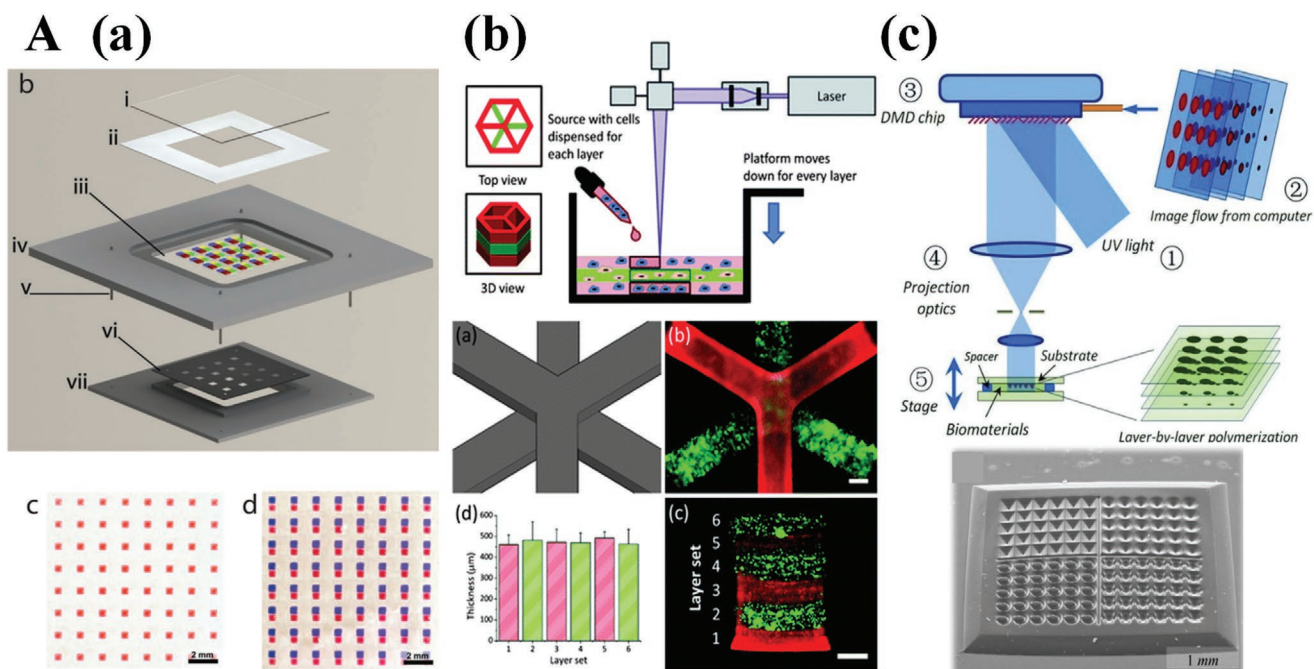
<sup>a)</sup>LAP: lithium acylphosphinate, ONB: *ortho*-nitrobenzyl, SCQ: sulfonyl camphorquinone, MeHA: methacrylate hyaluronic acid, NorHA norborene modified hyaluronic acid, PAAm: polyacrylamide, StG: styrenated gelatin, GelMA: gelatin methacryloyl, PEG: poly ethylene glycol, PEGA: PEG-monoacrylate, PEGDA: PEG-diacrylate, PEGdiPDA: PEG-di photodegradable acrylate, NHS-PC-4armPEG: *N*-hydroxysuccinimide-terminated photocleavable tetra-arm PEG, DBCO-PC-4armPEG: dibenzocyclooctyl-terminated photocleavable tetra arm-PEG, PETMP: pentaerythritol tetra (3-mercaptopropionate), TMPMP: trimethylolpropane tris(3-mercaptopropionate), HDT: 1,6-hexanedithiol, vinyl-NBE: (2-nitro-1,4-phenylene)*bis*(methylene)acetate, HMBS: 2-hydroxy-4-methoxy-benzophenone-5-sulfonic acid, UV absorber.

combines a spatial light modulator with a coordinated optical scanning system.<sup>[104a]</sup> This technique is scalable for manufacturing and can form hierarchical 3D topologies on photocurable materials with feature sizes that vary from tens of nanometers to several centimeters.<sup>[104a]</sup>

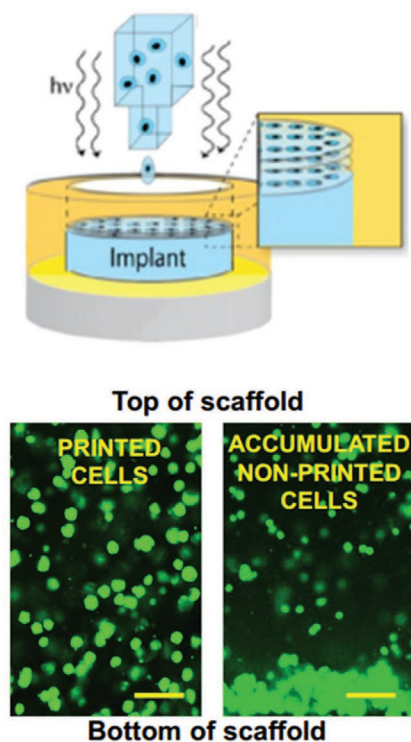
#### 2.4.2. Ink-Based Printing

In contrast to light-based printing, ink-based printing methods form patterns based on the shapes of the jets or extrusions from the printing nozzles.<sup>[3b,168,186]</sup> These methods are not only suitable for photocurable materials but also for precursors of other crosslinking mechanisms (e.g., thermal and ionic crosslinking). Ink-based printing can integrate several different types of materials in one structure through integration of multiple printing

nozzles.<sup>[168]</sup> Two approaches to ink-based printing exist: inkjet printing and extrusion printing.<sup>[186]</sup> In inkjet printing, droplets of ink are jetted onto a substrate to form desired patterns.<sup>[187]</sup> The droplets can be generated by either thermal or piezoelectric printing nozzles and are cured after the deposition of each layer.<sup>[166,188]</sup> To prevent clogging of the nozzle, inks must have low initial viscosity (1–30 mPa s<sup>-1</sup>) and, for cases in which cells are printed, low cell density (<10<sup>6</sup> cells mL<sup>-1</sup>).<sup>[189]</sup> The droplet volume, viscosity surface tension, and density must be controlled to tune droplet formation.<sup>[187b]</sup> Its resolution (typically 20–250 μm) is often lower than that of lithographic processes, and depends on droplet volume and the contact angle of the ink substrate.<sup>[187b]</sup> Early inkjet printing was developed for physically crosslinked hydrogels, such as collagen, alginate, and fibrin.<sup>[190]</sup> Droplet-based printing for PRHs was developed more recently. For example, Cui et al. developed a 3D inkjet printing system



**B (a)**



**(b)**

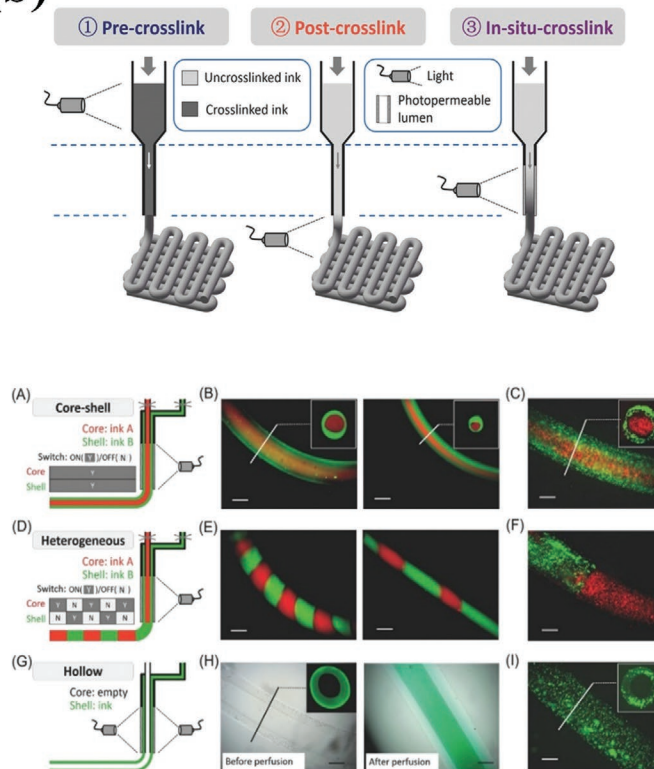


**Figure 7.** 3D printing methods for PRHs. A) Representative light-based printing techniques. a) Fabrication of patterned hydrogel structures by photo-mask-based stereolithography (scale bar: 2 mm). Reproduced with permission.<sup>[181]</sup> Copyright 2013, Wiley-VCH. b) Fabrication of a multilayer cell-laden hydrogel by laser-based stereolithography (scale bar: 1 mm). Reproduced with permission.<sup>[182a]</sup> Copyright 2010, Royal Society of Chemistry. c) Fabrication via digital micromirror device (DMD)-projection-based stereolithography and SEM images of microstructured wells (scale bar: 2 mm). Reproduced with permission.<sup>[179]</sup> Copyright 2012, Wiley-VCH. B) Representative ink-based printing techniques. a) Inkjet printing of cell-loaded photo-crosslinkable hydrogels and the resulting even cell distribution within the hydrogels (scale bar: 100  $\mu\text{m}$ ). Reproduced with permission.<sup>[191c]</sup> Copyright 2015, Springer. b) Extrusion printing of photo-crosslinkable hydrogels by three different fabrication strategies (pre-, post-, in situ photo-crosslinking) with fibers printed by an in situ photo-crosslinking strategy (scale bar: 500  $\mu\text{m}$ ). Reproduced with permission.<sup>[197]</sup> Copyright 2017, Wiley-VCH.

with simultaneous photopolymerization capability based on a modified commercial printer (Figure 7Ba), which is suitable for PEGDA-, PEGDMA-, and GelMA-based precursors.<sup>[191]</sup> To accelerate the curing process and keep the printed shapes, Biase et al. developed a Pluronic F127 diacrylate-based ink for inkjet printing, which adopted a tandem crosslinking mechanism of a rapid temperature-controlled gelation followed by photopolymerization.<sup>[192]</sup> In these applications, it is difficult to form a second layer for 3D structure with inkjet printing because the physical properties of the solidified surface are distinct from those of the substrate.<sup>[168]</sup> Despite this drawback, inkjet printing shows some advantages, such as the fact that it is mask-free, noncontact, and capable of generating small volume (1–100 pL) droplets.<sup>[187b,191a]</sup>

Extrusion printing continuously extrudes inks to generate a hydrogel filament (typical diameter of 150–300 μm) from the nozzle to the substrate by piston or screw.<sup>[189]</sup> Extrusion printing can tolerate inks with a larger range of viscosity that cover a much broader range of materials.<sup>[3b,168]</sup> The viscosity of extruded inks determines the parameters of printing processes and the shape fidelity after printing.<sup>[193]</sup> Aqueous solutions of photo-crosslinkable polymers usually have a low initial viscosity and limited crosslinking kinetics that limit their shape fidelity; Hence their use should be combined with other strategies such as adding guest–host bonding,<sup>[194]</sup> adjustment of temperature,<sup>[80b,195]</sup> or incorporation of viscous components (e.g., alginate, clay, gellan gum) for higher viscosity.<sup>[139b,196]</sup> As an alternative to these material-dependent strategies, Ouyang et al. proposed a “in situ” crosslinking strategy suitable for most PRHs, which allows light penetrating the printing head to crosslink the hydrogels immediately prior to deposition (Figure 7B).<sup>[197]</sup> It was shown that this strategy was suitable for a wide category of non-viscous bioinks, including aqueous solution of MeHA, GelMA, PEGDA, and NorHA without any modification of their properties. Additionally, it preserved a high shape fidelity and cytocompatibility.<sup>[197]</sup> Extrusion-based printing can print inks with a wider range of viscosity (0.03 to 60 000 Pa s) and cell density (up to 10<sup>8</sup> cells mL<sup>-1</sup>) than jetting-based printing techniques. Despite these advantages, extrusion printing also has challenges, such as a relatively lower printing resolution.<sup>[164c,188]</sup>

### 3. Mathematical Models for Predicting Elasticity of PRHs

Emerging mathematical models have been critical to developing advanced PRHs, and promise to guide further developments. Integration of models with novel quantitative experimental techniques such as network disassembly spectrometry<sup>[198]</sup> and isotopic labeling disassembly spectrometry<sup>[199]</sup> have helped with the development of a continuously expanding library of PRHs. This section summarizes the state of the art for modeling of photo-crosslinkable hydrogels, photodegradable hydrogels, and PRH-based nanocomposites.

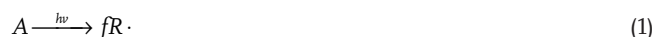
#### 3.1. Modeling the Elasticity of Photo-Crosslinkable Hydrogels

Hydrogel formation by photo-crosslinking begins by irradiating a precursor solution to develop a polymer network in

aqueous solution that can be crosslinked and extended until all monomers are consumed. The process involves two steps: phase transition (pre-gel) and stiffening (post-gel). The kinetics of these two steps determines the time evolution, architecture, and mechanics of the hydrogel. This section describes the three classes of models that are critical to understanding how the mechanics of these PRHs develop over time: i) models of how the degree of monomer conversion evolves over time as a function of reaction conditions; ii) models of how the relationship between the topology of the polymer network affects the degree of conversion; and iii) models of how hydrogel mechanics arises from the topology of the polymer network (Figure 8). These three classes of models link the four variables to prescribe the temporal evolution of conversion, network topology, and network mechanics, and thus define the spatiotemporal evolution of the mechanics of photo-crosslinkable hydrogels.

##### 3.1.1. Time Evolution of Photopolymerization

Photopolymerization develops over time as a result of the formation of radicals that drive formation of a polymer backbone. These kinetics are affected by factors such as optics, stoichiometry, diffusion, oxygen, and temperature, and involve three basic sub-processes: initiation, propagation, and termination.<sup>[200]</sup> A set of population balance equations can be established for describing these processes, and each process is governed by a rate coefficient. Type I initiator-induced photopolymerization can be described by the following equations<sup>[201]</sup>



where  $A$  represents the initiator,  $R$  represents the cleaved species of the initiator,  $M$  represents monomers, and represents a molecule in the radical state.

Determination of these rate coefficients is difficult and inaccurate due to complicated behaviors of radical polymerization systems and complex reaction conditions.<sup>[200]</sup> Thus, in most models, rate coefficients are fitting parameters for experimental data. Population balance equation-based kinetic models for photopolymerization have been helpful to understand reaction systems of photoinitiated thiol-ene polymerization,<sup>[202]</sup> copolymerization;<sup>[203]</sup> controlled radical polymerization,<sup>[204]</sup> and in understanding the roles of oxygen,<sup>[205]</sup> light intensity,<sup>[206]</sup> and diffusion<sup>[207]</sup> in photopolymerization systems. However, accounting for all possible processes in photopolymerization kinetics is cumbersome, and kinetic parameters are tedious to quantify, making these models hard to use in engineering practice.

To simplify these complex processes, Cabral et al. proposed a coarse kinetic model in which the whole photopolymerization

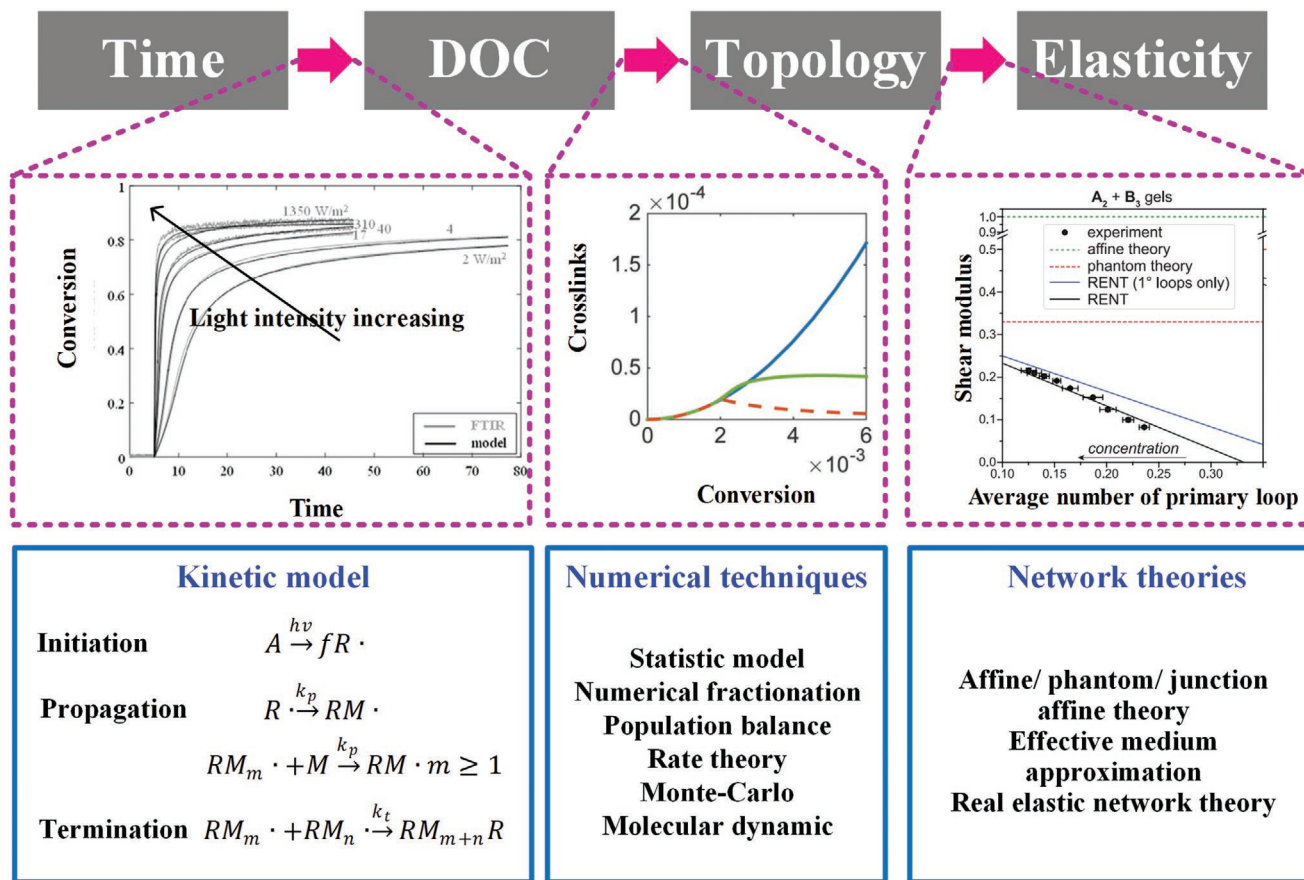


**Figure 8.** Basic principles for modeling the elasticity of photo-crosslinkable hydrogels. There are three tandem relationships underlying the evolution of mechanics in photo-crosslinkable hydrogels: the irradiation time-dependent degree of conversion (DoC), DoC-dependent network topology, and network topology-dependent elasticity. Theoretical methods have been developed for each relationship. From left to right, adapted with permission. [206] Copyright 2018, Elsevier. [215a] Copyright 2017, Wiley-VCH. [199b] Copyright 2016, American Association for the Advancement of Science.

process is represented by a single conversion constant. [184c] In combination with the Lambert–Beer law, the coarse kinetics model has been effective for understanding and controlling frontal kinetics in lithographic applications a range of conditions including photobleaching and photodarkening, [184c,208] heat generation and thermal diffusion, [209] mass diffusion, [210] temperature, [211] and 3D printing. [184b]

### 3.1.2. Topology of Polymer Network

Monomer population balance equations yield information about concentrations of chemical species but not about their structures. Moreover, these equations can be hard to solve due to a nearly infinite number of equations. To track network topology evolution, various numerical techniques have been proposed: i) statistical models, [212] ii) kinetic-derived methods (e.g., method of moments, [213] numerical fractionation technique (NFT), [214] and convolution methods [215]), and iii) first principles techniques (e.g., Monte-Carlo [216] and molecular dynamics simulation [217]).

Statistical models, including the treelike model (Flory/Stockmayer), [218] the cascade theory (Gordon), [219] and the recursive

model (Macosko/Miller) [212a,220] are classical methods for understanding the relationship between the crosslinks in polymer networks and the degree of polymerization. All theories are based on the following assumptions regarding ideal polymer networks: i) functional groups have equal reactivity and ii) cyclization reactions (i.e., intramolecular reactions) are negligible. They provide same critical criteria (gel point) of conversion for various types of reactive groups based on the concept of “infinitely large molecules.” For example, a homopolymerization system of monomers with  $f$  functional groups reaches the gel point when its conversion reaches  $\alpha_c = 1/(f - 1)$ . These theories also provide equivalent results regarding the distribution of molecular size and crosslinks. Combined with kinetic models based on rate equations, these statistical models show powerful predictive abilities regarding the evolving topology of ideal polymer networks. [38a,212b,221] For example, Reddy et al. developed a modeling framework for thiol-vinyl photopolymerization based on combined kinetic and statistical approaches, which can predict the molecular weight, crosslink density, and stiffness of gels crosslinked by either step growth or chain growth. [212b]

Kinetic-derived methods track the detailed molecular states of monomers or polymers based on the population balance

equations of these species during polymerization processes. The method of moments, one of the most widely applied kinetic-derived methods, is a simplified method of solving population balance equations in terms of the  $n$ th order moment ( $Q_n$ )<sup>[222]</sup>

$$Q_n = \sum_{r=0}^{\infty} r^n [P_r] \quad (5)$$

where  $r$  represents the length of a polymer chain, and  $[P_r]$  is the concentration of the polymer with the length of  $r$ . Through this method, the average chain length and dispersion of polymer chains can be predicted. Based on the method of moments, Teymour and Campbell developed a dynamic polymer model based on “numerical fractionation,” which numerically separates polymer populations into a series of subdistributions with similar size.<sup>[214a]</sup> This technique provides an approach for computing the gel point and gel fraction and finds applications in various photopolymerization systems.<sup>[214b,223]</sup> A variant exists that provides a reasonable estimation of rate constants for cyclization.<sup>[224]</sup> Kryven and co-workers proposed a related convolution-based calculation method for solving population balance equations, which also proved to be an efficient approach for predicting evolving topology.<sup>[215a,225]</sup>

Although statistical and kinetic-derived methods can predict crosslink concentrations, they cannot predict other key structures such as densities of loops that arise within polymer networks as a result of this crosslinking. Because these structural properties influence the mechanical properties of polymer networks,<sup>[199b]</sup> they are a focus of research involving Monte-Carlo and molecular dynamic simulations. Gillespie established a Monte-Carlo method based on the instantaneous reaction probabilities of chemical events capable of handling polymer network development.<sup>[226]</sup> By adding the position information of species on lattices, a kinetic gelation modeling for free radical polymerization can be developed, which is used to predict the structures of developed polymer networks and capture of radicals and reaction-diffusion.<sup>[216a,b,227]</sup> Johnson and co-workers developed a Monte-Carlo simulation method based on a purely topological perspective, ignoring spatial information about polymers and junctions and only counting special topological structures in the networks).<sup>[198,199,228]</sup> This approach shows good agreement with the results of experiments (network disassembly spectrometry, isotopic labeling disassembly spectrometry) and with kinetic graph theory predictions.

Another widely used computer simulation method for predicting hydrogel mechanical properties is molecular dynamics simulation. Molecular dynamics simulation is based on the motion of atoms obeying classical mechanics laws.<sup>[229]</sup> In comparison with the stochastic principles of Monte-Carlo models, it is a deterministic technique.<sup>[230]</sup> Molecular dynamics simulation have been used to investigate the effects of various parameters (e.g., degree of polymerization, chain rigidity, temperature, precursor topology) on the network structures (e.g., connectivity, dangling chains, pendants, looped structures, nanosized cavitation, amorphous and crystalline structures) created during crosslinking.<sup>[231]</sup> It can also be used to investigate the mechanical properties (e.g., stress-strain curve, extensibility, tensile strength) of polymer networks under stress.<sup>[232]</sup>

### 3.1.3. Elasticity of Polymer Networks

Numerical techniques for predicting topological structures such as crosslinks, primary and high-order loops, and dangling chains in photopolymerization systems are effective, but cannot predict the elasticity of the resulting hydrogel. The issue is that the mechanical responses of these materials arise from a combination of both the mechanics and structure of the constituents. This is a well-studied subject in mechanics, with a range of classical network elasticity theories such as affine/phantom/junction affine theories available. These presume that loops are negligible, and can be summarized by the following equation<sup>[233]</sup>

$$G = [v(C_0, p) - h\mu(C_0, p)] k_B T \quad (6)$$

where  $C_0$  is initial polymer concentration;  $k_B$  is Boltzmann's constant;  $T$  is the absolute temperature;  $v$  is number density of elastically effective chains;  $\mu$  is number density of elastically effective crosslinks;  $h$  is an empirical parameter, which is equal to 0 for an affine model, 1 for a phantom model, and  $0 < h < 1$  for a junction-affine model.

Sakai and co-workers adapted this relationship between elastic modulus and the degree of completion for disordered polymer networks<sup>[233]</sup>

$$G = [v(C_0, p) - h\mu(C_0, p)] g_1(C_0) \quad (7)$$

where  $g_1$  is a monotonic function of  $C_0$  and  $p$  denotes the connectivity probability. The variation of  $C_0$  with respect to the connectivity probability ( $G/G_0 - p$ ) falls onto a single master curve, where  $G_0$  is the elastic modulus at  $p = 1$ . However, this relation still remains limited to a network without loop defects.

Johnson and co-workers identified an important role for loop defects in polymer network elasticity through integrated rheology, disassembly spectrometry and a modified phantom network theory called the “real elastic network theory”).<sup>[199b]</sup> They found that, for crosslinked “ $A_2 + B_f$ ” monomers, classical phantom network theories need to be modified as follows<sup>[199b]</sup>

$$\frac{G'}{v_0 k_B T} = \frac{f-2}{f} \left( 1 - a_f n_{1,f} - b_f n_{2,f} - \sum_{i=3}^{\infty} c_{i,f} n_{i,f} \right) \quad (8)$$

where  $v_0$  is the total number density of polymer strands in the gel (loop and nonloop);  $n_{i,f}$  is the average number of loops per junction; and  $a_f$ ,  $b_f$ ,  $c_{i,f}$  are constants determined by the functionality number of B monomers ( $f$ ) and loop order ( $l$ )

$$a_f = \begin{cases} 5/2 & \text{for } f = 3 \\ 4/3 & \text{for } f = 4 \\ 2/f - 2 & \text{for } f \geq 5 \end{cases} \quad (9)$$

$$b_f = \frac{4(f-1)}{f^2(f-2)} \quad (10)$$

$$c_{i,f} = \frac{4}{f} \left[ \frac{1}{(f-1)^{2i-2} + 1} + \frac{1}{(f-1)^{2i-1} - 1} \right] \quad (11)$$

However, a full description of the elasticity of photo-crosslinkable hydrogels is still lacking, and multiscale mathematical models that serially connect chemical reactions, polymer network topologies represent an important need to guide the design of photo-crosslinkable hydrogels. Several promising approaches are under development. Kizilel's kinetic models for photopolymerization based on the numerical fractionation method are excellent but do not consider the mechanical properties of polymer networks.<sup>[203a,214b,223b]</sup> Wen's kinetic gelation model based on Monte Carlo methods could predict the evolution of network structures in free-radical polymerization, but has yet to be validated with experimental data.<sup>[216a,b,227]</sup> Wu et al. incorporated mechanical loading and nonlinear viscoelasticity into a photopolymerization model of PEGDA, which could capture the evolving properties of curing polymers.<sup>[234]</sup> Recently, our group investigated the role of the photochemical properties of initiators and side reactions (thiol-Michael addition) in the final elasticity of a thiol-acrylate hydrogel.<sup>[235]</sup> These efforts are all based upon simple synthetic polymers with clear chemical properties. Models for complex synthetic or natural polymers remain a critical need.

### 3.2. Modeling the Elasticity of Photodegradable Hydrogels

In photodegradation, light triggers the scission of photolabile linkages in polymer network, softening or even eroding the hydrogel. The network formation of a photodegradable hydrogel can be realized by many different chemical strategies, including radical reactions,<sup>[32a,175]</sup> Michael-type reactions,<sup>[236]</sup> click chemistry,<sup>[25a]</sup> and NHS chemistry.<sup>[25a,33b]</sup> Different chemical strategies obey different kinetic rules; thus, it is a challenge to establish a single unified model for predicting the crosslinking of all photodegradable hydrogels.

However, photodegradation of hydrogels does obey some similar principles. Similar to photo-crosslinkable hydrogels, the elastic modulus of photodegradable hydrogels is linked to their crosslink density, which is determined by photochemical kinetics. Thus, as in photo-crosslinkable hydrogels, photodegradable hydrogels display a tandem relationship between photochemical kinetics, network topology, and mechanical properties. Because of a lack of experimental characterization of how network topology arises during the synthesis of these materials, these tandem relationships are difficult to model and are usually simplified into a first-order exponential equation linking mechanics to light irradiation dosage directly<sup>[32a]</sup>

$$G(t)/G_0 = C(t)/C_0 = e^{-k_{\text{app}}t} \quad (12)$$

where  $G$  is the shear elastic modulus,  $G_0$  is the initial shear elastic modulus,  $C(t)$  is the concentration of uncleaved photolabile moieties after an exposure of time  $t$ ,  $C_0$  is the initial concentration of uncleaved photolabile moieties, and  $k_{\text{app}}$  is the apparent rate of degradation. Here,  $k_{\text{app}}$  is dependent on the quantum yield ( $\phi$ ), molar absorptivity ( $\epsilon$ ), incident irradiance ( $I_0$ ), and wavelength of light ( $\lambda$ )

$$k_{\text{app}} = \frac{\phi \epsilon \lambda I_0 (2.303 \times 10^{-6})}{N_A h c} \quad (13)$$

where  $N_A$  is Avogadro's number,  $h$  is Planck's constant, and  $c$  is the speed of light.

Anseth and co-workers found this relationship suitable not only for nitrobenzyl but also for coumarin-based photodegradable hydrogels.<sup>[32a,33a]</sup> Griffin and Kasko found that  $k_{\text{app}}$  could be increased by decreasing the amount of aryl ether on ONB or changing the functionality on benzylic site.<sup>[237]</sup>

A number of extensions to this relationship have been proposed (Figure 9). Lee et al. analyzed the effects of the solvent environment and polymer molecular weight on the photocleavage kinetics of ONB quantitatively.<sup>[32b]</sup> Tibbitt et al. extended this model framework to model changes in material properties and mass loss in photodegradable hydrogels by considering the release of cleavage products and light attenuation in the materials.<sup>[238]</sup> Yanagawa et al. also characterized the effect of light attenuation on the degradation depth of photodegradable hydrogels by the simple Beer-Lambert law.<sup>[33b]</sup> Based on Tibbitt's model, Norris et al. added diffusion of photoabsorbing species based on a series of mass-action equations and showed that the diffusion of absorbing species could play a significant role in determining the final state of photodegradable hydrogels.<sup>[239]</sup>

In comparison to extensively investigated models of photo-crosslinkable hydrogels, models for photodegradable hydrogels are less developed. Many features of the gel formation process remain unclear, as do effects of environmental factors on the degradation kinetics of photolabile groups.

### 3.3. Modeling the Mechanics of PRH-Based Nanocomposites

The field of homogenization theory has produced remarkably accurate methods to bound and estimate the mechanical responses of most engineering composite materials.<sup>[240]</sup> Unfortunately, standard techniques fail to capture the mechanics of PRH-based nanocomposites, as will be illustrated below. The key issues are that the surface energy and surface area of nanoscale reinforcing particles are high compared to those particles used in standard engineering composites, and that the polymeric matrix itself can be reconfigured and locally crystallized by interactions with the nanoscale reinforcement, including effects of nucleation and confinement.<sup>[241]</sup> The surface area effect is well known: for a filler particle of Young's modulus  $E_f$ , radius  $r$ , and surface energy  $\gamma$ ; that is subjected to an engineering strain  $\epsilon$  in one direction, the ratio of surface energy to strain energy is

$$\frac{U_{\text{surface}}}{U_{\text{strain}}} \approx \frac{4\pi r^2 \gamma}{\left(\frac{4}{3}\pi r^3\right)\left(\frac{1}{2}E_f \epsilon^2\right)} = \frac{6\gamma}{E_f \epsilon^2} \left(\frac{1}{r}\right) \quad (14)$$

For  $\gamma$  on the order of  $1 \text{ J m}^{-2}$ ,<sup>[242]</sup>  $E$  on the order of 100 GPa, and  $\epsilon$  on the order of 0.01, this is  $\approx 600 \text{ nm}/r$ , meaning that surface energy terms, not accounted for by classical homogenization theories, can become dominant for reinforcement at the nanoscale.

Computational approaches to estimate the mechanics of polymer-based nanocomposites exist which cover the range of scales from the molecular scale to the macroscale.<sup>[243]</sup> At the

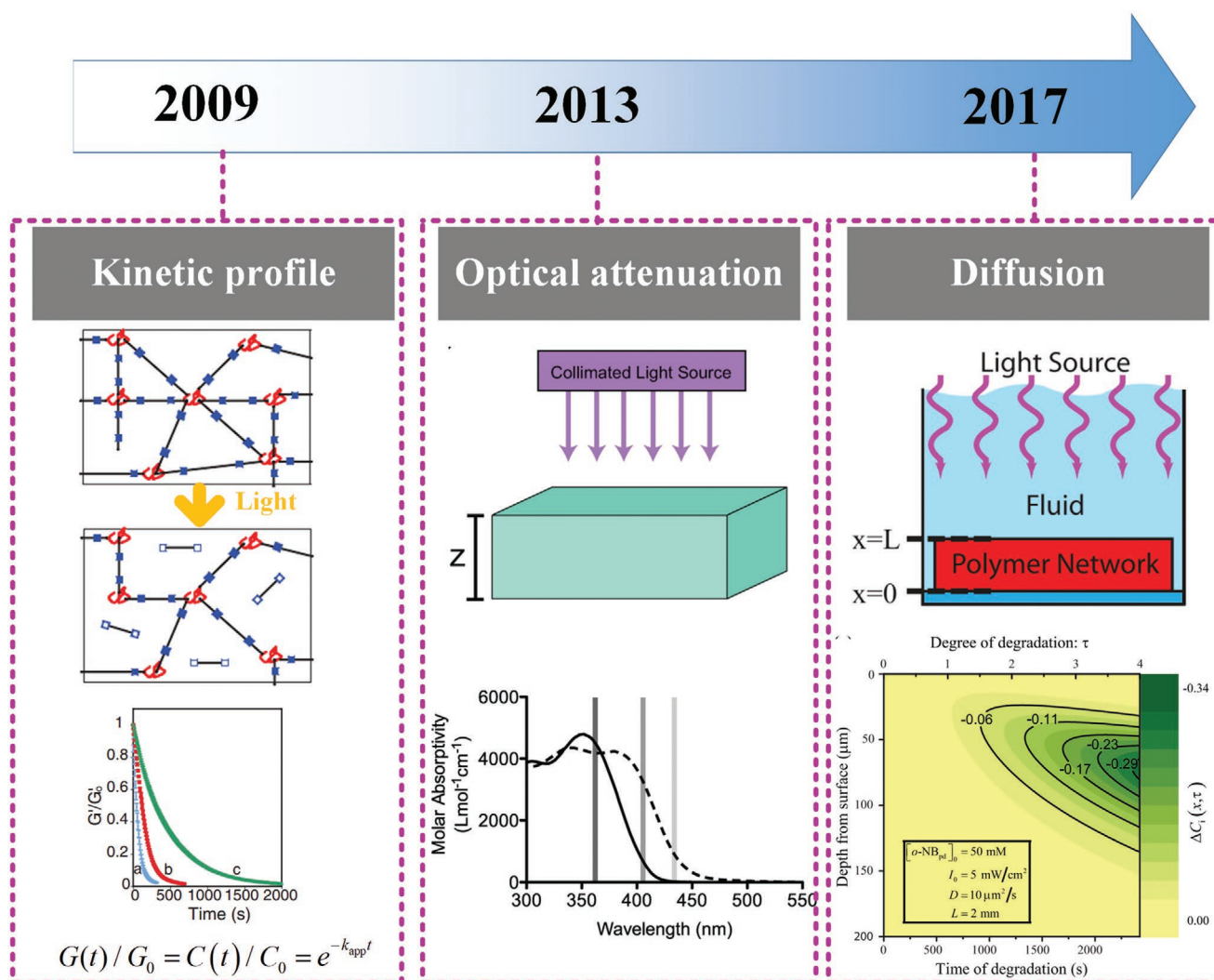


**Figure 9.** Development of models for the elasticity of photodegradable hydrogels. In 2009, a simple exponential function was introduced to express the irradiation time-dependent elastic moduli of photodegradable hydrogels. Adapted with permission.<sup>[32a]</sup> Copyright 2009, American Association for the Advancement of Science. Optical attenuation and mass loss were incorporated into models for optically thick hydrogels in 2013. Adapted with permission.<sup>[238]</sup> Copyright 2013, Wiley-VCH. Models accounting for degradation byproduct diffusion were developed in 2017. Adapted with permission.<sup>[239]</sup> Copyright 2017, Wiley-VCH.

molecular scale, MD models are effective for local interactions over very short timescales, but are ineffective for timescales associated with physiological loadings and photopolymerization.<sup>[243]</sup> Standard continuum models treat materials as continuous throughout their volume and ignore molecular and atomic structures.<sup>[244]</sup> Integration between these approaches is typically required, often by developing cohesive laws or by considering interphases that arise between matrix and filler.<sup>[245]</sup>

MD relates nano to microscale mechanical properties of a material to its molecular-level arrangement, thereby enabling short-range modeling of molecular interactions with nanofillers.<sup>[246]</sup> MD has been used to provide a molecular-scale analysis to evaluate the mechanical performance of the interface between nanofillers and the polymer matrices in various nanocomposites, such as surface-functionalized carbon fiber/epoxy<sup>[245b,c,247]</sup> and graphene/polyethylene.<sup>[248]</sup> However, key challenges are that MD simulations typically reach timescales

that are short compared to those of processes relevant to the physiological applications that underlie important applications of PRHs, and that they typically reach lengthscales that cannot account for effects of heterogeneity and disorder in PRHs.

For these reasons, continuum models continue to serve as the mainstay of efforts to understand and predict the mechanical properties of PRHs. A broad range of continuum homogenization models exist that take information on the structure and composition of a PRH, potentially along with coarse-grained molecular-scale interactions between nanofillers and the PRH, and yield an estimates of macroscopic mechanical properties.<sup>[240]</sup>

### 3.3.1. General Estimates and Bounds of Composites

The simplest continuum models combine only information about the mechanical properties and volume fractions of the

components of a composite, without any information about interactions or structure. Upper bounds on composite modulus ( $E_c$ ) are often approximated by the Voigt estimate (arithmetic or “rule of mixtures” average,  $E_{\text{Voigt}}$ ), and lower bounds by the Reuss estimate (harmonic average,  $E_{\text{Reuss}}$ ).<sup>[249]</sup> In one dimension, for a two-phase composite, these estimates are

$$E_{\text{Voigt}} = \phi E_f + (1 - \phi) E_m \quad (15)$$

$$\frac{1}{E_{\text{Reuss}}} = \phi \frac{1}{E_f} + (1 - \phi) \frac{1}{E_m} \quad (16)$$

where  $E_f$  is the Young’s modulus of filler,  $E_m$  is the Young’s modulus of the matrix, and  $\phi$  is the volume fraction of filler. The Voigt estimate is often reasonable for fibrous composites and particulate reinforced composites with a percolated reinforcement network, and the Reuss estimate is typically most reasonable for very small particulate volume fractions.<sup>[249]</sup> For composites with reinforcement and matrix that have no structure, the tighter Hashin–Shtrikman bounds are applicable.<sup>[240b,250]</sup>

Despite their ability to capture the monotonically increasing relationship between the Young’s modulus of a composite and the volume fraction of fillers, these estimates are typically poor for nanocomposites, for particulate or short fiber composites with higher volume fractions, and for composites with differing types of reinforcement. For lower volume fractions of particulate reinforcement, the Hashin–Shtrikman lower bound often provides a reasonable estimate.<sup>[251]</sup> As does the Mori–Tanaka estimate, the latter based upon the classical Eshelby solution for the elastic field of an ellipsoid included within an infinite matrix,<sup>[252]</sup> but modified to account for the far-field strain to consider the interactions between fillers.<sup>[253]</sup>

Modifications of these approaches can predict the rise of mechanical stiffness as volume fractions approach the percolation threshold.<sup>[254]</sup> At lower concentrations, reinforcement particles have minimal interactions, and their stiffening effects can be predicted by considering them in isolation; at the percolation threshold, reinforcement begins to deform nearly in registry with the surrounding matrix, and the mechanical contributions of contiguous reinforcement and matrix add in parallel.<sup>[255]</sup> Percolation phenomena can be accelerated by interactions among reinforcement,<sup>[255a]</sup> a phenomenon that has been observed in nanocomposites.<sup>[256]</sup>

Improvements to these traditional approaches have been made by considering of the interfacial effect. The earliest models for these effects are those that were developed for semicrystalline polymers, and are based upon models for laminated multiphase composite solids.<sup>[257]</sup> For example, rubbers could undergo phase transition induced by fillers and show distinct mechanical properties, which could be solved by a four-phase model considering the filler/matrix interface.<sup>[258]</sup> Further, the computational models have been applied to consider the scenario where particles draw so close that they create interphases with distinct mechanical properties,<sup>[259]</sup> and a wide range of continuum homogenization models exist to account for composites that contain multiple classes of reinforcing particles.<sup>[251b,260]</sup> Approximate methods such as shear lag approaches have been

applied, many of which approximate elastic fields around single fibers encased in concentric cylindrical shells of matrix.<sup>[261]</sup> These have been applied to CNT/polymer nanocomposites<sup>[261c]</sup> and cellulose/polymer nanocomposites,<sup>[104c]</sup> and have been modified to consider crystallization of polymers at the interfaces of nanotubes.<sup>[262]</sup>

However, many challenges still exist when applying these general estimates and bounds to a PRH composite. In the simplest of cases, the hydrogel is a three-phase composite of polymer backbone, filler, and solvent; as in models of bone,<sup>[251c]</sup> the equations should be adjusted to account for the fact that three phases exist, and that the filler replaces only solvent when added to the PRHs.

To illustrate the challenges with applying conventional homogenization theory to PRHs reinforced with nanoparticles, we plot several sets of data against the Voigt and Reuss estimates and the Hashin–Shtrikman bounds (**Figure 10**). Because such strong contrast exists between the moduli of typical filler and the moduli of PRHs, the bounds are almost perpendicular to each other at low volume fraction, and occupy much of the graph even with the vertical axis on a log scale; note that the bounds do eventually converge at a volume fraction of 100%. However, even with this very broad range, the bounds are informative.

The first observation of note is that the data do not in general follow the Mori–Tanaka estimate and Hashin–Shtrikman lower bound, as data for particulate reinforced or short fiber reinforced composites typically do. Only in the case of one of the three datasets from the literature on clay particulate reinforced nanocomposites approaches these; all other data for carbon nanotube, cellulose, clay particulate, and metal particle reinforced PRHs rise towards the upper bound, with several data sets exceeding the upper bound. One possibility is that the short fiber or plate-like nature of the filler particles contributes to this rapid rise, but this can be shown to be incorrect by comparing the data against the Halpin–Tsai equations, an estimate that works well over a broad range of concentrations.<sup>[263]</sup> The version used is that of Nielson,<sup>[264]</sup> and is specialized to the case of short fibers of aspect ratio  $A = 2l/d$

$$E_c = E_m \left( \frac{1 + A\eta\phi}{1 - \eta\psi\phi} \right) \quad (17)$$

$$\psi = 1 + \left( \frac{1 - \phi_{\text{max}}}{\phi_{\text{max}}^2} \right) \phi \quad (18)$$

$$\eta = \frac{E_f/E_m - 1}{E_f/E_m + A} \quad (19)$$

where  $E_c$  is the equivalent modulus of the composite,  $E_f$  is the modulus of the filler,  $E_m$  is the modulus of the matrix,  $\phi$  is the volume fraction of the filler, and  $\phi_{\text{max}} = 0.82$  is the maximum volume fraction of fibers for random packing. Although efforts have been made to special this to nanofilled composites,<sup>[265]</sup> the simple two-phase model suffices for evaluating the problem at hand. For the relatively stiff fillers under consideration,  $\eta \approx 1$ . Through these estimates, the cellulose data (**Figure 10B**) can be



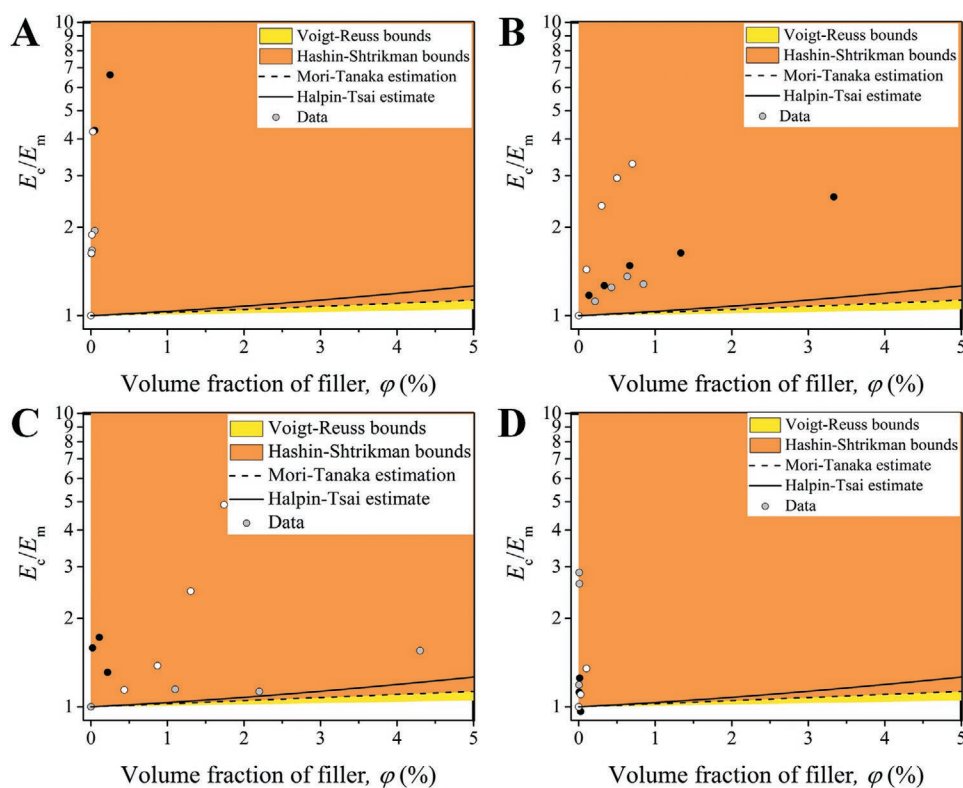


**Figure 10.** Relationships between the ratio of Young's modulus of nanocomposite ( $E_c$ ) and matrix ( $E_m$ ) and volume fraction of fillers ( $\phi$ ) for different nanocomposites. A) Carbon nanotube filled PRHs.<sup>[108c,129b,d]</sup> B) Cellulose reinforced PRHs.<sup>[108d,138,139c]</sup> C) Clay particulate reinforced PRHs.<sup>[144,145,148]</sup> D) Metal particle reinforced PRHs.<sup>[108e,152a,c]</sup> The dots are representative experimental data obtained from the literature. The estimates and bounds shown are two-phase homogenization results for a PRH matrix ( $E_m = 1$  kPa,  $\nu_m = 0.49$ ) reinforced by rigid spherical inclusions ( $E_f = 1$  TPa,  $\nu_f = 0.3$ ), where  $\nu_m$  and  $\nu_f$  are Poisson's ratios of matrix and filler, respectively. In many cases, predicted stiffening rises above thermodynamic limits for conventional composites due to surface energy effects such as recrystallization that arise from nanofillers.

explained as arising from the fibrous nature of the filler, with aspect ratio taken as 20. However, the surface energy effects clearly dominate for all other filler.

### 3.3.2. Computational Simulations

Aside from analytical solutions, finite element analysis (FEA) provides complementary information by solving the basic equations in micromechanics without significant simplifications. Two main steps need to be done in most of the FEA in determining the equivalent mechanical properties of nanocomposites. The first is to define a representative volume element (RVE) large enough to statistically represent a heterogeneous material such that the equivalent properties could be independent of boundary conditions.<sup>[259]</sup> The second is to calculate the effective mechanical properties of this RVE by simulation the detailed mechanical behavior of an element containing one or a few inclusions.<sup>[266]</sup> A recent example for utilizing FEA in graphene/polymer nanocomposites proved that the matrix modulus play an active role in stiffening due to modulus-mismatch dependent strain field distribution.<sup>[267]</sup>

Attempts have been made to use micromechanics to consider the atomic microstructures of nanofillers. The space frame structure where atoms and molecular bonds are described as nodes and nanoscale beams has proven to be useful to some

extent to replace MD on the bottom scale in multiscale simulations. It has successfully explained how the linear elastic behavior of nanocomposites is related to the volume fraction of nanofillers<sup>[268]</sup> and the aspect ratio of nanotubes.<sup>[261c]</sup>

Despite the various theoretical tools developed for nanocomposites, the challenges remain: i) the surface effects of nanoscale reinforcement can cause recrystallization effects that require a combination of multiscale analyses to predict. ii) Combination between kinetic-dependent PRH elasticity and composite micromechanics is needed to establish for more accurate predictions of curing time-dependent mechanical properties of PRH-based nanocomposites.

## 4. Programming of PRHs: Applications and Opportunities

The programmable mechanical properties of PRHs on both spatial and temporal scales provide abundant potential applications. Specifically, photo-crosslinkable hydrogels are attractive and widely used materials because light-controlled sol-gel transition processes endow them with the advantages of the easy formation of almost arbitrary shapes and of upwardly adjustable mechanical properties. These are often used to construct complex structures and guide the geometry of other materials.

Photodegradable hydrogels are emerging materials that can result in erosion and downwardly adjustable mechanical properties in a formed structure, which could be used to sculpt channels and pore structures, release cargos and soften the matrix. Both photo-crosslinkable and photodegradable hydrogels have contributed significantly to recent advances in biomedical applications. The following section will provide an overview of three widely investigated applications of PRHs: tissue engineering, drug delivery, and soft devices. A list of particularly promising applications is presented in **Table 3**.

#### 4.1. PRHs in Tissue Engineering

The goals of tissue engineering include efforts to cultivate biomaterials with ECM-like properties that elucidate cell–ECM interactions, establish in vitro organ models, and enable repair and regeneration of tissues in vivo.<sup>[4,164b,269]</sup> Among the many materials available in tissue engineering, hydrogels are receiving much attention due to their soft and tissue-like mechanical characteristics, biocompatibility, degradability, high water content, and tunable physicochemical properties.<sup>[270]</sup> PRHs show great superiority to other hydrogels in terms of spatiotemporal control and ease of the shape formation process, which are great advantages in tissue engineering applications.

##### 4.1.1. PRH-Based Cell Culture Platform

During the past two decades, the idea that matrix stiffness could significantly affect cell behaviors (e.g., adhesion, proliferation, differentiation, migration, apoptosis) for cells either growing upon a 2D substrate or in a 3D matrix has been supported by a range of evidence.<sup>[31a,91a,270a,271]</sup> However, some challenges remain in this field, such as identifying which other factors co-determine cell fate with matrix stiffness,<sup>[272]</sup> how to mimic the spatiotemporally changing mechanical properties of native ECM,<sup>[3e,31b]</sup> and how to investigate the cell–ECM interaction in a high-throughput way.<sup>[273]</sup> PRHs are ideal biomaterials to solve these problem due to their tissue-like mechanical properties, and the fact that they are easy to process and show excellent spatiotemporally controllability. Here, recent advances in PRH-based cell culture platforms will be briefly summarized.

*Temporally Varied ECM Elasticity:* In vivo, native ECM is constantly renewed by cells, which show temporally changed elasticity in various (path-)physiological process (e.g., embryonic development, healing, aging, cancers).<sup>[274]</sup> To study the complex dynamics of cell–ECM interaction processes, model systems are established by controlling material properties in multiple time scales. These in vitro experiments show that the time scale of ECM elasticity is a crucial factor for various cell behaviors.<sup>[275]</sup> PRHs with temporally increasing or decreasing elasticity can be used as an active mechanical signal to regulate cell behaviors, which may reveal the role of the dynamic mechanical microenvironment on cells. Hence, in this part, temporal strategies for tuning ECM elasticity based on PRHs and the cell responses to these active signals will be introduced.

*Stiffening Strategies:* ECM stiffening is a common phenomenon that occurs in amounts of (patho-)physiological processes,

such as embryogenesis,<sup>[276]</sup> fibrogenesis,<sup>[98b,169b]</sup> and tumorigenesis.<sup>[277]</sup> For example, fibrosis of murine lung leads to a sixfold increase in tissue stiffness in comparison to normal tissue.<sup>[169b]</sup> The elastic moduli of PRHs can be stiffened across several magnitudes within only a few minutes, which provides a powerful tool for studying cell behaviors in stiffening ECM at various time scales.

Sequential crosslinking of PRHs is a commonly used time-dependent stiffening strategy, in which hydrogels are stiffened by the reactions of either remaining monomers or newly added monomers in photopolymerization systems. For example, with thiol-Michael addition and I2959-initiated photopolymerization, Guvendiren and Burdick designed a stiffened 2D MeHA hydrogel with a stiffness ranging from 3 to 30 kPa and observed the short-term and long-term effects of stiffening on MSC behaviors (**Figure 11A**).<sup>[278]</sup> It was proved that cells maintained low spreading when seeded on a soft substrate for 1 day, while subsequent stiffening would increase cell spreading, traction force, and motility within 4 h.<sup>[278]</sup> During 14 days of culture, the substrate was stiffened at different culturing times (1–7 days), and the adipogenic/osteogenic population would increase with culturing time on a soft substrate.<sup>[278]</sup> Through a similar strategy of using LAP as an initiator, Caliarì et al. constructed a stiffenable 2D MeHA hydrogel with a stiffness ranging from 1.75 to 33.0 kPa for hepatic stellate cells.<sup>[279]</sup> Similar to MSCs, the spreading area of hepatic stellate cells also increased rapidly (within 24 h) after stiffening.<sup>[279]</sup> During 14 days of culture, delayed stiffening (6-day culture on soft substrates) increased YAP/TAZ nuclear translocation, and  $\alpha$ -smooth muscle actin ( $\alpha$ -SMA) fiber assembly compared to that with early stiffening (1-day culture on soft substrates).<sup>[279]</sup> These findings indicate that a delayed stiffening strategy could accelerate the myofibroblast differentiation of hepatic stellate cells.<sup>[279]</sup> The role of time scale in changing ECM elasticity is also being investigated in 3D cell cultures. For example, through LAP-initiated thiol-norborene PEG hydrogels with elastic moduli ranging from 0.24 to 13 kPa, Anseth and co-workers observed the morphology and fibroblast phenotype variation of valvular interstitial cells (VICs) in a 3D environment.<sup>[98b]</sup> After 3 days culturing on soft substrates (0.24 kPa), the ECM stiffened within a few second to 1.2 or 13 kPa, and a decrease of  $\alpha$ -SMA expression was observed in comparison with cells in a soft environment, which is counter to observations of VICs on 2D substrates.<sup>[98b]</sup>

*Softening Strategies:* As a reverse process of stiffening, softening or degradation of ECM also has profound (path-)physiological significance, especially for diseases such as cardiac dysfunction,<sup>[280]</sup> osteoarthritis,<sup>[281]</sup> and destructive lung diseases.<sup>[282]</sup> Photodegradable hydrogels, the mechanical properties of which could be predictably manipulated with light intensity, wavelength, and irradiation time, provide a softening even erodible environment for cells. This further affects the cell behavior dynamically, which could guide the modelling of ECM-softening related (path-)physiological processes and help us understand the mechanical cues in ECM.

Anseth and co-workers fabricated a photodegradable PEG hydrogel platform based on ONB and redox-initiated radical polymerization, which could be softened by one- or two-photon irradiance.<sup>[32a]</sup> Based on this temporally controlled platform, they could manipulate the behaviors of various cell types at

**Table 3.** Typical applications based on PRHs with various mechanical properties.

PSCs <sup>a)</sup>	Polymer matrix	Additives	Fabrication techniques	Young's modulus	Applications	Ref.
<b>Cell culture</b>						
I2959	MeHA, DTT	RGD	–	3–30 kPa	MSC culture	[278]
LAP	MeHA, DTT	RGD	–	1–33 kPa	Hepatic stellate cell culture	[279]
LAP	PEG8NorB, PEG8SH	RGD	–	0.2–12 kPa	VIC culture	[98b]
o-NB	PEGA, PEGdiPDA	Fibronectin	Photomask	7–32 kPa	VIC culture	[52]
o-NB	PEG4DIFO3, Peptide-di(azide)	RGD	Photomask, TPA	0–5.1 kPa	3T3 fibroblast culture	[25a]
o-NB	PEG4DBCO, PEG8NBA	YIGSR	TPA	0–3.6 kPa	ESMN culture	[283a]
o-NB	PEGA, PEGdiPDA	RGD	Photomask, TPA	–	MSC culture	[32a]
o-NB	PEGA, PEGdiPDA	RGD	Photomask	2–10 kPa	MSC culture	[174b]
o-NB	PEGDA, PEGdiPDA	RGD	DMD projection	12–220 kPa	MSC culture	[177b]
<b>Organ model</b>						
LAP	GelMA, GMHA	–	Stereolithography	3.5–4.5 kPa	Liver model	[183]
I2959	PEGDA	–	Extrusion printing	5–75 kPa	Aortic valve model	[196a]
I2959	MeHA, GelMA	–	Extrusion printing	4–13 kPa	Aortic valve model	[297]
I2959	GelMA, Pluronic F127	–	Extrusion printing	1–20 kPa	Vascularized tissue model	[91b]
I2959	GelMA, PLA	VEGF, PDA, BMP2	FDM, Stereolithography	–	Vascularized bone model	[298]
<b>Implant</b>						
I2959	PVAMA, CSMA	–	Electrospun	–	Cartilage repair	[78]
I2959	PEG8NB, PEGDT	–	Stereolithography	–	Cartilage repair	[299]
I2959	PEGDMA	NFC	–	40–160 kPa	Nucleus pulposus replacement	[300a]
I2959	PEG4A, dextran, gelatin	–	–	2–60 kPa	Nucleus pulposus replacement	[300b]
Eosin Y	PEGDA, HA	–	–	60–110 kPa	Soft tissue restoration	[39c]
o-NB	PAAm, oNB-PAMPS	–	–	Around 664 kPa	Gastrointestinal tract stents	[301]
<b>Drug delivery</b>						
LAP	GelMA	Abaloparotide	–	–	Repairing bone defects	[310]
I2959	GelMA, chitosan	Angiogenic growth factor	–	–	Angiogenesis	[311]
I2959	PEGDA	Penicillin, streptomycin	–	–	Treat urothelial diseases	[312]
I2959	CTS-g-GMA, PEGDA	Bone ash, amoxicillin	–	20–30 MPa	Treat gastric ulcer	[313]
I2959	PEGDA	SDF1-GPVI	–	–	Treat cardiovascular ischemic disease	[314]
I2959	MeHA	MSN, DOX	–	–	Sonodynamic therapy	[315]
I2959	MeHA	SiO <sub>2</sub> , Fe <sub>3</sub> O <sub>4</sub> , DOX	–	–	Targeted cancer therapy	[316]
I2959	PEGDA	Ropinirole HCl	Inkjet printing	–	Oral dosage forms	[317b]
DPPO	PEGDA	4-aminosalicylic acid, paracetamol	Stereolithography	–	Oral dosage forms	[317a]
o-NB	PEG4bicyclononyne, PEGdiazide	Fluorescein	Photomask	–	Drug release	[320]
o-NB	PEG-Peptide	DOX	–	0.2–20 kPa	Drug release	[319]
Coumarin	Hydrogelator	Cytarabine	–	–	Drug release	[318]
<b>Conductors</b>						
AP	PAAm	NaCl	Laser cutter	3–400 kPa	Ionic conductor	[324]
AP	PAAm	NaCl	Laser cutter	–	Ionic skin	[325a]
AP	PAAm	LiCl	Laser cutter	–	Ionic cable	[327]
AP	PAAm	LiCl	Mold	12 kPa	Touch panel	[325e]
AP	PAAm	NaCl	–	–	Capacitive sensor	[325b]

**Table 3.** Continued.

PSCs <sup>a)</sup>	Polymer matrix	Additives	Fabrication techniques	Young's modulus	Applications	Ref.
AP	PAA, PEGDA	Fe <sub>3</sub> O <sub>4</sub>	–	7–36 kPa	Strain sensor	[325d]
AP	PAAm, PDA	rGO	–	–	Cell stimulator	[326a]
I2959	PEGDA, PEGDMA	Na <sub>2</sub> SO <sub>4</sub> , Na <sub>2</sub> HPO <sub>4</sub>	Mold	–	Ionic circuits	[326b]
I2959	PAAm, Ca <sup>2+</sup> PAA	Au nanowires	DMD photolithography	–	Wearable pressure sensor	[325c]
riboflavin	PAA, AETA	SiO <sub>2</sub> -SO <sub>3</sub> <sup>-</sup> Na <sup>+</sup>	Stereolithography	0.8–120 kPa	Conductors	[323b]
<b>Sensors</b>						
AP	MEO <sub>2</sub> MA, OEGMA	NFC	–	4–10 kPa	Temperature sensor	[329b]
DEAP	PAAm, PVA	PCCA, PBA	–	–	Glucose sensor	[329c]
I2959	PEGDA	CNT, DNA	Mold	–	Implantable chemical sensor	[330]
<b>Actuators</b>						
I2959	PAAm, Ca <sup>2+</sup> alginate	–	Stereolithography	14–84 kPa	Camouflaged gripper, robots	[334]
I2959	PEGDA, Fe <sup>3+</sup> PAA	NaOH, EDTA	Stereolithography	4–32 kPa	Gripper	[335]
I1173	PEGDA	–	Mold	–	Walking devices	[333]
<b>Robotics</b>						
AP	PAAm	LiCl	Mold	–	Electronic fish	[321a]
DMPA	NIPAAm, PAAm, PEGDA	Fe <sub>3</sub> O <sub>4</sub>	Photomask	–	Swimmer	[337]
I2959	PEGDA, GelMA	CNT	Photomask	37–651 kPa	Batoid-fish like robot	[338]

<sup>a)</sup>AP: ammonium persulfate, BMP2: bone morphogenetic protein 2, CNT: carbon nanotube, CTS-g-GMA: chitosan-grafted-glycidyl methacrylate, DEAP: diethoxyacetophenone, DMD: digital micromirror device, DMPA: 2,2-dimethoxy-2-phenylacetophenone, DPPO: diphenyl(2,4,6-trimethylbenzoyl) phosphine oxide, DTT: dithiothreitol, DOX: doxorubicin, ESMN: embryonic stem cell-derived motor neuron, FDM: Fused deposition modelling, GelMA: gelatin methacryloyl, GMHA: glycidyl methacrylate-hyaluronic acid, GPVI: glycoprotein VI, LAP: lithium acylphosphinate, NFC: nanofibrillated cellulose, MeHA: methacrylated hyaluronic acid, MEO<sub>2</sub>MA: 2-(2'-methoxyethoxy)ethyl methacrylate, NIPAAm: poly(*N*-isopropylacrylamide), OEGMA: oligo(ethylene glycol)methacrylate, *o*-NB: *ortho*-nitrobenzyl, PAA: poly(acrylic acid), PAAm: poly(acrylamide), PAMPS: poly(2-acrylamido-2-methylpropane sulfonic acid), PBA: phenylboronic acid, PCCA: polymerized crystalline colloidal array, PDA: poly(dopamine), PEG: poly(ethylene glycol), PEGA: PEG-monoacrylate, PEGDA: PEG-diacrylate, PEGdiPDA: PEG-di photodegradable acrylate, PEG4DIFO3: PEG-tetra cyclooctyne, PEG-4DBC0: PEG-tetra dibenzylcyclooctyne, PEG8NBA: PEG-octa nitrobenzyl-azide, PEG8NorB: PEG-octa norbornene, PEG8SH: PEG-octa thiol, PLA: poly(lactide), PVA: poly(vinyl alcohol), RGD: Peptide sequence containing Arg-Gly-Asp, rGO: reduced graphene oxide, SDF1: stromal cell-derived factor 1, TMSpMA: 3-(trimethoxysilyl) propyl methacrylate, TPA: two-photon absorption techniques, VIC: valvular interstitial cell, VEGF: vascular endothelial growth factor, YIGSR: Peptide sequence containing Tyr-Ile-Gly-Ser-Arg.

desired time points and spatial positions.<sup>[25a,52,283]</sup> In such a special case, MSCs were cultured in a 2D microenvironment based on this photodegradable hydrogel (Figure 11B).<sup>[283b]</sup> MSCs were cultured on a stiff substrate (10 kPa) initially for various culture times (1–10 days), and then the substrate was stiffened in situ (to 2 kPa), and culturing was continued for up to 10 days.<sup>[283b]</sup> It was observed that cells could remember the previous stiff substrate by activation of YAP and RUNX2, while softening the substrate would reverse the activation of these two factors. However, the reversibility by the softening strategy decreased with the culture time on a stiff substrate.<sup>[283b]</sup> This study showed that PRHs could block inherent complications (trypsin treatment and stiff-to-soft substrata passage) in conventional experimental designs and revealed the role of mechanical dosing in cell behaviors. In addition to PEG, HA could also enable photodegradation through modifying with ONB functional groups.<sup>[284]</sup> Interestingly, after a first softening step by UV irradiation, the MeHA-based hydrogel could initiate stiffening by the photopolymerization of pendant methacrylates.<sup>[284]</sup> When this strategy was applied, the hydrogel showed a reversible change in elasticity (14.8–3.5–27.7 kPa).<sup>[284]</sup> MSCs were cultured on this reversible system (initially stiff on day 0, stiff-soft

on day 1, soft-stiff on day 3); it was found that cell morphology, spreading, and nuclear/cytoplasm localization of YAP/TAZ could change reversely according to the reversible system.<sup>[284]</sup>

*Spatially Varied ECM Elasticity:* Besides heterogeneities in time scale, native ECM elasticity also shows great heterogeneities in spatial scale. Elasticities of different tissues vary by several magnitudes, and even within the same organ, the elasticity is not uniform.<sup>[285]</sup> For example, the elastic moduli in human tissues show gradients in osteochondral tissues,<sup>[286]</sup> blood vessels,<sup>[287]</sup> and skin layers.<sup>[288]</sup> PRHs could provide spatially controlled ECM elasticity through printing-based photochemistry, which opens opportunities for creating new tissue scaffolds with mechanical properties closer to those of native niches and understanding the effects of ECM's mechanical properties on cell behaviors.<sup>[3e,189a,289]</sup> There have been many cell culture studies based on PRH-based ECM with spatial heterogeneous mechanical properties, such as "durotaxis" studies,<sup>[26a,290]</sup> high-throughput cell mechanotransduction studies<sup>[169a,170a,273c,291]</sup> and subcellular elastic-heterogeneity studies<sup>[174b,292]</sup> (Figure 12). Although there have been many studies on cell culturing on mechanical heterogeneous substrates, their conclusions are still not in agreement due to unclear mechanisms behind these

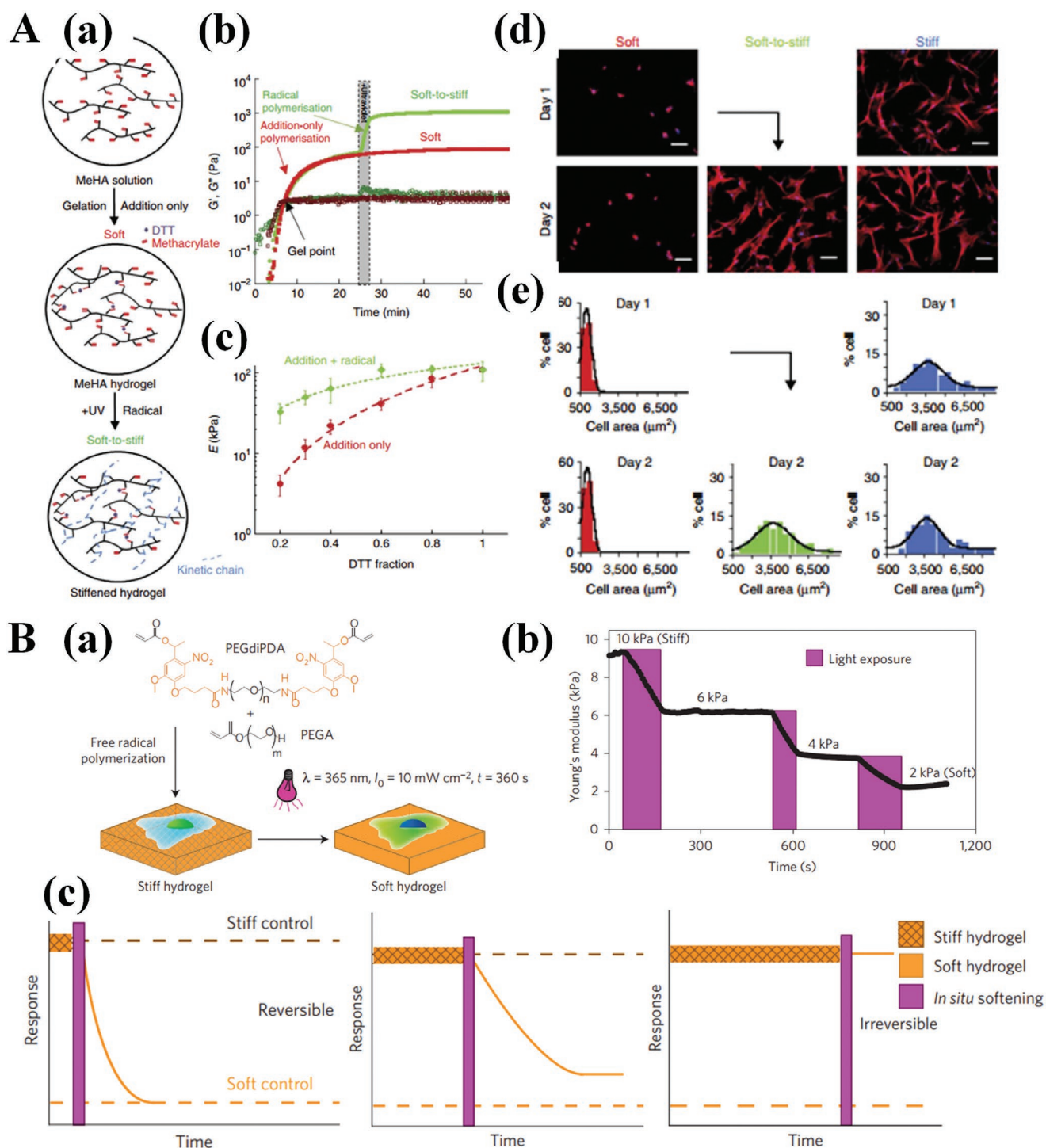


**Figure 11.** Cell culture platforms based on PRH with temporally controlled elasticity. A) A representative matrix-stiffening strategy for PRHs used in cell culture. Reproduced under the terms of the CC-BY License.<sup>[278]</sup> Copyright 2012, the Authors. Published by Nature Publishing Group. a) Schematic of the sequential crosslinking process in methacrylated hyaluronic acid (MeHA). b) Rheology profiles over the course of the hydrogel formation process. c) Atomic force microscopy estimates of the Young's moduli of MeHA substrates at various DTT concentrations (scale bar: 100  $\mu\text{m}$ ). d) Fluorescence images of MSCs cultured on MeHA substrates (soft, soft-to-stiff, stiff) for 1 and 2 days. e) Distributions of cell areas when cultured on the static and dynamic substrates in (d). B) Representative softening strategy for PRHs used in cell culture. Reproduced with permission.<sup>[283b]</sup> Copyright 2014, Nature Publishing Group. a) Schematic of the softening of a photodegradable hydrogel. b) Young's moduli of photodegradable hydrogel at various light exposure doses. c) Cell responses (nuclear co-localization of YAP and RUNX2) to mechanical dosing on stiff hydrogels.

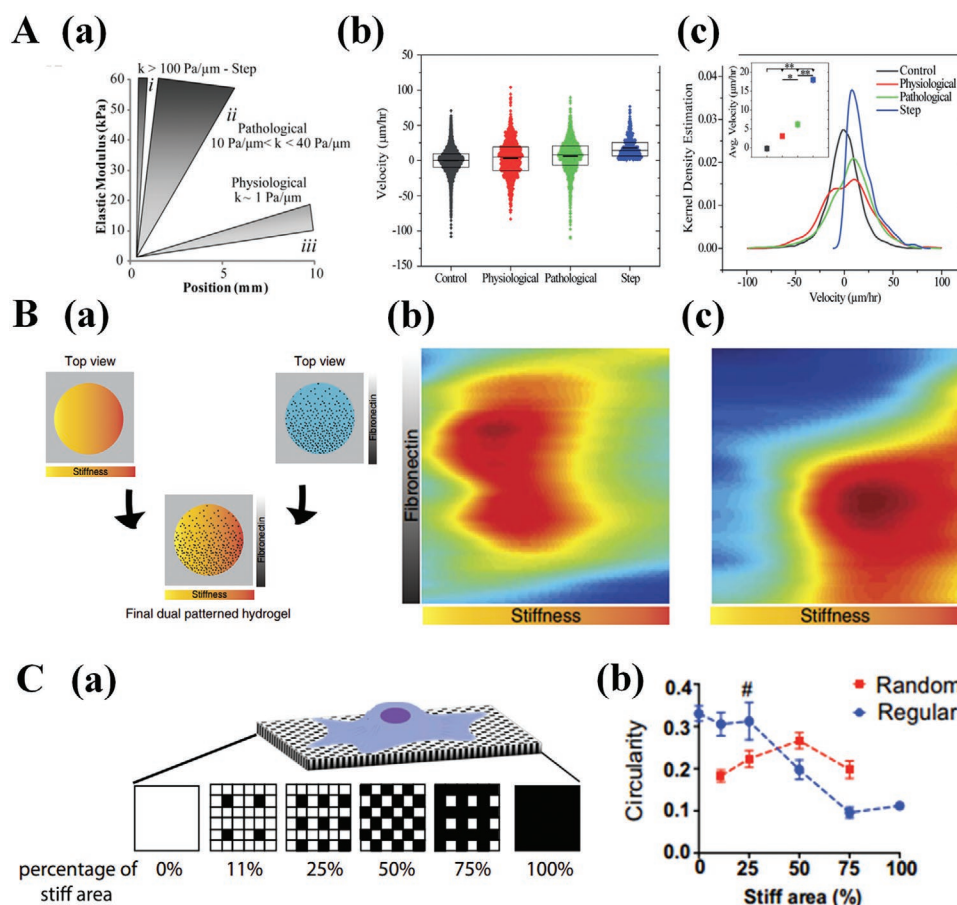


**Figure 12.** Cell culture platforms based on PRHs with spatially heterogeneous elasticity. A) Representative cell migration study based on mechanically patterned substrates. Reproduced with permission.<sup>[290b]</sup> Copyright 2013, Wiley-VCH. a) Three different strengths of stiffness gradients (step, pathological, and physiological), and b) velocities of mesenchymal stem cells (MSCs) migrating along these gradients. c) Kernel density estimation of cell velocities on the three stiffness gradients. B) High-throughput cell behavior study based on mechanically patterned substrates. Reproduced under the terms of the CC-BY License.<sup>[169a]</sup> Copyright 2015, the Authors. Published by Nature Publishing Group. a) Orthogonal gradients of both stiffness and fibronectin concentrations produced by lithography. b) Statistical results of osteogenic staining of MSCs on orthogonal gradient hydrogels. c) Statistical results of adipogenic staining of MSCs on the orthogonal gradient hydrogels. C) A representative study showing cellular responses to subcellular elastic heterogeneity arising on mechanically patterned substrates. Reproduced under the terms of the CC-BY License.<sup>[174b]</sup> Copyright 2016, the Authors. Published by National Academy of Sciences. a) MSCs on mechanically patterned hydrogel surfaces with various stiff-to-soft ratios. Black indicates stiff regions, and white indicates soft regions. b) Dependence of cell morphology (cellular circularity) on substrate composition for substrates with various percentages of stiff regions and a range of patterns.

observed phenomena; therefore, there is a need for further research in this area. For example, through DMD-projection-based photolithography, Norris et al. created a 2D substrate with sub-micrometer elastic gradients using photodegradable hydrogels.<sup>[177b]</sup> They observed that MSCs could congregate in the softest region of the gel, which was converse to the conclusions reached by other studies.<sup>[290b,293]</sup>

**Outlook:** The range of PRH materials that are available for probing mechanobiology is broad, but, as described above, many conflicting results need still to be resolved. Additionally, the viscoelastic aspect of ECM remodeling is an open frontier: although it is well known that cells change the elastic and viscoelastic responses of their ECM over time,<sup>[294]</sup> the study of how these factors affect cell mechanobiology is in its infancy, and few options exist to adapt hydrogel viscoelasticity over time.<sup>[75,295]</sup> Doing so with high spatial control represents an important open frontier.

#### 4.1.2. PRH-Based Organ Models

Natural tissues and organs are complex and multiscale hybrids of cells and materials. Reconstructing native-tissue-like organ models in vitro is a promising solution for exploring the underlying mechanisms of (patho-)physiological processes, screening drugs, and cultivating novel drug delivery systems.<sup>[164c,296]</sup> However, traditional organ models are mostly limited to 2D cell culture or simple 3D cell spheroid culture, which lack the structural complexity and cell diversity seen in native tissues. Based on advanced 3D bioprinting technologies, novel organ models have emerged for exploring almost all the organ systems of the human body.<sup>[164c]</sup> In these studies, PRHs have been proved to be efficient ingredients in inks for these 3D bioprinting technologies, which allow the precise deposition of multiple types of cells and provide a mechanically diverse environment for these cells. For example, Ma et al. built a 3D biomimetic

liver model by a DMD-SL printing technique based on photocrosslinkable hydrogels (GelMA and GMHA) with multiple cells (hepatic cells, vein endothelial cells, adipose derived stem cells) (Figure 13).<sup>[183]</sup> Compared to 2D monolayer culture and 3D culture of only hepatic cells, the 3D liver model show improvements in both phenotype and functionality, which could be used in drug screening and disease modeling.<sup>[183]</sup> PRHs have also been used to construct trileaflet aortic valve models<sup>[196a,297]</sup> and vascularized tissue models,<sup>[91b,298]</sup> which open avenues for fundamental studies of (path-)physiology processes, drug screening, and multicellular tissue regeneration.

#### 4.1.3. PRH-Based Implantable Biomaterials

As seen in various cell platforms and organ models, PRHs show tunable chemical and physical properties, biocompatibility, facile fabrication, and precise spatiotemporal controllability. Thus, PRHs are being further explored for implantation into the body for tissue support, replacement or aesthetic surgery (e.g., cartilage repair,<sup>[78,299]</sup> nucleus pulposus replacement,<sup>[300]</sup> soft tissue restoration,<sup>[39c]</sup> and stents in gastrointestinal tract<sup>[301]</sup>) by either implantation of constructed structures or direct injection into the body.

Articular cartilage is a vulnerable tissue that lacks the ability to self-repair due to its avascular-nature-determined insufficient mass transport.<sup>[302]</sup> Traditional surgeries (e.g., autografting, microfracture technique and autologous chondrocyte transplantation) present drawbacks, such as limited donor availability, high cost, uncertain prognosis, and low clinical efficacy.<sup>[162a,303]</sup> Recently, several novel implantable biomaterials based on stimuli-responsiveness (especially PRHs) have been proposed as an available strategy for cartilage repair.<sup>[304]</sup> For example, Coburn et al. proposed recapitulating the fibrous collagen network of native ECM and constructed low-density, fibrous scaffolds by electrospinning photo-crosslinkable hydrogels (I2959-initiated PVAMA and CSMA).<sup>[78]</sup> The nanofiber scaffolds could enhance chondrogenic differentiation of MSCs *in vitro* and chondrogenesis *in vivo*, suggesting their potential application in cartilage repair.<sup>[78]</sup> In another work, Aisenbrey et al. designed a hybrid scaffold for repairing cartilage defects, which was constructed using an SLA printed support structure and an injected photocrosslinkable hydrogel (I2959-initiated norbornene-8armPEG and PEG-dithiol) (Figure 14A).<sup>[299]</sup> The defect chondral tissues that filled the hybrid scaffold showed significantly less damage under either cyclic loading or free swelling than untreated defect tissues, which indicates that the hybrid scaffold is a potential therapy approach for treating cartilage defects and degeneration.<sup>[299]</sup>

Nucleus pulposus (NP) is the core of the intervertebral disc, the degeneration of which causes pain and disability.<sup>[300]</sup> PRHs are considered potential materials for NP regeneration due to their similarities to NP and spatiotemporal controllability. Schmockler et al. made the first attempt to cultivate photocrosslinkable hydrogel (NFC/PEGDMA nanocomposite) materials for NP replacement.<sup>[300a]</sup> A surgical probe consisting of a cannula and optical fiber was used for injecting and irradiating the hydrogel.<sup>[300a]</sup> After implantation of the composite hydrogel, disc height was re-established, indicating that this method is

promising for nucleus pulposus regeneration.<sup>[300a]</sup> Gan et al. evaluated an interpenetrating network (IPN) of photocrosslinkable acrylated 4arm PEG (PEG4A) and dextran and gelatin for nucleus pulposus regeneration (Figure 14B).<sup>[300b]</sup> The IPN hydrogel was injected into the nucleus pulposus cavity and then irradiated by a minimally invasive illumination device.<sup>[300b]</sup> It was found that the IPN hydrogel could support long-term cell retention and survival in rat intervertebral discs.<sup>[300b]</sup>

Adipose tissue restoration has gained increasing attention because it is related to aesthetic surgeries and disease (e.g., congenital defects, trauma, surgical resections) treatments.<sup>[305]</sup> Commercially available soft tissue fillers (e.g., collagen, HA, PMMA) have the disadvantages of high cost, foreign body reaction and inflammation, shape distortion, and the need for repeated injections.<sup>[305]</sup> Thus, novel soft fillers based on PRHs for adipose tissue restoration have been developed recently. For example, Hillel et al. designed an injectable and photocrosslinkable PEGDA-HA composite hydrogel for soft tissue restoration.<sup>[39c]</sup> The hydrogel could be injected into the dermis and then massaged into the desired shape, and finally be cured by a transdermal photo-crosslinking method (Figure 14C).<sup>[39c]</sup> The implanted hydrogel could maintain its volume for a long time (up to 59% after 9 months), and its properties (elasticity, persistence, and reversibility) could be tuned for special applications (e.g., superficial dermal injections, deep tissue injections).<sup>[39c]</sup>

## 4.2. PRHs in Drug Delivery

Drugs, which are usually bioactive molecules (e.g., polysaccharides, proteins, nucleic acids, and small chemical molecules), can lose therapeutic activity due to biodegradation or changes in environmental factors (e.g., pH, temperature). Moreover, they can cause strong side effects, severe pain or overdosing due to frequent administration and sharply increased drug concentration shortly after administration.<sup>[306]</sup> Thus, there is a growing need to develop controlled drug delivery systems to improve drug therapeutic efficiency.<sup>[306]</sup> These drug delivery systems should have high loading efficiency, and should protect drugs from breakdown. They should have biocompatibility and be able to provide on-demand, dose-controlled release only at desired sites.<sup>[306a,307]</sup> PRHs are desirable materials to construct such drug delivery systems because they can not only load and protect the drugs, but also release drugs at desired times and sites in a noninvasive manner.<sup>[269,307,308]</sup> Thus, PRH plays a crucial role in the development of personalized drug delivery systems. In particular, photocrosslinkable hydrogels could be used to construct vehicles with complex structures at various scales. On the other hand, photodegradable hydrogels could provide precise spatiotemporal control for drug release. Regarding these two types of hydrogels, the role of PRHs in drug delivery systems is introduced in the following section.

### 4.2.1. Photo-Crosslinkable Hydrogels for Drug Vehicle Construction

According to various routes of administration (e.g., ocular delivery, buccal delivery, pulmonary delivery, systemic delivery,

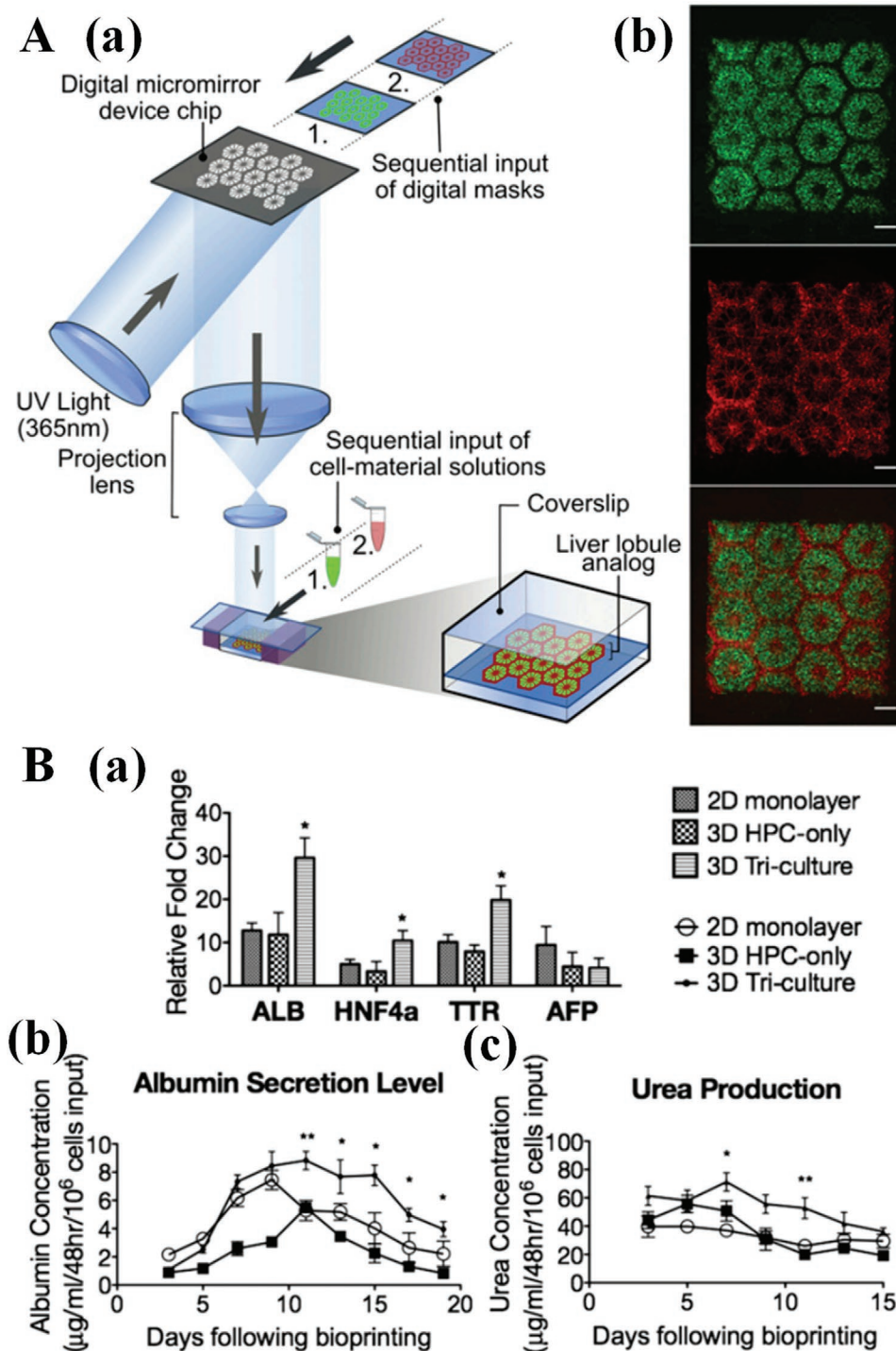


**Figure 13.** Hepatic triculture model constructed from multiple cell-loaded PRHs. Reproduced with permission.<sup>[183]</sup> Copyright 2016, National Academy of Sciences. A) Schematic of fabrication processes a) and fluorescence images b) of a printed triculture hepatic model. In green are human-induced pluripotent stem cell (hiPSC)-derived hepatic progenitor cells (HPCs), and in red are supporting cells (scale bar: 500 µm). B) Gene expression a), albumin secretion levels b), and urea secretion levels c) of the hepatic model. Results showed more mature gene expression and better anabolic and catabolic functionality of hiPSCs–HPCs in the printed triculture models than in other culture conditions.

oral delivery, transdermal delivery, vaginal delivery, and surgical implantation) and different drug dosing for each individual, the vehicles for drug delivery need to be designed into different structures from nano to macroscale.<sup>[306a,309]</sup> Fabricated

PRHs have showed versatile adaptation for various drug vehicle designs.

A widely adopted strategy for drug delivery is noncovalently embedding drugs into a photo-crosslinkable hydrogel



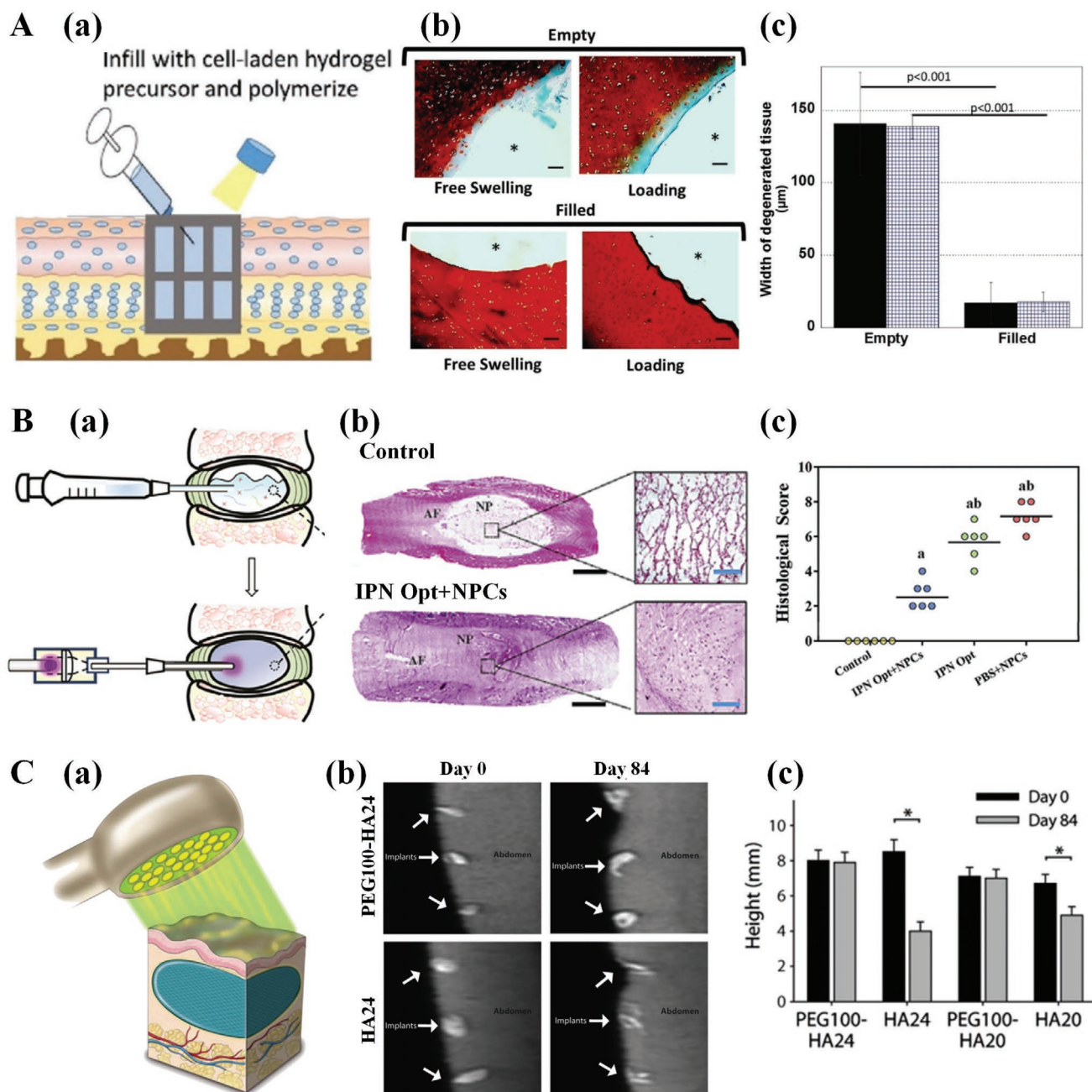


**Figure 14.** Implantable biomaterials based on PRHs. A) PRH-based 3D-printed hybrid scaffold for cartilage defect repair. Reproduced with permission.<sup>[299]</sup> Copyright 2018, Wiley-VCH. a) Design and application of the hybrid scaffold. After a 3D printed support structure was placed in the defect, a cell-laden photo-crosslinkable hydrogel was injected into the support structure and polymerized via light. b) Representative histological images of stained sulfated glycosaminoglycans in empty and scaffold-filled porcine chondral defects under either free swelling or dynamic strain loading after 4-week culture. Here, \* means the position of the defect or scaffold (scale bar: 100  $\mu\text{m}$ ). c) Semiquantification of the width of degenerated tissue in empty and scaffold-filled defects under free swelling (solid) and dynamic strain loading (striped). These results indicate that the PRH-based scaffold could prevent degeneration of cartilage adjacent to a defect. B) PRH-based nucleus pulposus (NP) regeneration strategy. Reproduced with permission.<sup>[300b]</sup> Copyright 2017, Elsevier. a) Schematic showing a nucleus pulposus cell (NPC)-laden photo-crosslinkable precursor of an interpenetrating network (IPN) hydrogel injected into the NP cavity and then crosslinked by a minimally invasive illumination device. b) Representative hematoxylin and eosin stained tissue of the untreated (control) and cell-laden hydrogel-treated (IPN Opt + NPC) porcine disc degeneration model at 12 weeks after implantation (scale bar: black is 2000  $\mu\text{m}$ , blue is 100  $\mu\text{m}$ ). c) Histological score obtained from untreated (control), cell-laden hydrogel (IPN Opt + NPC), hydrogel only (IPN Opt), and cell only (NPC + PBS) groups at 12 weeks after implantation. Results demonstrate that the photo-crosslinkable IPN hydrogel facilitated regeneration of porcine degenerative NPs. C) PRH-based soft tissue restoration strategy. Reproduced with permission.<sup>[39c]</sup> Copyright 2011, American Association for the Advancement of Science. a) Schematic showing transdermal photo-crosslinking of injected PEGDA–HA hydrogels. b) Magnetic resonance imaging (MRI) of implanted PEGDA–HA hydrogels in human abdominal skin at days 0 and 84. c) Persistent height of the implanted hydrogel with various compositions, showing effectiveness of this photo-crosslinkable hydrogel in the restoration of soft tissue.

to prolong the release time. For example, Ning et al. designed an injectable abaloparatide (drug for treating postmenopausal osteoporosis)-loaded GelMA hydrogel that could prolong drug release by slowly biodegrading and showed that sustained release of abaloparatide from GelMA could promote the healing of damaged bones (Figure 15A).<sup>[310]</sup> Similar strategies to realize sustained release of drugs could also be used in angiogenesis,<sup>[311]</sup> the treatment of urothelial diseases,<sup>[312]</sup> treatment of gastric ulcers,<sup>[313]</sup> and treatment of cardiovascular ischemic disease.<sup>[314]</sup> In another way, photo-crosslinkable hydrogels could also be used to coat nano/microparticles or fabricate nano/microgels for target delivery. For example, Ding et al. developed MeHA-coated and doxorubicin (DOX)-loaded mesoporous silica nanoparticles (MSN) for sonodynamic therapy (SDT) (Figure 15B).<sup>[315]</sup> Their results showed that MeHA shells would be degraded by hyaluronidase in a tumor environment, and subsequent ultrasound treatment could not only trigger SDT but also promote DOX release from MSN.<sup>[315]</sup> Yu et al. fabricated a DOX-loaded nanogel with endosome membrane components (EM-NG) from MeHA-coated SiO<sub>2</sub>/Fe<sub>3</sub>O<sub>4</sub>, which showed an ability to target cancer and better therapeutic efficiency than bare DOX-loaded HA nanogels.<sup>[316]</sup>

In addition, in combination with 3D printing techniques, photo-crosslinkable hydrogels could also be used to construct more complex and personalized medicine.<sup>[309,317]</sup> For example, Wang et al. explored the feasibility of constructing a drug-load tablet by stereolithography, and showed that the release profile of the tablet is dependent on the initial composition rather than the environmental pH (Figure 15C).<sup>[317a]</sup> In a similar work, Clark et al. prepared Ropinirole HCl (drug for Parkinson's and restless legs syndrome)-loaded PEGDA pharmaceutical tablets by a UV-curing inkjet printing technique, and showed that the tablets could release Ropinirole HCl by Fickian diffusion and could be used in solid oral dosage forms.<sup>[317b]</sup>

#### 4.2.2. Photodegradable Hydrogels for Programmable Drug Release

Photodegradable hydrogels can also be used to design novel drug delivery strategies. In these hydrogels, drugs can be loaded through either covalent tethering or physical entrapment and hydrophobic absorption, and then released by light-triggered cleavage of pendants or disruption of hydrogels.<sup>[318]</sup> Recently, Zhao et al. reported a novel photodegradable hydrogel formed by hydrophobic interactions of a four-arm star polymer, poly(ethylene glycol)-*b*-poly( $\gamma$ -*o*-nitrobenzyl-L-glutamate), which is capable of self-healing and is injectable simultaneously. They showed that UV irradiation could trigger cleavage of *o*-nitrobenzyl and then disrupt the hydrophobic crosslinks in this photodegradable hydrogel, and drugs could then be released and kill cancer cells efficiently.<sup>[319]</sup>

Beside single photodegradation-based drug release approaches, orthogonal chemistries facilitate drug release strategies with unprecedented complexity. For example, Ruskowitz et al. designed a degradable hydrogel that incorporates multi-stimuli (light, chemical reductant, enzyme)-sensitive components, which could release tethered therapeutics from the gel following Boolean logics (YES, OR, and AND) through different

input combinations (Figure 15D).<sup>[320]</sup> They showed that light first could trigger the release of drugs by a mask-defined pattern, and then a chemical reductant could sequentially release all the remaining pendant drugs.<sup>[320]</sup> Such sequential delivery strategies that provide additional control of drug release are expected to improve disease treatment.

### 4.3. PRHs in Soft Robotics

Conventional devices and robots based on stiff and dry materials (e.g., metal, silica, elastomer) are unsuitable for biomedical applications due to their low biocompatibility, high resistance to deformation, limited stretchability, easy erosion in complex chemical conditions in vivo, and high cost.<sup>[321]</sup> Thus, there is a growing trend to develop flexible materials for soft device designs or human-machine interface construction.<sup>[160b,322]</sup> PRHs are soft, stretchable, biocompatible, and smart materials, which not only could be responsive to stimuli (e.g., light, stress, humidity) themselves, but also could be used to realize complex structures in combination with 3D printing techniques, and multiple functionalities by combination with various other functional materials (e.g., cells, magnetic nanoparticles, electrical conductors). Thus, PRHs (especially photo-crosslinkable hydrogels) are favored functional and base materials in the fabrication of soft devices and soft robotics.

#### 4.3.1. PRH-Based Conductors

Electrical conductors are common materials not only widely persisting in living tissues (e.g., brain, heart, and muscle) but also artificial devices (e.g., batteries, fuel cells, and capacitors).<sup>[322a]</sup> Traditional artificial conductors are based on metal and carbons, which have distinct mechanical properties with living tissues. Thus, in most bioelectronic applications (e.g., electronic skins, implantable or wearable biosensors, artificial tissues, soft robotics), a bridging interface is needed to connect biological tissues and electronic devices and minimize their mechanical property gap.<sup>[105a,322b]</sup> Conductive hydrogels, which are synthesized by combining hydrogels with conductive materials (e.g., ions, carbon, metal, conductive polymer), are fantastic materials to serve as the bridging interface because they are not only electronically conductive but also soft, stretchable, and transparent.<sup>[124b,322b,323]</sup> Compared to other conductive hydrogels, PRH-based conductors have the advantages of simple fabrication, precise patterning, and real-time controllability. So far, PRH-based conductors have shown versatile functionalities in various electronic devices, such as electrical actuators,<sup>[324]</sup> mechanical sensors (e.g., touch, pressure, bend, stretch),<sup>[325]</sup> bioelectrodes,<sup>[326]</sup> and signal conduits.<sup>[327]</sup> Water soluble ionic species are the most common conductive materials in PRH-based conductors. For example, Keplinger et al. developed high-voltage frequency-tolerant, stretchable, and transparent ionic conductors based on the incorporation of NaCl ions into a UV-cured PAAm hydrogel (Figure 16A).<sup>[324]</sup> By sandwiching into two layers of dielectric elastomer, the PRH could expand under applied voltage, which could be further utilized in a class of devices (e.g., loudspeaker).<sup>[324]</sup>

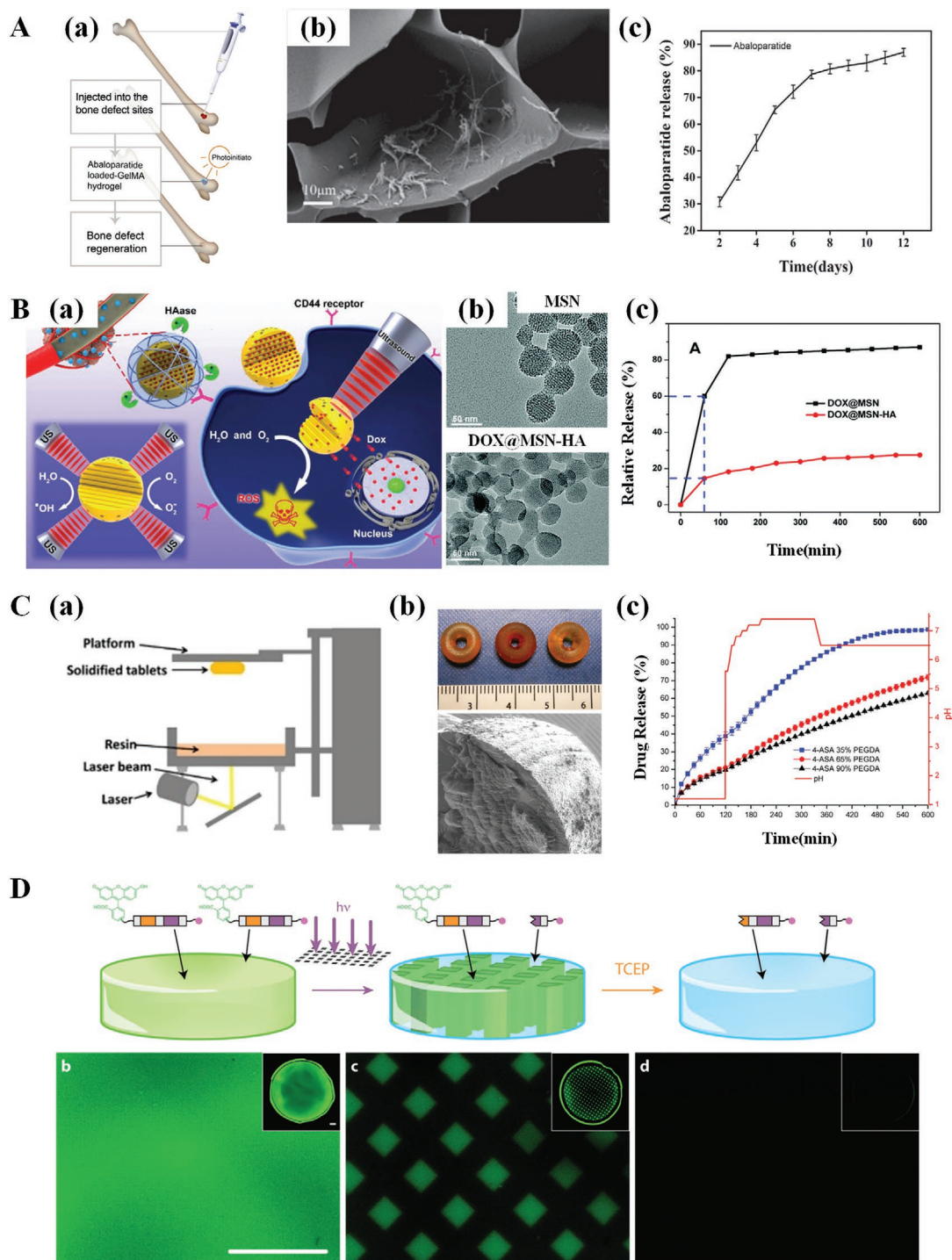


**Figure 15.** Drug delivery strategies based on PRHs. A) Prolonged drug release strategy based on abaloparatide-loaded GelMA hydrogels. Reproduced with permission.<sup>[310]</sup> Copyright 2019, Wiley-VCH. a) Schematic for in vivo treatment of bone defect by loaded GelMA hydrogels. b) SEM image of dried abaloparatide-loaded GelMA hydrogels (scale bar: 10  $\mu\text{m}$ ). c) In vitro drug release profiles of the hydrogels. B) Methacrylated hyaluronic acid (MeHA)-coated mesoporous silica nanoparticles (MSN) used for ultrasound treatment. Reproduced with permission.<sup>[315]</sup> Copyright 2017, Royal Society of Chemistry. a) Schematic of targeted delivery and synergic sonodynamic therapy and chemotherapy of tumor by doxorubicin-loaded MSN–HA (DOX@MSN–HA). b) TEM images of MSN and DOX@MSN–HA (scale bar: 50 nm). c) Drug release profile of DOX from DOX@MSN and DOX@MSN–HA without hyaluronidase and sonication. C) 3D printed oral dosage form based on PEGDA hydrogel. Reproduced with permission.<sup>[317a]</sup> Copyright 2016, Elsevier. a) Laser-based stereolithography platform for manufacturing drug-loaded tablets. b) Photograph and SEM image of 4-aminosalicylic acid (4-ASA)-loaded PEGDA hydrogel. c) Drug release profile of 4-ASA from printed tablets under dynamic pH conditions. D) Sequentially triggered release strategy based on multiple stimuli, namely light- and chemical-induced cleavage in hydrogels (scale bar: 1 mm). Reproduced with permission.<sup>[320]</sup> Copyright 2019, Royal Society of Chemistry.

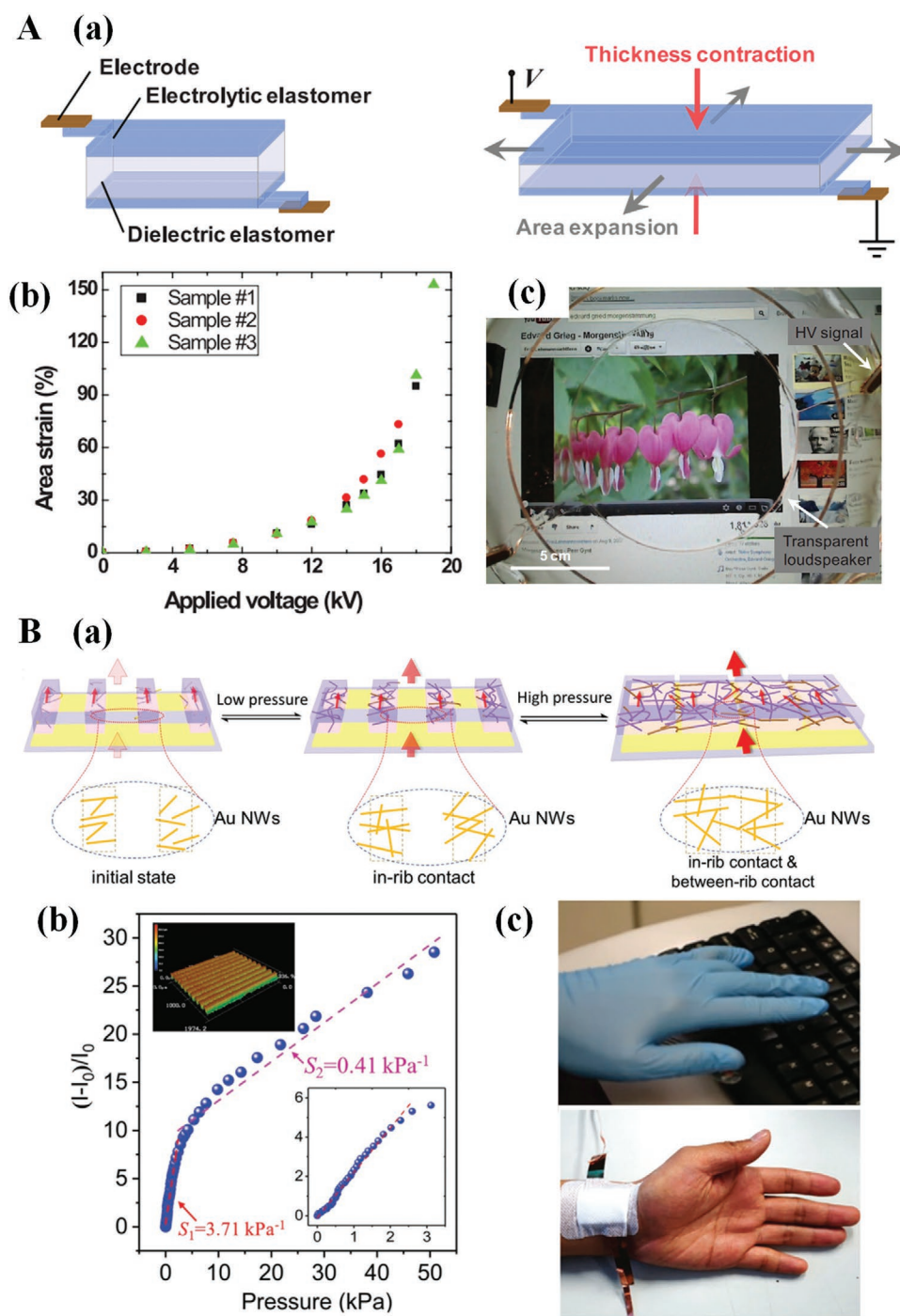


**Figure 16.** Electrical gauges based on PRHs. A) A NaCl containing ionic conductive PAAm hydrogel and its applications. Reproduced with permission.<sup>[324]</sup> Copyright 2013, American Association for the Advancement of Science. a) Construction and working principles of an electrical actuator formed by ionic hydrogels and dielectric elastomer. b) Expanded area of the electrical actuator under varying applied voltages on electrodes. c) A transparent loudspeaker generated from the electrical actuator. B) Gold nanowire (Au NW)-filled conductive PAAm hydrogel and its applications. Reproduced with permission.<sup>[325c]</sup> Copyright 2018, Wiley-VCH. a) Working principles of a pressure sensor based on the conductive hydrogel. Pressure drives inner-rib and between-rib contact of Au NWs in the hydrogel sensor, reducing the resistance of the conductive hydrogels. b) Representative current responses and pressure sensitivities of the pressure sensors. c) Photographs of a wearable pressure sensor constructed from the conductive hydrogel.

Beside the ions, electronic conductive materials could also be incorporated into PRHs to form soft conductors. For example, Yin et al. incorporated Au nanowires (diameter 3 nm,

length 0.9–10  $\mu\text{m}$ ) into a photo-crosslinkable PAAm and  $\text{Ca}^{2+}$ -crosslinked PAA double-network hydrogel (Figure 16B).<sup>[325c]</sup> In this work, DMD projection-based photolithography was

used to pattern microribs onto the PRH electrode, which could change the conductivity by pressure-induced in-rib and between-rib contacts of Au nanowires.<sup>[325c]</sup> The patterned PRH electrode could be used to construct various wearable pressure sensors.<sup>[325c]</sup>

#### 4.3.2. PRH-Based Sensors

Sensors transform an input signal into another more quantifiable signal. PRH-based sensors can detect input signals in two ways.<sup>[328]</sup> The first is based on the fact that the mechanical, electrical, or optical properties (e.g., swelling/deswelling, shape, electrical conductivity, transparency) of PRHs can change according to environmental parameters (e.g., pH, temperature, electrical field, strain, chemical species).<sup>[328,329]</sup> The second is that PRHs can also serve as protection for sensitive components for implantable sensors. For example, Lee et al. incorporated an NIR fluorescence nanosensor into photo-crosslinked PEGDA hydrogels for chemical detection in marine organisms (Figure 17).<sup>[330]</sup> The nanosensor is composed of DNA-wrapped SWNT, which changes the NIR fluorescence (intensity quenching and wavelength shift) in response to riboflavin binding.<sup>[330]</sup> PEGDA hydrogel, as an implantable material, can maintain the fluorescence signal of nanosensors and protect nanosensors from erratic movement in the bodies of moving marine organisms.

#### 4.3.3. PRH-Based Actuators

Actuators are transducers that translate input stimuli (e.g., electrical, thermal, optical, magnetic, or biological signals) into mechanical action, which is a vital component for accomplishing various functions (e.g., moving and grasping).<sup>[331]</sup> Rigid material-based actuators are limited due to their bulky and geometrically fixed nature.<sup>[332]</sup> Thus, various soft materials (e.g., hydrogels, shape-memory polymers, elastomer) have emerged for the development of soft actuators. Compared to other soft materials, PRHs are both smart and hydrophilic, which are especially suitable for the construction of actuators in aqueous environment.

In addition to application of the aforementioned conductive PRHs as electrical actuators, PRHs could also be used to construct actuators triggered by other signals (e.g., humidity, osmotic pressure, hydraulic pressure, and swelling). For example, Lv et al. fabricated a humidity-responsive hydrogel film by photopolymerization-fabricated PEGDA, which could function as a walking actuator on a rough ratchet substrate driven by water vapor (Figure 18A).<sup>[333]</sup> Yuk et al. developed a soft hydraulic actuator based on a double-network hydrogel consisting of photo-crosslinkable PAAm and Ca<sup>2+</sup>-crosslinked alginate (Figure 18B).<sup>[334]</sup> The structures of the actuator are constructed by an SL printer.<sup>[334]</sup> The performance of the actuator could be tuned by mechanical properties and the supplied water volume.<sup>[334]</sup> The actuator showed advantages at high

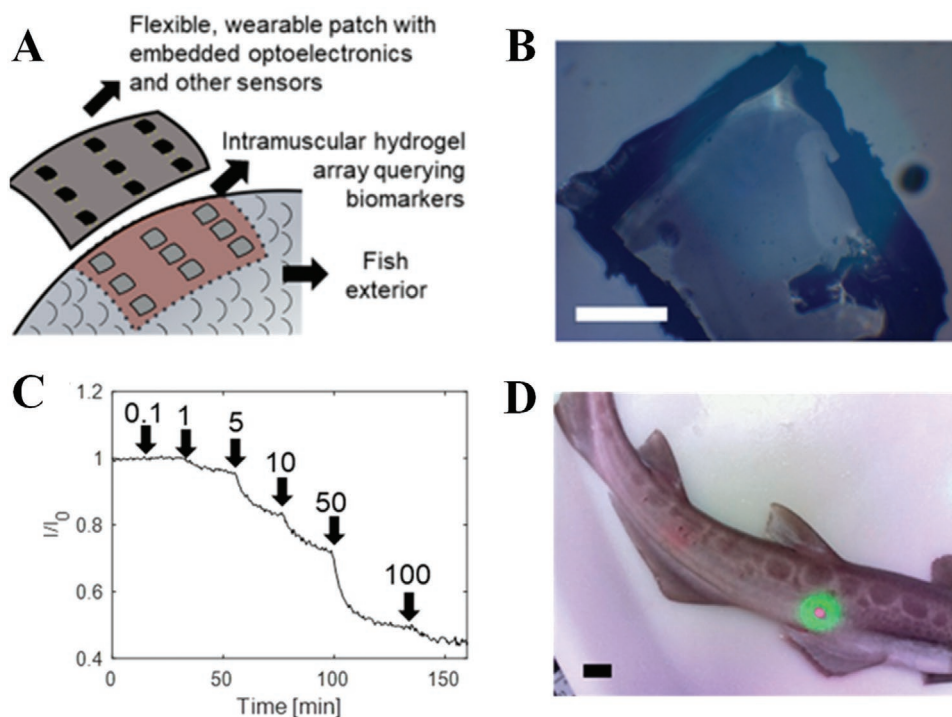


**Figure 17.** Implantable sensor for marine organisms based on PRHs. Reproduced with permission. <sup>[330]</sup> Copyright 2019, American Chemical Society. A) Design schematic for implantable hydrogel sensors for physiological monitoring of marine organisms. B) Photograph of the fluorescent hydrogel sensor, which consists of DNA-wrapped SWNTs and PEGDA (scale bar: 0.5 mm). C) In vitro tests of the sensor showing that the fluorescent signal of the hydrogel sensor decreases with step increases in riboflavin concentration. D) Overlay of brightfield and fluorescence images of a fluorescent hydrogel implanted beneath the skin of *Galeus melastomus* (scale bar: 20 mm).

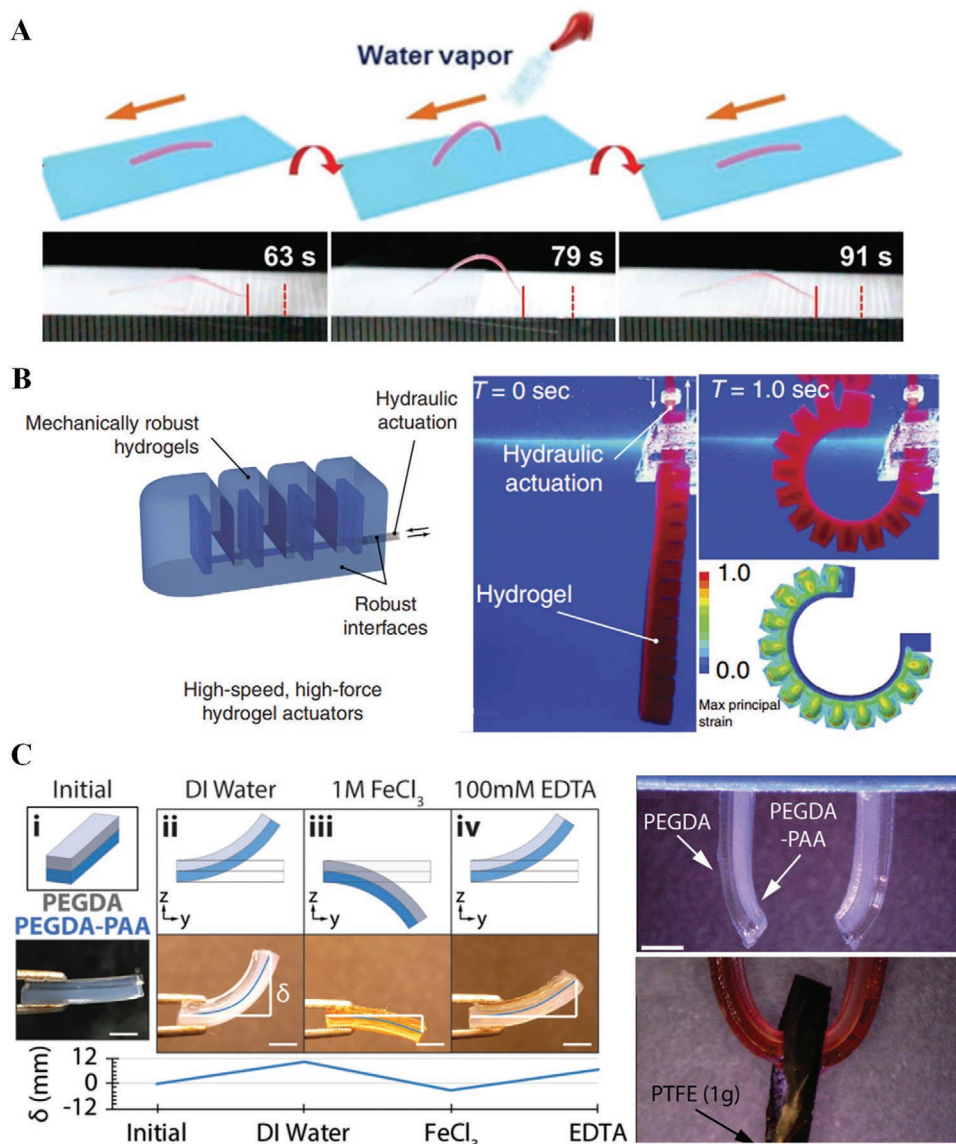


**Figure 18.** Actuators based on PRHs. A) Humidity-driven actuator based on photo-crosslinked PEGDA hydrogel films. Reproduced with permission.<sup>[333]</sup> Copyright 2017, Wiley-VCH. When water vapor is applied to the film, the upper side absorbs the water and swells, which induces bending of the film. When water evaporates, the film is gradually stretched, which leads the device to move forward. B) Hydraulic hydrogel actuator fabricated from photo-crosslinkable PAAm hydrogels. Reproduced under the terms of the CC-BY License.<sup>[334]</sup> Copyright 2017, the Authors. Published by Nature Publishing Group. Inflation by water influx triggers the originally straight hydrogel to bend into a circle, and withdrawal of water restores its straight shape. C) Ion-responsive composite hydrogel based on photo-crosslinkable PEGDA and PAA hydrogels. Reproduced with permission.<sup>[335]</sup> Copyright 2019, Royal Society of Chemistry. Cations ( $\text{Fe}^{3+}$ ) trigger the crosslinking of anionic polymer chains (PAA), which results in contraction of the hydrogels. The mismatched contraction of the ion-responsive layer (PEGDA) and non-ion-responsive layer (PEGDA–PAA) could result in bending or twisting actuation, which can further be used to design grippers (scale bar: 5 mm).

optical and sonic transparency as well as high actuation force and speed, which could be used to camouflage hydrogel actuators and robots in water.<sup>[334]</sup> Valentin et al. showed that different  $\text{Fe}^{3+}$  concentrations could drive the actuation of a PEGDA–PAA double-network hydrogel through ionic crosslinking and swelling, which could be utilized to control the bending and twisting actuation (Figure 18C).<sup>[335]</sup> The photo-crosslinkable properties of PEGDA enable 3D printing of the hydrogel, which could pattern the hydrogel into complex freestanding structures.<sup>[335]</sup>

#### 4.3.4. PRH-Based Robotics

Robots, which are autonomous integrals of various devices (sensors, actuators, power/signal conductor, controls, and power systems) that can carry out a series of complex tasks (e.g., grasping, sensing, locomotion, and communication), are applied in many contexts (e.g., manufacture, aerospace, clinics).<sup>[336]</sup> In contrast to conventional rigid material-based robots, soft robots based on PRH-based soft components show larger scale flexibility, deformability, and environmental

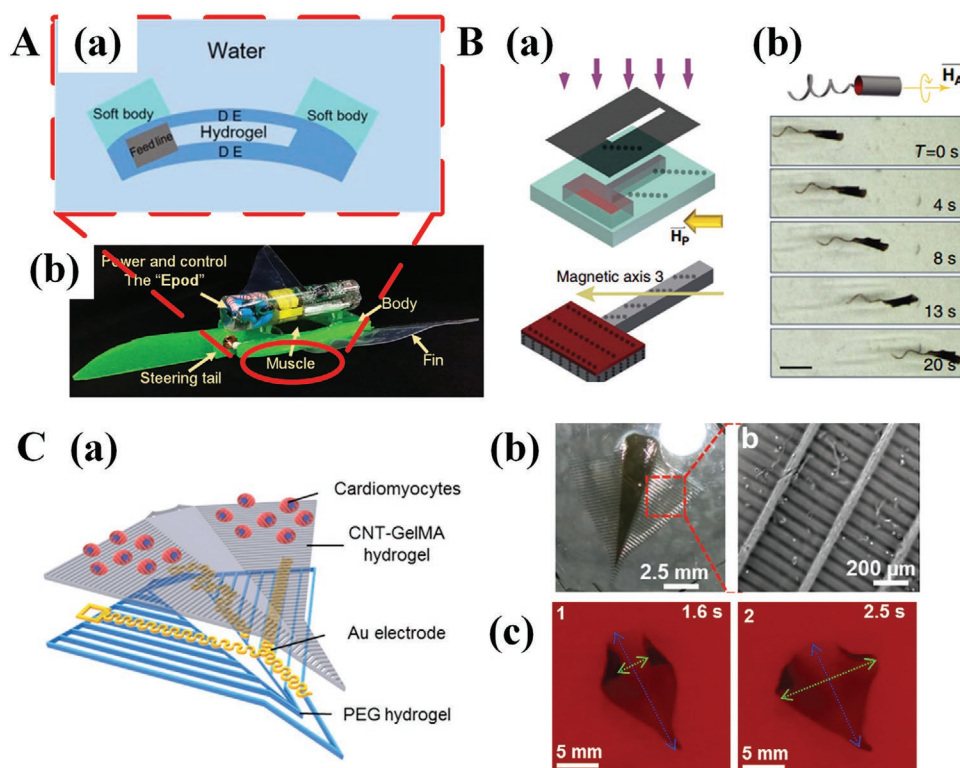


**Figure 19.** Robots based on PRHs. A) Soft electronic fish with PRH-based components. Reproduced under the terms of the CC-BY License.<sup>[321a]</sup> Copyright 2017, the Authors. Published by American Association for the Advancement of Science. a) Design of the robot fish muscle, composed of an ionic hydrogel and dielectric elastomer. b) Tilted view showing the entire construction of the electronic fish. B) Soft microswimmers fabricated from PRHs (scale bar: 2 mm). Reproduced under the terms of the CC-BY License.<sup>[337]</sup> Copyright 2016, the Authors. Published by Nature Publishing Group. a) The soft microswimmer was fabricated by photopatterning of magnetic hydrogel. b) A moving microswimmer driven by rotating uniform magnetic fields (scale bar: 5 mm). C) Bioinspired soft robot constructed from cell-loaded PRHs. Reproduced with permission.<sup>[338]</sup> Copyright 2018, Wiley-VCH. a) Construction scheme showing the layer-by-layer structure of the bioinspired soft robot. b) Photograph and SEM image showing the patterns of PEGDA and CNT/GelMA hydrogels on the robot. c) Photograph showing the cell-actuating robots at over a contraction cycle.

adaptability, and have generated much attention recently. For example, based on an ionic conductive PRH actuator, Li et al. designed an electronic fish (Figure 19A).<sup>[321a]</sup> An integrated onboard system was used to provide power and remote control of the electronic fish.<sup>[321a]</sup> The soft robotic fish showed advantages of high mobility, environmental tolerance, and long endurance, the design principle of which could be potentially extended to other soft robots.<sup>[321a]</sup> In another example, Huang et al. developed a self-folding, magnetically powered microswimmer with complex body plans, reconfigurable shape and controllable motility based on a magnetic nanoparticle (MNP)-doped PRH (Figure 19B).<sup>[337]</sup> Photopatterning, magnetic alignment, and NIR heating could provide programming methods for morphology and motility characteristics of the soft micromachine.<sup>[337]</sup>

Living cells could also be incorporated into these PRH-based robots for self-actuating movement. For example, inspired by the movement of batoid fish, Shin et al. developed a bioinspired soft robotic system, which integrated self-actuating cardiac muscles on a multilayered (PEGDA-CNT/GelMA) and Au electrode-incorporated scaffold (Figure 19C).<sup>[338]</sup> A stiff PEGDA hydrogel (651 kPa) was used to provide a mechanically stable structure, and a soft CNT/GelMA composite hydrogel (37 kPa) served as a cell culture substrate for creating the actuation.<sup>[338]</sup>

The CNT/GelMA layer could be driven by contraction in the direction of aligned cardiomyocytes on its surface, and the beating behaviors of cardiomyocytes could be controlled by electrical stimulation through Au electrodes.<sup>[338]</sup> This proof-of-concept study has potential applications in point-of-care sample analysis and regenerative medicine.<sup>[338]</sup>

## 5. Conclusion and Outlook

In this review, we have presented recent progress in the control and utilization of spatiotemporally varied mechanical properties of PRHs. Through the design of photochemistry, polymer matrices, nanofillers, and architecture, the mechanical properties (e.g., elasticity, toughness, stretchability) of PRHs can be tuned for applications in tissue engineering, drug delivery, and soft devices. Theoretical frameworks and mathematical models now exist for PRH design. However, despite the aforementioned achievements in the design and application of mechanical properties of PRHs, there remain challenges and opportunities in this field.

First of all, despite the useful insights that theoretical models have provided that have helped us understand the mechanisms of photo-crosslinking, photodegradation, and nanofiller

enhancement in PRHs, there is still a major gap between theoretical calculations and practical engineering of PRHs. Environmental conditions (e.g., light intensity, oxygen, temperature, pH) and chemical compositions (e.g., photoinitiators/photolabile moieties, polymer matrices, nanofillers) of PRHs affect the chemical kinetics, topologies, and mechanical properties of PRH networks. Existing models can only explain the roles of one or several factors of PRHs. Thus, there is still a lack of integrated mathematical models that consider these factors simultaneously. These fundamental problems hinder the precise fabrication of PRHs. Designing of PRHs calls for more integral, accurate, and efficient mathematic models based on in-depth knowledge of the formation–structure–property relationships in PRHs.

Second, for in situ control of the mechanical properties of PRHs within the human body (e.g., injectable filler for soft tissue restoration), NIR excitation techniques are superior to traditional UV–vis excitation in terms of tissue penetration and minimization of photo damage. However, the efficiency of existing NIR excitation techniques for PRHs, such as two-photon absorption-based or UCNP-assisted photochemistry, is still too low for clinical applications. Thus, developing a more efficient NIR excitation technique is also a promising direction in the fabrication of PRHs.

Third, high resolution mechanical patterns and complex 3D structures of PRHs rely on advanced fabrication techniques. Improvements in these fabrication techniques require advances in not only precision, efficiency, reliability, and biocompatibility, but also the chemical and physical properties of the inks (e.g., biochemical cues, crosslinking kinetics, swelling characteristics, light absorption properties, mechanical properties).<sup>[182b,339]</sup> Thus, how to ideally design inks for 3D printing based on PRHs will continue to be a topic of importance.

Finally, novel chemical mechanisms (e.g., orthogonal chemistry, photocage, photoisomerization) are expanding the library of PRHs, which could either improve the original mechanical properties of PRHs or endow PRHs with desirable properties (e.g., reversible responses to light, multi-mode crosslinkability/degradability). These developments in chemical reactions would benefit the design of multi-stimuli-responsive cell culture platforms and drug release strategies.

Engineering and utilizing PRHs with tailored mechanical properties will continue to be important to tissue engineering, drug delivery, and soft devices. Addressing the aforementioned challenges in engineering and utilizing PRHs calls for crossdisciplinary approaches across mechanics, engineering, chemistry, biology, and medicine.

## Acknowledgements

This work was supported by the National Natural Science Foundation of China (11772253, 11532009), the Shaanxi Province Youth Talent Support Program, the Young Talent Support Plan of Xi'an Jiaotong University, the National Institutes of Health (U01EB016422 and R21AR076008), and the NSF Science and Technology Center for Engineering Mechanobiology (CMMI 1548571).

## Conflict of Interest

The authors declare no conflict of interest.

## Keywords

hydrogels, mechanical properties, models, photo-crosslinking, photodegradation

Received: January 21, 2020

Revised: March 16, 2020

Published online: June 18, 2020

- [1] K. Uto, J. H. Tsui, C. A. DeForest, D.-H. Kim, *Prog. Polym. Sci.* **2017**, *65*, 53.
- [2] M. E. Wechsler, R. E. Stephenson, A. C. Murphy, H. F. Oldenkamp, A. Singh, N. A. Peppas, *Biomed. Microdevices* **2019**, *21*, 31.
- [3] a) T. J. Wallin, J. Pikul, R. F. Shepherd, *Nat. Rev. Mater.* **2018**, *3*, 84; b) R. L. Truby, J. A. Lewis, *Nature* **2016**, *540*, 371; c) R. Wang, M. K. Sing, R. K. Avery, B. S. Souza, M. Kim, B. D. Olsen, *Acc. Chem. Res.* **2016**, *49*, 2786; d) I. Tomatsu, K. Peng, A. Kros, *Adv. Drug Delivery Rev.* **2011**, *63*, 1257; e) Y. Ma, M. Lin, G. Huang, Y. Li, S. Wang, G. Bai, T. J. Lu, F. Xu, *Adv. Mater.* **2018**, *30*, 1705911; f) Y. Dong, G. Jin, Y. Hong, H. Zhu, T. J. Lu, F. Xu, D. Bai, M. Lin, *ACS Appl. Mater. Interfaces* **2018**, *10*, 12374.
- [4] Y. S. Zhang, A. Khademhosseini, *Science* **2017**, *356*, eaaf3627.
- [5] T. Matsuda, R. Kawakami, R. Namba, T. Nakajima, J. P. Gong, *Science* **2019**, *363*, 504.
- [6] G. Zabow, S. J. Dodd, A. P. Koretsky, *Nature* **2015**, *520*, 73.
- [7] a) L.-W. Xia, R. Xie, X.-J. Ju, W. Wang, Q. Chen, L.-Y. Chu, *Nat. Commun.* **2013**, *4*, 2226; b) Y. S. Kim, M. Liu, Y. Ishida, Y. Ebina, M. Osada, T. Sasaki, T. Hikima, M. Takata, T. Aida, *Nat. Mater.* **2015**, *14*, 1002; c) X. Fan, L. Zhu, K. Wang, B. Wang, Y. Wu, W. Xie, C. Huang, B. P. Chan, Y. Du, *Adv. Healthc. Mater.* **2017**, *6*, 1601152.
- [8] M. N. Yousof, B. T. Houseman, M. Mrksich, *Proc. Natl. Acad. Sci. USA* **2001**, *98*, 5992.
- [9] S. Tasoglu, C. H. Yu, H. I. Gungordu, S. Guven, T. Vural, U. Demirci, *Nat. Commun.* **2014**, *5*, 4702.
- [10] a) H. Yao, J. Wang, S. Mi, *Polymers* **2018**, *10*, 11; b) B. P. Purcell, D. Lobb, M. B. Charati, S. M. Dorsey, R. J. Wade, K. N. Zellars, H. Doviak, S. Pettaway, C. B. Logdon, J. A. Shuman, *Nat. Mater.* **2014**, *13*, 653; c) M. F. Maitz, U. Freudenberg, M. V. Tsurkan, M. Fischer, T. Beyrich, C. Werner, *Nat. Commun.* **2013**, *4*, 2168; d) M. Nakahata, Y. Takashima, H. Yamaguchi, A. Harada, *Nat. Commun.* **2011**, *2*, 511; e) S.-J. Jeon, A. W. Hauser, R. C. Hayward, *Acc. Chem. Res.* **2017**, *50*, 161.
- [11] a) K. N. Long, T. F. Scott, H. Jerry Qi, C. N. Bowman, M. L. Dunn, *J. Mech. Phys. Solids* **2009**, *57*, 1103; b) J. Ma, X. Mu, C. N. Bowman, Y. Sun, M. L. Dunn, H. J. Qi, D. Fang, *J. Mech. Phys. Solids* **2014**, *70*, 84.
- [12] L. Li, J. M. Scheiger, P. A. Levkin, *Adv. Mater.* **2019**, *31*, 1807333.
- [13] S. Dadashi-Silab, S. Doran, Y. Yagci, *Chem. Rev.* **2016**, *116*, 10212.
- [14] S. Wu, J. P. Blinco, C. Barner-Kowollik, *Chem. - Eur. J.* **2017**, *23*, 8325.
- [15] a) P. Xiao, J. Zhang, F. Dumur, M. A. Tehfe, F. Morlet-Savary, B. Graff, D. Gigmes, J. P. Fouassier, J. Lalevée, *Prog. Polym. Sci.* **2015**, *41*, 32; b) P. Payamyar, B. T. King, H. C. Ottinger, A. D. Schluter, *Chem. Commun.* **2016**, *52*, 18; c) P. Derboven, D. R. D'hooge, M. M. Stamenovic, P. Espeel, G. B. Marin, F. E. Du Prez, M.-F. Reyniers, *Macromolecules* **2013**, *46*, 1732; d) J. Xu, C. Boyer, *Macromolecules* **2015**, *48*, 520.
- [16] C. N. Bowman, C. J. Kloxin, *AIChE J.* **2008**, *54*, 2775.
- [17] a) C. E. Hoyle, C. N. Bowman, *Angew. Chem., Int. Ed.* **2010**, *49*, 1540; b) C. E. Hoyle, A. B. Lowe, C. N. Bowman, *Chem. Soc. Rev.* **2010**, *39*, 1355.
- [18] a) N. B. Cramer, C. N. Bowman, *J. Polym. Sci., Part A: Polym. Chem.* **2001**, *39*, 3311; b) T.-Y. Lin, J. C. Bragg, C.-C. Lin, *Macromol.*



- Biosci.* **2016**, *16*, 496; c) S. Chung, H. Lee, H.-S. Kim, M.-G. Kim, L. P. Lee, J. Y. Lee, *Nanoscale* **2016**, *8*, 14213; d) C. D. Pritchard, T. M. O'shea, D. J. Siegwart, E. Calo, D. G. Anderson, F. M. Reynolds, J. A. Thomas, J. R. Slotkin, E. J. Woodard, R. Langer, *Biomaterials* **2011**, *32*, 587; e) A. E. Rydholm, C. N. Bowman, K. S. Anseth, *Biomaterials* **2005**, *26*, 4495.
- [19] S. Dadashi-Silab, C. Aydogan, Y. Yagci, *Polym. Chem.* **2015**, *6*, 6595.
- [20] D. P. Hari, B. Konig, *Chem. Commun.* **2014**, *50*, 6688.
- [21] a) S. J. Bryant, C. R. Nuttelman, K. S. Anseth, *J. Biomater. Sci., Polym. Ed.* **2000**, *11*, 439; b) C. G. Williams, A. N. Malik, T. K. Kim, P. N. Manson, J. H. Elisseeff, *Biomaterials* **2005**, *26*, 1211; c) K. Chatterjee, S. Lin-Gibson, W. E. Wallace, S. H. Parekh, Y. J. Lee, M. T. Cicerone, M. F. Young, C. G. Simon Jr, *Biomaterials* **2010**, *31*, 5051; d) S. Khetan, M. Guvendiren, W. R. Legant, D. M. Cohen, C. S. Chen, J. A. Burdick, *Nat. Mater.* **2013**, *12*, 458.
- [22] a) C. L. E. Nijst, J. P. Bruggeman, J. M. Karp, L. Ferreira, A. Zumbuehl, C. J. Bettinger, R. Langer, *Biomacromolecules* **2007**, *8*, 3067; b) L. I. Jamie, F. P. Robert, A. B. Jason, *Biomed. Mater.* **2008**, *3*, 034104; c) B. W. Tuft, S. Li, L. Xu, J. C. Clarke, S. P. White, B. A. Guymon, K. X. Perez, M. R. Hansen, C. A. Guymon, *Biomaterials* **2013**, *34*, 42; d) Y. Hou, C. A. Schoener, K. R. Regan, D. Munoz-Pinto, M. S. Hahn, M. A. Grunlan, *Biomacromolecules* **2010**, *11*, 648; e) K. E. Smith, S. L. Hyzy, M. Sunwoo, K. A. Gall, Z. Schwartz, B. D. Boyan, *Biomaterials* **2010**, *31*, 6131.
- [23] a) B. D. Fairbanks, M. P. Schwartz, C. N. Bowman, K. S. Anseth, *Biomaterials* **2009**, *30*, 6702; b) B. D. Fairbanks, M. P. Schwartz, A. E. Halevi, C. R. Nuttelman, C. N. Bowman, K. S. Anseth, *Adv. Mater.* **2009**, *21*, 5005; c) T. Greene, C.-C. Lin, *ACS Biomater. Sci. Eng.* **2015**, *1*, 1314; d) T. Greene, T.-Y. Lin, O. M. Andrisani, C.-C. Lin, *J. Appl. Polym. Sci.* **2017**, *134*, 1.
- [24] a) R. Popielarz, O. Vogt, *J. Polym. Sci., Part A: Polym. Chem.* **2008**, *46*, 3519; b) C. Bahney, T. J. Lujan, C. Hsu, M. Bottlang, J. West, B. Johnstone, *Eur. Cells Mater.* **2011**, *22*, 43.
- [25] a) C. A. DeForest, K. S. Anseth, *Nat. Chem.* **2011**, *3*, 925; b) H. Shih, C.-C. Lin, *Macromol. Rapid Commun.* **2013**, *34*, 269; c) Y. Hao, C.-C. Lin, *J. Biomed. Mater. Res., Part A* **2014**, *102*, 3813.
- [26] a) S. Kidoaki, H. Sakashita, *PLoS One* **2013**, *8*, e78067; b) T. Kuboki, W. Chen, S. Kidoaki, *Langmuir* **2014**, *30*, 6187.
- [27] a) T. R. Evans, P. A. Leermakers, *J. Am. Chem. Soc.* **1967**, *89*, 4380; b) E. Charney, L. Tsai, *J. Am. Chem. Soc.* **1971**, *93*, 7123; c) C. K. Luk, F. S. Richardson, *J. Am. Chem. Soc.* **1974**, *96*, 2006.
- [28] a) J. Jakubiak, X. Allonas, J. P. Fouassier, A. Sionkowska, E. Andrzejewska, L. Å. Linden, J. F. Rabek, *Polymer* **2003**, *44*, 5219; b) S. Lin-Gibson, F. A. Landis, P. L. Drzal, *Biomaterials* **2006**, *27*, 1711; c) T. Kuboki, F. Kantawong, R. Burchmore, M. J. Dalby, S. Kidoaki, *Cell Struct. Funct.* **2012**, *37*, 127; d) K. Wang, G. Ma, X. Qin, M. Xiao, J. Nie, *Polym. J.* **2010**, *42*, 450.
- [29] a) A. D. Rouillard, C. M. Berglund, J. Y. Lee, W. J. Polacheck, Y. Tsui, L. J. Bonassar, B. J. Kirby, *Tissue Eng., Part C* **2011**, *17*, 173; b) P. Occhetta, N. Sadr, F. Piraino, A. Redaelli, M. Moretti, M. Rasponi, *Biofabrication* **2013**, *5*, 035002.
- [30] D. Ahn, S. S. Sathe, B. H. Clarkson, T. F. Scott, *Dent. Mater.* **2015**, *31*, 1075.
- [31] a) G. Huang, F. Li, X. Zhao, Y. Ma, Y. Li, M. Lin, G. Jin, T. J. Lu, G. M. Genin, F. Xu, *Chem. Rev.* **2017**, *117*, 12764; b) T. E. Brown, K. S. Anseth, *Chem. Soc. Rev.* **2017**, *46*, 6532.
- [32] a) A. M. Kloxin, A. M. Kasko, C. N. Salinas, K. S. Anseth, *Science* **2009**, *324*, 59; b) M. E. Lee, E. Gungor, A. M. Armani, *Macromolecules* **2015**, *48*, 8746.
- [33] a) M. A. Azagarsamy, D. D. McKinnon, D. L. Alge, K. S. Anseth, *ACS Macro Lett.* **2014**, *3*, 515; b) F. Yanagawa, S. Sugiura, T. Takagi, K. Sumaru, G. Camci-Unal, A. Patel, A. Khademhosseini, T. Kanamori, *Adv. Healthcare Mater.* **2015**, *4*, 246; c) M. Tamura, F. Yanagawa, S. Sugiura, T. Takagi, K. Sumaru, T. Kanamori, *Sci. Rep.* **2015**, *5*, 15060.
- [34] a) C. Bao, L. Zhu, Q. Lin, H. Tian, *Adv. Mater.* **2015**, *27*, 1647; b) H. Zhao, E. S. Sterner, E. B. Coughlin, P. Theato, *Macromolecules* **2012**, *45*, 1723; c) S. R. Trenor, A. R. Shultz, B. J. Love, T. E. Long, *Chem. Rev.* **2004**, *104*, 3059.
- [35] K. M. C. Tsang, N. Annabi, F. Ercole, K. Zhou, D. J. Karst, F. Li, J. M. Haynes, R. A. Evans, H. Thissen, A. Khademhosseini, J. S. Forsythe, *Adv. Funct. Mater.* **2015**, *25*, 977.
- [36] a) T. Furuta, S. S.-H. Wang, J. L. Dantzker, T. M. Dore, W. J. Bybee, E. M. Callaway, W. Denk, R. Y. Tsien, *Proc. Natl. Acad. Sci. USA* **1999**, *96*, 1193; b) J. Babin, M. Pelletier, M. Lepage, J. F. Allard, D. Morris, Y. Zhao, *Angew. Chem., Int. Ed.* **2009**, *48*, 3329; c) C. Zhu, C. J. Bettinger, *J. Mater. Chem. B* **2014**, *2*, 1613.
- [37] L. Fournier, I. Aujard, T. Le Saux, S. Maurin, S. Beaupierre, J. B. Baudin, L. Jullien, *Chem. - Eur. J.* **2013**, *19*, 17494.
- [38] a) M. Claudino, X. Zhang, M. D. Alim, M. Podgórski, C. N. Bowman, *Macromolecules* **2016**, *49*, 8061; b) Z. Liu, Q. Lin, Y. Sun, T. Liu, C. Bao, F. Li, L. Zhu, *Adv. Mater.* **2014**, *26*, 3912; c) G. Bort, T. Gallavardin, D. Ogden, I. Dalko Peter, *Angew. Chem., Int. Ed.* **2013**, *52*, 4526.
- [39] a) B. Li, L. Wang, F. Xu, X. Gang, U. Demirci, D. Wei, Y. Li, Y. Feng, D. Jia, Y. Zhou, *Acta Biomater.* **2015**, *22*, 59; b) R.-Z. Lin, Y.-C. Chen, R. Moreno-Luna, A. Khademhosseini, J. M. Melero-Martin, *Biomaterials* **2013**, *34*, 6785; c) A. T. Hillel, S. Untermaier, Z. Nahas, B. Reid, J. M. Coburn, J. Axelman, J. J. Chae, Q. Guo, R. Trow, A. Thomas, Z. Hou, S. Lichtsteiner, D. Sutton, C. Matheson, P. Walker, N. David, S. Mori, J. M. Taube, J. H. Elisseeff, *Sci. Transl. Med.* **2011**, *3*, 93ra67.
- [40] J. Mendez-Ramos, J. C. Ruiz-Morales, P. Acosta-Mora, N. M. Khaidukov, *J. Mater. Chem. C* **2016**, *4*, 801.
- [41] R. Liu, H. Chen, Z. Li, F. Shi, X. Liu, *Polym. Chem.* **2016**, *7*, 2457.
- [42] Y.-Q. Sun, J. Liu, X. Lv, Y. Liu, Y. Zhao, W. Guo, *Angew. Chem., Int. Ed.* **2012**, *51*, 7634.
- [43] J.-F. Xing, M.-L. Zheng, X.-M. Duan, *Chem. Soc. Rev.* **2015**, *44*, 5031.
- [44] S. Wu, H. J. Butt, *Adv. Mater.* **2016**, *28*, 1208.
- [45] M. Rumi, J. W. Perry, *Adv. Opt. Photonics* **2010**, *2*, 451.
- [46] R. G. Wylie, M. S. Shoichet, *J. Mater. Chem.* **2008**, *18*, 2716.
- [47] S. You, J. Li, W. Zhu, C. Yu, D. Mei, S. Chen, *J. Mater. Chem. B* **2018**, *6*, 2187.
- [48] Z. Li, J. Torgersen, A. Ajami, S. Muhleder, X. Qin, W. Husinsky, W. Holthöner, A. Ovsianikov, J. Stampfl, R. Liska, *RSC Adv.* **2013**, *3*, 15939.
- [49] A. Ovsianikov, A. Deiwick, S. Van Vlierberghe, M. Pflaum, M. Wilhelmi, P. Dubrue, B. Chichkov, *Materials* **2011**, *4*, 288.
- [50] M. Farsari, G. Filippidis, K. Sambani, T. S. Drakakis, C. Fotakis, *J. Photochem. Photobiol., A* **2006**, *181*, 132.
- [51] a) L. Brigo, A. Urciuolo, S. Giulitti, G. Della Giustina, M. Tromayer, R. Liska, N. Elvassore, G. Brusatin, *Acta Biomater.* **2017**, *55*, 373; b) S. Baudis, D. Bomze, M. Markovic, P. Gruber, A. Ovsianikov, R. Liska, *J. Polym. Sci., Part A: Polym. Chem.* **2016**, *54*, 2060; c) X.-H. Qin, X. Wang, M. Rottmar, B. J. Nelson, K. Maniura-Weber, *Adv. Mater.* **2018**, *30*, 1705564.
- [52] M. W. Tibbitt, A. M. Kloxin, K. U. Dyamenahalli, K. S. Anseth, *Soft Matter* **2010**, *6*, 5100.
- [53] a) M. Álvarez, A. Best, A. Unger, J. M. Alonso, A. del Campo, M. Schmelzeisen, K. Koynov, M. Kreiter, *Adv. Funct. Mater.* **2010**, *20*, 4265; b) J. H. Wosnick, M. S. Shoichet, *Chem. Mater.* **2008**, *20*, 55; c) M. Álvarez, A. Best, S. Pradhan-Kadam, K. Koynov, U. Jonas, M. Kreiter, *Adv. Mater.* **2008**, *20*, 4563.
- [54] a) V. V. Rocheva, A. V. Koroleva, A. G. Savelyev, K. V. Khaydukov, A. N. Generalova, A. V. Nechaev, A. E. Guller, V. A. Semchishen, B. N. Chichkov, E. V. Khaydukov, *Sci. Rep.* **2018**, *8*, 3663; b) N. A. Chartrain, C. B. Williams, A. R. Whittington, *Acta Biomater.* **2018**, *74*, 90.
- [55] S. Wu, H.-J. Butt, *Phys. Chem. Chem. Phys.* **2017**, *19*, 23585.
- [56] G. Liu, *Chem. Soc. Rev.* **2015**, *44*, 1635.

- [57] J. V. Garcia, J. Yang, D. Shen, C. Yao, X. Li, R. Wang, G. D. Stucky, D. Zhao, P. C. Ford, F. Zhang, *Small* **2012**, *8*, 3800.
- [58] L. Tu, X. Liu, F. Wu, H. Zhang, *Chem. Soc. Rev.* **2015**, *44*, 1331.
- [59] E. M. Chan, *Chem. Soc. Rev.* **2015**, *44*, 1653.
- [60] H. Zhu, M. Lin, G. Jin, T. J. Lu, F. Xu, *J. Lumin.* **2017**, *185*, 292.
- [61] Y.-F. Wang, G.-Y. Liu, L.-D. Sun, J.-W. Xiao, J.-C. Zhou, C.-H. Yan, *ACS Nano* **2013**, *7*, 7200.
- [62] a) A. Stepuk, D. Mohn, R. N. Grass, M. Zehnder, K. W. Krämer, F. Pellé, A. Ferrier, W. J. Stark, *Dent. Mater.* **2012**, *28*, 304; b) S. Beyazit, S. Ambrosini, N. Marchyk, E. Palo, V. Kale, T. Soukka, B. Tse Sum Bui, K. Haupt, *Angew. Chem., Int. Ed.* **2014**, *53*, 8919.
- [63] a) C.-J. Carling, F. Nourmohammadian, J.-C. Boyer, N. R. Branda, *Angew. Chem.* **2010**, *122*, 3870; b) E. Ruggiero, A. Habtemariam, L. Yate, J. C. Mareque-Rivas, L. Salassa, *Chem. Commun.* **2014**, *50*, 1715; c) Z. Chen, W. Sun, H. J. Butt, S. Wu, *Chem. - Eur. J.* **2015**, *21*, 9165.
- [64] a) C.-J. Carling, J.-C. Boyer, N. R. Branda, *J. Am. Chem. Soc.* **2009**, *131*, 10838; b) L. Wang, H. Dong, Y. Li, C. Xue, L.-D. Sun, C.-H. Yan, Q. Li, *J. Am. Chem. Soc.* **2014**, *136*, 4480; c) W. Wu, L. Yao, T. Yang, R. Yin, F. Li, Y. Yu, *J. Am. Chem. Soc.* **2011**, *133*, 15810.
- [65] Z. Li, X. Zou, F. Shi, R. Liu, Y. Yagci, *Nat. Commun.* **2019**, *10*, 3560.
- [66] a) W. Li, J. Wang, J. Ren, X. Qu, *J. Am. Chem. Soc.* **2014**, *136*, 2248; b) Z. Chen, S. He, H. J. Butt, S. Wu, *Adv. Mater.* **2015**, *27*, 2203.
- [67] Z. Yan, H. Qin, J. Ren, X. Qu, *Angew. Chem., Int. Ed.* **2018**, *57*, 11182.
- [68] J. Thiele, Y. Ma, M. C. Bruekers Stéphanie, S. Ma, T. S. Huck Wilhelm, *Adv. Mater.* **2014**, *26*, 125.
- [69] K. Shapira-Schweitzer, D. Seliktar, *Acta Biomater.* **2007**, *3*, 33.
- [70] E. E. Antoine, P. P. Vlachos, M. N. Rylander, *Tissue Eng., Part B* **2014**, *20*, 683.
- [71] B. J. Klotz, D. Gawlitza, A. J. W. P. Rosenberg, J. Malda, F. P. W. Melchels, *Trends Biotechnol.* **2016**, *34*, 394.
- [72] R. Fridman, G. Benton, I. Aranoutova, H. K. Kleinman, R. D. Bonfil, *Nat. Protoc.* **2012**, *7*, 1138.
- [73] a) G. Zhao, H. Qing, G. Huang, G. M. Genin, T. J. Lu, Z. Luo, F. Xu, X. Zhang, *NPG Asia Mater.* **2018**, *10*, 982; b) H. Qing, G. Jin, G. Zhao, G. Huang, Y. Ma, X. Zhang, B. Sha, Z. Luo, T. J. Lu, F. Xu, *ACS Appl. Mater. Interfaces* **2018**, *10*, 39228.
- [74] J. A. Burdick, G. D. Prestwich, *Adv. Mater.* **2011**, *23*, H41.
- [75] O. Chaudhuri, L. Gu, D. Klumpers, M. Darnell, S. A. Bencherif, J. C. Weaver, N. Huebsch, H.-p. Lee, E. Lippens, G. N. Duda, D. J. Mooney, *Nat. Mater.* **2016**, *15*, 326.
- [76] G. Wu, X. Deng, J. Song, F. Chen, *J. Photochem. Photobiol., B* **2018**, *178*, 27.
- [77] D. Ye, Q. Cheng, Q. Zhang, Y. Wang, C. Chang, L. Li, H. Peng, L. Zhang, *ACS Appl. Mater. Interfaces* **2017**, *9*, 43154.
- [78] J. M. Coburn, M. Gibson, S. Monagle, Z. Patterson, J. H. Elisseeff, *Proc. Natl. Acad. Sci. USA* **2012**, *109*, 10012.
- [79] K. Yue, G. Trujillo-de Santiago, M. M. Alvarez, A. Tamayol, N. Annabi, A. Khademhosseini, *Biomaterials* **2015**, *73*, 254.
- [80] a) P. Occhetta, R. Visone, L. Russo, L. Cipolla, M. Moretti, M. Rasponi, *J. Biomed. Mater. Res., Part A* **2015**, *103*, 2109; b) T. Billiet, E. Gevaert, T. De Schryver, M. Cornelissen, P. Dubruel, *Biomaterials* **2014**, *35*, 49; c) W. Schuurman, A. Levett Peter, W. Pot Michiel, R. van Weeren Paul, J. A. Dhert Wouter, W. Huttmacher Dietmar, P. W. Melchels Ferry, J. Klein Travis, J. Malda, *Macromol. Biosci.* **2013**, *13*, 551; d) P. Kerscher, J. A. Kaczmarek, S. E. Head, M. E. Ellis, W. J. Seeto, J. Kim, S. Bhattacharya, V. Suppiramaniam, E. A. Lipke, *ACS Biomater. Sci. Eng.* **2017**, *3*, 1499; e) W. Liu, M. A. Heinrich, Y. Zhou, A. Akpek, N. Hu, X. Liu, X. Guan, Z. Zhong, X. Jin, A. Khademhosseini, Y. S. Zhang, *Adv. Healthcare Mater.* **2017**, *6*, 1601451; f) S. Darvishi, M. Souissi, M. Kharaziha, F. Karimzadeh, R. Sahara, S. Ahadian, *Electrochim. Acta* **2018**, *261*, 275; g) C.-H. Lin, J. J.-M. Su, S.-Y. Lee, Y.-M. Lin, *J. Tissue Eng. Regen. Med.* **2018**, *12*, 2099; h) Y. Sun, R. Deng, X. Ren, K. Zhang, J. Li, *ACS Appl. Bio Mater.* **2019**, *2*, 570; i) Z. Wang, H. Kumar, Z. Tian, X. Jin, J. F. Holzman, F. Menard, K. Kim, *ACS Appl. Mater. Interfaces* **2018**, *10*, 26859.
- [81] Z. Muñoz, H. Shih, C.-C. Lin, *Biomater. Sci.* **2014**, *2*, 1063.
- [82] L. Tytgat, L. Van Damme, J. Van Hoorick, H. Declercq, H. Thienpont, H. Ottevaere, P. Blondeel, P. Dubruel, S. V. Vlierberghe, *Acta Biomater.* **2019**, *94*, 340.
- [83] V. X. Truong, K. M. Tsang, G. P. Simon, R. L. Boyd, R. A. Evans, H. Thissen, J. S. Forsythe, *Biomacromolecules* **2015**, *16*, 2246.
- [84] a) A. Mora-Boza, M. Puertas-Bartolomé, B. Vázquez-Lasa, J. San Román, A. Pérez-Caballer, M. Olmeda-Lozano, *Eur. Polym. J.* **2017**, *95*, 11; b) I. L. Kim, R. L. Mauck, J. A. Burdick, *Biomaterials* **2011**, *32*, 8771.
- [85] a) J. A. Burdick, C. Chung, X. Jia, M. A. Randolph, R. Langer, *Biomacromolecules* **2005**, *6*, 386; b) I. E. Erickson, A. H. Huang, S. Sengupta, S. Kestle, J. A. Burdick, R. L. Mauck, *Osteoarthritis Cartilage* **2009**, *17*, 1639; c) S. K. Seidlits, Z. Z. Khaing, R. R. Petersen, J. D. Nickels, J. E. Vanscoy, J. B. Shear, C. E. Schmidt, *Biomaterials* **2010**, *31*, 3930; d) B. Ananthanarayanan, Y. Kim, S. Kumar, *Biomaterials* **2011**, *32*, 7913; e) L. Bian, C. Hou, E. Tous, R. Rai, R. L. Mauck, J. A. Burdick, *Biomaterials* **2013**, *34*, 413; f) P. A. Levett, F. P. W. Melchels, K. Schrobback, D. W. Huttmacher, J. Malda, T. J. Klein, *Acta Biomater.* **2014**, *10*, 214; g) A. Khanlari, J. E. Schulteis, T. C. Suekama, M. S. Detamore, S. H. Gehrke, *J. Appl. Polym. Sci.* **2015**, *132*, 42009; h) P. Maturavongsadit, X. Bi, K. Metavarayuth, J. A. Luckanagul, Q. Wang, *ACS Appl. Mater. Interfaces* **2017**, *9*, 3318.
- [86] J. B. Leach, K. A. Bivens, C. W. Patrick, C. E. Schmidt, *Biotechnol. Bioeng.* **2003**, *82*, 578.
- [87] Q. Feng, M. Zhu, K. Wei, L. Bian, *PLoS One* **2014**, *9*, e99587.
- [88] W. M. Gramlich, I. L. Kim, J. A. Burdick, *Biomaterials* **2013**, *34*, 9803.
- [89] J. L. Young, J. Tuler, R. Braden, P. Schüp-Magoffin, J. Schaefer, K. Kretschmer, K. L. Christman, A. J. Engler, *Acta Biomater.* **2013**, *9*, 7151.
- [90] A. D. Shubin, T. J. Felong, B. E. Schutrum, D. S. L. Joe, C. E. Ovitt, D. S. W. Benoit, *Acta Biomater.* **2017**, *50*, 437.
- [91] a) F. Han, C. Zhu, Q. Guo, H. Yang, B. Li, *J. Mater. Chem. B* **2016**, *4*, 9; b) D. B. Kolesky, R. L. Truby, A. S. Gladman, T. A. Busbee, K. A. Homan, J. A. Lewis, *Adv. Mater.* **2014**, *26*, 3124.
- [92] M. L. Oyen, *Int. Mater. Rev.* **2014**, *59*, 44.
- [93] C. E. Kandow, P. C. Georges, P. A. Janmey, K. A. Benningo, *Methods in Cell Biology*, Vol. 83, Academic Press, New York **2007**, p. 29.
- [94] a) M. Pouria, F. C. Luciano da, C. Andreas, P. L. Stephanie, F. James, G. Jochen, F. Kristian, *J. Phys. Condens. Mater.* **2010**, *22*, 194114; b) A. K. Denisin, B. L. Pruitt, *ACS Appl. Mater. Interfaces* **2016**, *8*, 21893.
- [95] a) A. Vashist, A. Kaushik, A. Vashist, V. Sagar, A. Ghosal, Y. K. Gupta, S. Ahmad, M. Nair, *Adv. Healthcare Mater.* **2018**, *7*, 1701213; b) S. Nemir, H. N. Hayenga, J. L. West, *Biotechnol. Bioeng.* **2010**, *105*, 636; c) A. M. Kloxin, C. J. Kloxin, C. N. Bowman, K. S. Anseth, *Adv. Mater.* **2010**, *22*, 3484; d) S. M. Hodgson, S. A. McNelles, L. Abdullahu, I. A. Marozas, K. S. Anseth, A. Adronov, *Biomacromolecules* **2017**, *18*, 4054.
- [96] C.-C. Lin, *RSC Adv.* **2015**, *5*, 39844.
- [97] a) M. C. Mosley, H. J. Lim, J. Chen, Y.-H. Yang, S. Li, Y. Liu, L. A. Smith Callahan, *J. Biomed. Mater. Res., Part A* **2017**, *105*, 824; b) M. Peter, P. Tayalia, *RSC Adv.* **2016**, *6*, 40878; c) Q. Wang, L. Ren, C. Xu, Z. Zhai, J. A. Zhou, Y. Yao, H. Xia, Y. Wang, *J. Appl. Polym. Sci.* **2013**, *128*, 89; d) V. T. Michael, S. Sonja, C. L. Jeffery, P. Georgia, *Biomed. Mater.* **2013**, *8*, 025001.
- [98] a) J. J. Roberts, S. J. Bryant, *Biomaterials* **2013**, *34*, 9969; b) K. M. Mabry, R. L. Lawrence, K. S. Anseth, *Biomaterials* **2015**, *49*, 47; c) H.-Y. Liu, T. Greene, T.-Y. Lin, C. S. Dawes, M. Korc, C.-C. Lin, *Acta Biomater.* **2017**, *48*, 258; d) C. I. Fiedler, E. A. Aisenbrey,

- J. A. Wahlquist, C. M. Heveran, V. L. Ferguson, S. J. Bryant, R. R. McLeod, *Soft Matter* **2016**, *12*, 9095; e) H. Shih, C.-C. Lin, *Bio-macromolecules* **2012**, *13*, 2003; f) C.-C. Lin, A. Raza, H. Shih, *Bio-materials* **2011**, *32*, 9685.
- [99] H. Qi, M. Ghodousi, Y. Du, C. Grun, H. Bae, P. Yin, A. Khademhosseini, *Nat. Commun.* **2013**, *4*, 2275.
- [100] A. Kumar, S. S. Han, *Int. J. Polym. Mater. Polym. Biomater.* **2017**, *66*, 159.
- [101] Y. Zhou, C. Zhang, K. Liang, J. Li, H. Yang, X. Liu, X. Yin, D. Chen, W. Xu, *Int. J. Biol. Macromol.* **2018**, *106*, 227.
- [102] R. A. Bader, W. E. Rochefort, *J. Biomed. Mater. Res., Part A* **2008**, *86A*, 494.
- [103] a) X.-H. Qin, K. Labuda, J. Chen, V. Hruschka, A. Khadem, R. Liska, H. Redl, P. Slezak, *Adv. Funct. Mater.* **2015**, *25*, 6606; b) Y. Zhou, S. Zhao, C. Zhang, K. Liang, J. Li, H. Yang, S. Gu, Z. Bai, D. Ye, W. Xu, *Carbohydr. Polym.* **2018**, *184*, 383.
- [104] a) X. Zheng, W. Smith, J. Jackson, B. Moran, H. Cui, D. Chen, J. Ye, N. Fang, N. Rodriguez, T. Weisgraber, C. M. Spadaccini, *Nat. Mater.* **2016**, *15*, 1100; b) K. Radi, D. Jauffrès, S. Deville, C. L. Martin, *J. Mech. Phys. Solids* **2019**, *126*, 101; c) K.-Y. Lee, Y. Aitomäki, L. A. Berglund, K. Oksman, A. Bismarck, *Compos. Sci. Technol.* **2014**, *105*, 15.
- [105] a) S. Choi, S. I. Han, D. Kim, T. Hyeon, D.-H. Kim, *Chem. Soc. Rev.* **2019**, *48*, 1566; b) A. Alam, Y. Zhang, H.-C. Kuan, S.-H. Lee, J. Ma, *Prog. Polym. Sci.* **2018**, *77*, 1; c) S. Sayyar, D. L. Officer, G. G. Wallace, *J. Mater. Chem. B* **2017**, *5*, 3462.
- [106] H.-L. Tan, S.-Y. Teow, J. Pushpamalar, *Bioengineering* **2019**, *6*, 17.
- [107] C. Dannert, T. B. Stokke, S. R. Dias, *Polymers* **2019**, *11*, 275.
- [108] a) C. Cha, S. R. Shin, X. Gao, N. Annabi, M. R. Dokmeci, X. Tang, A. Khademhosseini, *Small* **2014**, *10*, 514; b) S. R. Shin, S. M. Jung, M. Zalabany, K. Kim, P. Zorlutuna, S. b. Kim, M. Nikkha, M. Khabiry, M. Azize, J. Kong, K.-t. Wan, T. Palacios, M. R. Dokmeci, H. Bae, X. Tang, A. Khademhosseini, *ACS Nano* **2013**, *7*, 2369; c) S. R. Shin, C. Zihlmann, M. Akbari, P. Assawes, L. Cheung, K. Zhang, V. Manoharan, Y. S. Zhang, M. Yüsekçkaya, K.-t. Wan, M. Nikkha, M. R. Dokmeci, X. Tang, A. Khademhosseini, *Small* **2016**, *12*, 3677; d) V. C.-F. Li, X. Kuang, A. Mulyadi, C. M. Hamel, Y. Deng, H. J. Qi, *Cellulose* **2019**, *26*, 3973; e) K. Zhu, S. R. Shin, T. van Kempen, Y.-C. Li, V. Ponraj, A. Nasajpour, S. Mandla, N. Hu, X. Liu, J. Leijten, Y.-D. Lin, M. A. Hussain, Y. S. Zhang, A. Tamayol, A. Khademhosseini, *Adv. Funct. Mater.* **2017**, *27*, 1605352.
- [109] P. Sarkar, E. Bosneaga, M. Auer, *J. Exp. Bot.* **2009**, *60*, 3615.
- [110] a) M. Roman, *Ind. Biotechnol.* **2015**, *11*, 25; b) R. T. Cullen, B. G. Miller, A. D. Jones, J. M. G. Davis, *Ann. Occup. Hyg.* **2002**, *46*, 81.
- [111] a) A. Wagner, A. P. White, T. A. Stueckle, D. Banerjee, K. A. Sierros, Y. Rojanasakul, S. Agarwal, R. K. Gupta, C. Z. Dinu, *ACS Appl. Mater. Interfaces* **2017**, *9*, 32323; b) N. K. Verma, E. Moore, W. Blau, Y. Volkov, P. Ramesh Babu, *J. Nanopart. Res.* **2012**, *14*, 1137.
- [112] a) S. Lin, M. Mortimer, R. Chen, A. Kaminen, J. E. Riviere, T. P. Davis, F. Ding, P. C. Ke, *Environ. Sci.: Nano* **2017**, *4*, 1433; b) J. Shannahan, *Nanotechnol. Rev.* **2017**, *6*, 345.
- [113] a) X. Guo, N. Mei, *J. Food Drug Anal.* **2014**, *22*, 105; b) B. Fadeel, C. Bussy, S. Merino, E. Vázquez, E. Flahaut, F. Mouchet, L. Evariste, L. Gauthier, A. J. Koivisto, U. Vogel, C. Martín, L. G. Delogu, T. Buerki-Thurnherr, P. Wick, D. Beloin-Saint-Pierre, R. Hischier, M. Pelin, F. Candotto Carniel, M. Tretiach, F. Cesca, F. Benfenati, D. Scaini, L. Ballerini, K. Kostarelos, M. Prato, A. Bianco, *ACS Nano* **2018**, *12*, 10582.
- [114] a) Y. Ma, Y. Ji, M. You, S. Wang, Y. Dong, G. Jin, M. Lin, Q. Wang, A. Li, X. Zhang, F. Xu, *Acta Biomater.* **2016**, *42*, 199; b) M. Lin, Y. Gao, T. J. Diefenbach, J. K. Shen, F. J. Hornicek, Y. I. Park, F. X. Xu, T. J. Lu, M. M. Amiji, Z. Duan, *ACS Appl. Mater. Interfaces* **2017**, *9*, 7941; c) G. Jin, R. He, Q. Liu, Y. Dong, M. Lin, W. Li, F. Xu, *ACS Appl. Mater. Interfaces* **2018**, *10*, 10634.
- [115] a) S.-M. Lee, H. J. Kim, S. Y. Kim, M.-K. Kwon, S. Kim, A. Cho, M. Yun, J.-S. Shin, K.-H. Yoo, *Biomaterials* **2014**, *35*, 2272; b) P. Thoniyot, M. J. Tan, A. A. Karim, D. J. Young, X. J. Loh, *Adv. Sci.* **2015**, *2*, 1400010; c) A. Gnach, T. Lipinski, A. Bednarkiewicz, J. Rybka, J. A. Capobianco, *Chem. Soc. Rev.* **2015**, *44*, 1561.
- [116] a) P. Somasundaran, X. Fang, S. Ponnuram, B. Li, *KONA Powder Part. J.* **2010**, *28*, 38; b) H. A. Jeng, J. Swanson, *J. Environ. Sci. Health, Part A: Toxic/Hazard. Subst. Environ. Eng.* **2006**, *41*, 2699.
- [117] a) S. Prabhu, E. K. Poulouse, *Int. Nano Lett.* **2012**, *2*, 32; b) A. M. Alkilany, C. J. Murphy, *J. Nanopart. Res.* **2010**, *12*, 2313.
- [118] C. Beer, R. Foldbjerg, Y. Hayashi, D. S. Sutherland, H. Autrup, *Toxicol. Lett.* **2012**, *208*, 286.
- [119] S. Gottlieb, J. Shuren, Statement from FDA Commissioner Scott Gottlieb, M.D. and Jeff Shuren, M.D., Director of the Center for Devices and Radiological Health, on efforts to evaluate materials in medical devices to address potential safety questions, <https://www.fda.gov/news-events/press-announcements/statement-fda-commissioner-scott-gottlieb-md-and-jeff-shuren-md-director-center-devices-and-3> (accessed: March, 2020).
- [120] a) C. Lee, X. Wei, J. W. Kysar, J. Hone, *Science* **2008**, *321*, 385; b) I. A. Kinloch, J. Suhr, J. Lou, R. J. Young, P. M. Ajayan, *Science* **2018**, *362*, 547; c) P.-C. Ma, N. A. Siddiqui, G. Marom, J.-K. Kim, *Composites, Part A* **2010**, *41*, 1345.
- [121] J. Jang, J. Hong, C. Cha, *J. Mech. Behav. Biomed. Mater.* **2017**, *69*, 282.
- [122] a) C. Cheng, S. Li, A. Thomas, N. A. Kotov, R. Haag, *Chem. Rev.* **2017**, *117*, 1826; b) K. Hu, D. D. Kulkarni, I. Choi, V. V. Tsukruk, *Prog. Polym. Sci.* **2014**, *39*, 1934; c) T. Kuilla, S. Bhadra, D. Yao, N. H. Kim, S. Bose, J. H. Lee, *Prog. Polym. Sci.* **2010**, *35*, 1350.
- [123] a) Y. Hernandez, V. Nicolosi, M. Lotya, F. M. Blighe, Z. Sun, S. De, I. T. McGovern, B. Holland, M. Byrne, Y. K. Gun'Ko, J. J. Boland, P. Niraj, G. Duesberg, S. Krishnamurthy, R. Goodhue, J. Hutchison, V. Scardaci, A. C. Ferrari, J. N. Coleman, *Nat. Nanotechnol.* **2008**, *3*, 563; b) U. Khan, A. O'Neill, M. Lotya, S. De, J. N. Coleman, *Small* **2010**, *6*, 864.
- [124] a) S. R. Shin, B. Aghaei-Ghareh-Bolagh, T. T. Dang, S. N. Topkaya, X. Gao, S. Y. Yang, S. M. Jung, J. H. Oh, M. R. Dokmeci, X. Tang, A. Khademhosseini, *Adv. Mater.* **2013**, *25*, 6385; b) H. Jo, M. Sim, S. Kim, S. Yang, Y. Yoo, J.-H. Park, T. H. Yoon, M.-G. Kim, J. Y. Lee, *Acta Biomater.* **2017**, *48*, 100; c) X. Zhou, M. Nowicki, H. Cui, W. Zhu, X. Fang, S. Miao, S.-J. Lee, M. Keidar, L. G. Zhang, *Carbon* **2017**, *116*, 615.
- [125] R. Xiong, A. M. Grant, R. Ma, S. Zhang, V. V. Tsukruk, *Mater. Sci. Eng., R* **2018**, *125*, 1.
- [126] X. Yan, J. Yang, F. Chen, L. Zhu, Z. Tang, G. Qin, Q. Chen, G. Chen, *Compos. Sci. Technol.* **2018**, *163*, 81.
- [127] J. E. Shin, H. W. Kim, B. M. Yoo, H. B. Park, *J. Appl. Polym. Sci.* **2018**, *135*, 45417.
- [128] H.-P. Cong, P. Wang, S.-H. Yu, *Small* **2014**, *10*, 448.
- [129] a) R. Kouser, A. Vashist, M. Zafaryab, M. A. Rizvi, S. Ahmad, *Mater. Sci. Eng., C* **2018**, *84*, 168; b) S. R. Shin, H. Bae, J. M. Cha, J. Y. Mun, Y.-C. Chen, H. Tekin, H. Shin, S. Farshchi, M. R. Dokmeci, S. Tang, A. Khademhosseini, *ACS Nano* **2012**, *6*, 362; c) J. Ramón-Azcón, S. Ahadian, M. Estili, X. Liang, S. Ostrovidov, H. Kaji, H. Shiku, M. Ramalingam, K. Nakajima, Y. Sakka, A. Khademhosseini, T. Matsue, *Adv. Mater.* **2013**, *25*, 4028; d) S. Ahadian, J. Ramon-Azcon, M. Estili, X. Liang, S. Ostrovidov, H. Shiku, M. Ramalingam, K. Nakajima, Y. Sakka, H. Bae, T. Matsue, A. Khademhosseini, *Sci. Rep.* **2015**, *4*, 4271.
- [130] J. Simak, Investigation of Potential Toxic Effects of Engineered Nanoparticles and Biologic Microparticles in Blood

- and Their Biomarker Applications, <https://www.fda.gov/vaccines-blood-biologics/biologics-research-projects/investigation-potential-toxic-effects-engineered-nanoparticles-and-bio-logic-microparticles-blood-and> (accessed: March 2020).
- [131] S. H. De Paoli Lacerda, J. Semberova, K. Holada, O. Simakova, S. D. Hudson, J. Simak, *ACS Nano* **2011**, *5*, 5808.
- [132] S. H. De Paoli, L. L. Diduch, T. Z. Tegegn, M. Orecna, M. B. Strader, E. Karnaukhova, J. E. Bonevich, K. Holada, J. Simak, *Biomaterials* **2014**, *35*, 6182.
- [133] R. M. A. Domingues, M. E. Gomes, R. L. Reis, *Biomacromolecules* **2014**, *15*, 2327.
- [134] a) M. Younas, A. Noreen, A. Sharif, A. Majeed, A. Hassan, S. Tabasum, A. Mohammadi, K. M. Zia, *Int. J. Biol. Macromol.* **2019**, *124*, 591; b) S. J. Eichhorn, *Soft Matter* **2011**, *7*, 303.
- [135] H. Liu, H. Qing, Z. Li, Y. L. Han, M. Lin, H. Yang, A. Li, T. J. Lu, F. Li, F. Xu, *Mater. Sci. Eng., R* **2017**, *112*, 1.
- [136] J. Yang, C.-R. Han, J.-F. Duan, F. Xu, R.-C. Sun, *ACS Appl. Mater. Interfaces* **2013**, *5*, 3199.
- [137] A. Khoushabi, A. Schmockler, D. P. Pioletti, C. Moser, C. Schizas, J. A. Manson, P. E. Bourban, *Compos. Sci. Technol.* **2015**, *119*, 93.
- [138] A. Khoushabi, C. S. Wyss, B. Caglar, D. Pioletti, P. E. Bourban, *Compos. Sci. Technol.* **2018**, *168*, 88.
- [139] a) N. B. Palaganas, J. D. Mangadla, A. C. C. de Leon, J. O. Palaganas, K. D. Pangilinan, Y. J. Lee, R. C. Advincula, *ACS Appl. Mater. Interfaces* **2017**, *9*, 34314; b) A. Sydney Gladman, E. A. Matsumoto, R. G. Nuzzo, L. Mahadevan, J. A. Lewis, *Nat. Mater.* **2016**, *15*, 413; c) K. Hou, Y. Li, Y. Liu, R. Zhang, B. S. Hsiao, M. Zhu, *Polymer* **2017**, *123*, 55.
- [140] a) S. Zhumagalieva, R. Iminova, G. Kairalapova, M. M. Beysebekov, M. K. Beysebekov, Z. Abilov, *Eurasian Chem.-Technol. J.* **2017**, *19*, 279; b) W. D. Keller, *AAPG Bull.* **1956**, *40*, 2689.
- [141] L. Z. Zhao, C. H. Zhou, J. Wang, D. S. Tong, W. H. Yu, H. Wang, *Soft Matter* **2015**, *11*, 9229.
- [142] Y. Zheng, A. Zaoui, *Phys. A* **2018**, *505*, 582.
- [143] B. Strachota, J. Hodan, L. Matějka, *Eur. Polym. J.* **2016**, *77*, 1.
- [144] L. Xiong, X. Hu, X. Liu, Z. Tong, *Polymer* **2008**, *49*, 5064.
- [145] E. Helvacioğlu, V. Aydin, T. Nugay, N. Nugay, B. G. Uluocak, S. Şen, *J. Polym. Res.* **2011**, *18*, 2341.
- [146] G. Gao, G. Du, Y. Sun, J. Fu, *ACS Appl. Mater. Interfaces* **2015**, *7*, 5029.
- [147] X. Su, S. Mahalingam, M. Edirisinghe, B. Chen, *ACS Appl. Mater. Interfaces* **2017**, *9*, 22223.
- [148] C.-W. Chang, A. van Spreuwel, C. Zhang, S. Varghese, *Soft Matter* **2010**, *6*, 5157.
- [149] X. Zhai, Y. Ma, C. Hou, F. Gao, Y. Zhang, C. Ruan, H. Pan, W. W. Lu, W. Liu, *ACS Biomater. Sci. Eng.* **2017**, *3*, 1109.
- [150] B. Wu, A. Heidelberg, J. J. Boland, *Nat. Mater.* **2005**, *4*, 525.
- [151] a) M. I. González-Sánchez, S. Perni, G. Tommasi, N. G. Morris, K. Hawkins, E. López-Cabarcos, P. Prokopovich, *Mater. Sci. Eng., C* **2015**, *50*, 332; b) K. Vimala, K. Samba Sivudu, Y. Murali Mohan, B. Sreedhar, K. Mohana Raju, *Carbohydr. Polym.* **2009**, *75*, 463.
- [152] a) T. Xu, J. Zhang, Y. Zhu, W. Zhao, C. Pan, H. Ma, L. Zhang, *Nanotechnology* **2018**, *29*, 395101; b) A. Navaei, N. Moore, R. T. Sullivan, D. Truong, R. Q. Migrino, M. Nikkhah, *RSC Adv.* **2017**, *7*, 3302; c) A. Navaei, H. Saini, W. Christenson, R. T. Sullivan, R. Ros, M. Nikkhah, *Acta Biomater.* **2016**, *41*, 133.
- [153] B. R. Thompson, T. S. Horozov, S. D. Stoyanov, V. N. Paunov, *J. Mater. Chem. A* **2019**, *7*, 8030.
- [154] E. Prince, E. Kumacheva, *Nat. Rev. Mater.* **2019**, *4*, 99.
- [155] J. U. Surjadi, L. Gao, H. Du, X. Li, X. Xiong, N. X. Fang, Y. Lu, *Adv. Eng. Mater.* **2019**, *21*, 1800864.
- [156] T. Xia, W. Liu, L. Yang, *J. Biomed. Mater. Res., Part A* **2017**, *105*, 1799.
- [157] Q. Zhang, X. Yang, P. Li, G. Huang, S. Feng, C. Shen, B. Han, X. Zhang, F. Jin, F. Xu, T. J. Lu, *Prog. Mater. Sci.* **2015**, *74*, 332.
- [158] B. Grigoryan, S. J. Paulsen, D. C. Corbett, D. W. Sazer, C. L. Fortin, A. J. Zaita, P. T. Greenfield, N. J. Calafat, J. P. Gounley, A. H. Ta, F. Johansson, A. Randles, J. E. Rosenkrantz, J. D. Louis-Rosenberg, P. A. Galie, K. R. Stevens, J. S. Miller, *Science* **2019**, *364*, 458.
- [159] G. M. Genin, S. Thomopoulos, *Nat. Mater.* **2017**, *16*, 607.
- [160] a) M. Kadic, G. W. Milton, M. van Hecke, M. Wegener, *Nat. Rev. Phys.* **2019**, *1*, 198; b) A. Rafsanjani, K. Bertoldi, A. R. Studart, *Sci. Rob.* **2019**, *4*, eaav7874; c) K. Bertoldi, V. Vitelli, J. Christensen, M. van Hecke, *Nat. Rev. Mater.* **2017**, *2*, 17066.
- [161] K. J. De France, F. Xu, T. Hoare, *Adv. Healthcare Mater.* **2018**, *7*, 1700927.
- [162] a) A. De Mori, M. Peña Fernández, G. Blunn, G. Tozzi, M. Roldo, *Polymers* **2018**, *10*, 285; b) G. Zhao, X. Zhang, T. J. Lu, F. Xu, *Adv. Funct. Mater.* **2015**, *25*, 5726.
- [163] a) S. Wang, L. Li, D. Su, K. Robin, K. A. Brown, *ACS Appl. Mater. Interfaces* **2018**, *10*, 34604; b) N. Broguiere, A. Husch, G. Palazzolo, F. Bradke, S. Madduri, M. Zenobi-Wong, *Biomaterials* **2019**, *200*, 56; c) S. Jiang, C. Lyu, P. Zhao, W. Li, W. Kong, C. Huang, G. M. Genin, Y. Du, *Nat. Commun.* **2019**, *10*, 3491.
- [164] a) B. W. Walker, R. Portillo Lara, E. Mogadam, C. Hsiang Yu, W. Kimball, N. Annabi, *Prog. Polym. Sci.* **2019**, *92*, 135; b) A. M. Pekkanen, R. J. Mondschein, C. B. Williams, T. E. Long, *Biomacromolecules* **2017**, *18*, 2669; c) S. Vijayavenkataraman, W. C. Yan, W. F. Lu, C. H. Wang, J. Y. H. Fuh, *Adv. Drug Delivery Rev.* **2018**, *132*, 296.
- [165] L. Moroni, T. Boland, J. A. Burdick, C. De Maria, B. Derby, G. Forgacs, J. Groll, Q. Li, J. Malda, V. A. Mironov, C. Mota, M. Nakamura, W. Shu, S. Takeuchi, T. B. F. Woodfield, T. Xu, J. J. Yoo, G. Vozzi, *Trends Biotechnol.* **2018**, *36*, 384.
- [166] S. C. Ligon, R. Liska, J. Stampfl, M. Gurr, R. Mülhaupt, *Chem. Rev.* **2017**, *117*, 10212.
- [167] A. Velasco-Hogan, J. Xu, M. A. Meyers, *Adv. Mater.* **2018**, *30*, 1800940.
- [168] Y. Zhang, F. Zhang, Z. Yan, Q. Ma, X. Li, Y. Huang, J. A. Rogers, *Nat. Rev. Mater.* **2017**, *2*, 17019.
- [169] a) A. D. Rape, M. Zibinsky, N. Murthy, S. Kumar, *Nat. Commun.* **2015**, *6*, 8129; b) F. Liu, J. D. Mih, B. S. Shea, A. T. Kho, A. S. Sharif, A. M. Tager, D. J. Tschumperlin, *J. Cell Biol.* **2010**, *190*, 693.
- [170] a) R. Sunyer, A. J. Jin, R. Nossal, D. L. Sackett, *PLoS One* **2012**, *7*, e46107; b) S. García, R. Sunyer, A. Olivares, J. Noailly, J. Atencia, X. Trepas, *Lab Chip* **2015**, *15*, 2606; c) A. M. Kloxin, J. A. Benton, K. S. Anseth, *Biomaterials* **2010**, *31*, 1; d) W. Yang, H. Yu, G. Li, B. Wang, Y. Wang, L. Liu, *Biomater. Sci.* **2016**, *4*, 863.
- [171] F. Yanagawa, S. Sugiura, T. Kanamori, *Regener. Ther.* **2016**, *3*, 45.
- [172] S. M. Mehta, T. Jin, I. Stanculescu, K. J. Grande-Allen, *Acta Biomater.* **2018**, *75*, 52.
- [173] J. E. Samorezov, C. M. Morlock, E. Alsberg, *Bioconjugate Chem.* **2015**, *26*, 1339.
- [174] a) K. A. Mosiewicz, L. Kolb, A. J. van der Vlies, M. P. Lutolf, *Biomater. Sci.* **2014**, *2*, 1640; b) C. Yang, F. W. DelRio, H. Ma, A. R. Killars, L. P. Basta, K. A. Kyburz, K. S. Anseth, *Proc. Natl. Acad. Sci. USA* **2016**, *113*, E4439.
- [175] S. V. Radl, C. Schipfer, S. Kaiser, A. Moser, B. Kaynak, W. Kern, S. Schlogl, *Polym. Chem.* **2017**, *8*, 1562.
- [176] a) B. Chollet, L. D'Eramo, E. Martwong, M. Li, J. Macron, T. Q. Mai, P. Tabeling, Y. Tran, *ACS Appl. Mater. Interfaces* **2016**, *8*, 24870; b) T. F. Scott, B. A. Kowalski, A. C. Sullivan, C. N. Bowman, R. R. McLeod, *Science* **2009**, *324*, 913; c) I. Mironi-Harpaz, L. Hazanov, G. Engel, D. Yelin, D. Seliktar, *Adv. Mater.* **2015**, *27*, 1933.
- [177] a) J. L. Curley, S. R. Jennings, M. J. Moore, *J. Visualized Exp.* **2011**, *48*, 2636; b) S. C. P. Norris, P. Tseng, A. M. Kasko, *ACS Biomater. Sci. Eng.* **2016**, *2*, 1309; c) R. Gauvin, Y.-C. Chen, J. W. Lee, P. Soman, P. Zorlutuna, J. W. Nichol, H. Bae, S. Chen, A. Khademhosseini, *Biomaterials* **2012**, *33*, 3824.

- [178] a) N. Annabi, A. Tamayol, J. A. Uquillas, M. Akbari, L. E. Bertassoni, C. Cha, G. Camci-Unal, M. R. Dokmeci, N. A. Peppas, A. Khademhosseini, *Adv. Mater.* **2014**, *26*, 85; b) F. Yanagawa, T. Mizutani, S. Sugiura, T. Takagi, K. Sumaru, T. Kanamori, *Colloids Surf., B* **2015**, *126*, 575.
- [179] A. P. Zhang, X. Qu, P. Soman, K. C. Hribar, J. W. Lee, S. Chen, S. He, *Adv. Mater.* **2012**, *24*, 4266.
- [180] D. Xue, Y. Wang, J. Zhang, D. Mei, Y. Wang, S. Chen, *ACS Appl. Mater. Interfaces* **2018**, *10*, 19428.
- [181] U. A. Gurkan, Y. Fan, F. Xu, B. Erkmen, E. S. Urkac, G. Parlakgul, J. Bernstein, W. Xing, E. S. Boyden, U. Demirci, *Adv. Mater.* **2013**, *25*, 1192.
- [182] a) V. Chan, P. Zorlutuna, J. H. Jeong, H. Kong, R. Bashir, *Lab Chip* **2010**, *10*, 2062; b) P. Zorlutuna, J. H. Jeong, H. Kong, R. Bashir, *Adv. Funct. Mater.* **2011**, *21*, 3642.
- [183] X. Ma, X. Qu, W. Zhu, Y.-S. Li, S. Yuan, H. Zhang, J. Liu, P. Wang, C. S. E. Lai, F. Zanella, G.-S. Feng, F. Sheikh, S. Chien, S. Chen, *Proc. Natl. Acad. Sci. USA* **2016**, *113*, 2206.
- [184] a) H. Seo, S. G. Heo, H. Lee, H. Yoon, *RSC Adv.* **2017**, *7*, 28684; b) A. Vitale, T. J. Cabral, *Materials* **2016**, *9*, 760; c) J. T. Cabral, S. D. Hudson, C. Harrison, J. F. Douglas, *Langmuir* **2004**, *20*, 10020.
- [185] J. R. Tumbleston, D. Shirvanyants, N. Ermoshkin, R. Januszewicz, A. R. Johnson, D. Kelly, K. Chen, R. Pinschmidt, J. P. Rolland, A. Ermoshkin, E. T. Samulski, J. M. DeSimone, *Science* **2015**, *347*, 1349.
- [186] J. A. Lewis, *Adv. Funct. Mater.* **2006**, *16*, 2193.
- [187] a) P. Valvert, *Science* **2007**, *318*, 208; b) R. E. Saunders, B. Derby, *Int. Mater. Rev.* **2014**, *59*, 430.
- [188] J. Jang, J. Y. Park, G. Gao, D.-W. Cho, *Biomaterials* **2018**, *156*, 88.
- [189] a) I. Donderwinkel, J. C. M. van Hest, N. R. Cameron, *Polym. Chem.* **2017**, *8*, 4451; b) T. Jungst, W. Smolan, K. Schacht, T. Scheibel, J. Groll, *Chem. Rev.* **2016**, *116*, 1496.
- [190] T. Boland, T. Xu, B. Damon, X. Cui, *Biotechnol. J.* **2006**, *1*, 910.
- [191] a) X. Cui, K. Breitenkamp, M. G. Finn, M. Lotz, D. D. D' Lima, *Tissue Eng., Part A* **2012**, *18*, 1304; b) X. Cui, G. Gao, T. Yonezawa, G. Dai, *J. Vis. Exp.* **2014**, <https://doi.org/10.3791/51294>; c) G. Gao, A. F. Schilling, K. Hubbell, T. Yonezawa, D. Truong, Y. Hong, G. Dai, X. Cui, *Biotechnol. Lett.* **2015**, *37*, 2349.
- [192] M. Di Biase, P. de Leonardis, V. Castelletto, I. W. Hamley, B. Derby, N. Tirelli, *Soft Matter* **2011**, *7*, 4928.
- [193] H. Yuk, X. Zhao, *Adv. Mater.* **2018**, *30*, 1704028.
- [194] L. Ouyang, C. B. Highley, C. B. Rodell, W. Sun, J. A. Burdick, *ACS Biomater. Sci. Eng.* **2016**, *2*, 1743.
- [195] a) M. Michael, B. Jana, S. Matthias, Z.-W. Marcy, *Biofabrication* **2015**, *7*, 035006; b) M. Kesti, M. Müller, J. Becher, M. Schnabelrauch, M. D'Este, D. Eglin, M. Zenobi-Wong, *Acta Biomater.* **2015**, *11*, 162.
- [196] a) L. A. Hockaday, K. H. Kang, N. W. Colangelo, P. Y. C. Cheung, B. Duan, E. Malone, J. Wu, L. N. Girardi, L. J. Bonassar, H. Lipson, C. C. Chu, J. T. Butcher, *Biofabrication* **2012**, *4*, 035005; b) L. Riccardo, V. Jetze, A. P. Josep, E. Elisabeth, M. Jos, A. M.-T. Miguel, *Biofabrication* **2014**, *6*, 035020.
- [197] L. Ouyang, C. B. Highley, W. Sun, J. A. Burdick, *Adv. Mater.* **2017**, *29*, 1604983.
- [198] H. Zhou, J. Woo, A. M. Cok, M. Wang, B. D. Olsen, J. A. Johnson, *Proc. Natl. Acad. Sci. USA* **2012**, *109*, 19119.
- [199] a) H. Zhou, E.-M. Schön, M. Wang, M. J. Glassman, J. Liu, M. Zhong, D. Díaz Díaz, B. D. Olsen, J. A. Johnson, *J. Am. Chem. Soc.* **2014**, *136*, 9464; b) M. Zhong, R. Wang, K. Kawamoto, B. D. Olsen, J. A. Johnson, *Science* **2016**, *353*, 1264.
- [200] E. Andrzejewska, *Prog. Polym. Sci.* **2001**, *26*, 605.
- [201] G. Terrones, A. J. Pearlstein, *Macromolecules* **2001**, *34*, 8894.
- [202] a) N. B. Cramer, S. K. Reddy, A. K. O'Brien, C. N. Bowman, *Macromolecules* **2003**, *36*, 7964; b) N. B. Cramer, T. Davies, A. K. O'Brien, C. N. Bowman, *Macromolecules* **2003**, *36*, 4631; c) S. K. Reddy, N. B. Cramer, C. N. Bowman, *Macromolecules* **2006**, *39*, 3681; d) S. K. Reddy, N. B. Cramer, C. N. Bowman, *Macromolecules* **2006**, *39*, 3673.
- [203] a) S. Kizilel, V. H. Pérez-Luna, F. Teymour, *Macromol. Theory Simul.* **2006**, *15*, 686; b) J. C. Hernández-Ortiz, E. Vivaldo-Lima, A. Penlidis, *Macromol. Theory Simul.* **2012**, *21*, 302.
- [204] X. Pan, M. A. Tasdelen, J. Laun, T. Junkers, Y. Yagci, K. Matyjaszewski, *Prog. Polym. Sci.* **2016**, *62*, 73.
- [205] a) K. Kastrup, A. Aguirre-Soto, C. Wang, C. N. Bowman, J. W. Stansbury, H. D. Sikes, *Polym. Chem.* **2016**, *7*, 592; b) M. D. Dickey, R. L. Burns, E. Kim, S. C. Johnson, N. A. Stacey, C. G. Willson, *AIChE J.* **2005**, *51*, 2547; c) A. K. O'Brien, C. N. Bowman, *Macromolecules* **2006**, *39*, 2501.
- [206] P. D. Iedema, V. Schamböck, H. Boonen, J. Koskamp, S. Schellekens, R. Willemse, *Chem. Eng. Sci.* **2018**, *176*, 491.
- [207] S. Park, D. Kim, S. Y. Ko, J.-O. Park, S. Akella, B. Xu, Y. Zhang, S. Fraden, *Lab Chip* **2014**, *14*, 1551.
- [208] J. T. Cabral, J. F. Douglas, *Polymer* **2005**, *46*, 4230.
- [209] M. G. Hennessy, A. Vitale, J. T. Cabral, O. K. Matar, *Phys. Rev. E* **2015**, *92*, 022403.
- [210] a) M. G. Hennessy, A. Vitale, O. K. Matar, J. T. Cabral, *Phys. Rev. E* **2015**, *91*, 062402; b) M. G. Hennessy, A. Vitale, O. K. Matar, J. T. Cabral, *Soft Matter* **2017**, *13*, 9199.
- [211] a) A. Vitale, M. G. Hennessy, O. K. Matar, J. T. Cabral, *Adv. Mater.* **2015**, *27*, 6118; b) A. Vitale, M. G. Hennessy, O. K. Matar, J. T. Cabral, *Macromolecules* **2015**, *48*, 198.
- [212] a) D. R. Miller, C. W. Macosko, *Rubber Chem. Technol.* **1976**, *49*, 1219; b) S. K. Reddy, O. Okay, C. N. Bowman, *Macromolecules* **2006**, *39*, 8832; c) M. Gordon, *Proc. R. Soc. London, Ser. A* **1962**, *268*, 240; d) P. J. Flory, J. Rehner, *J. Chem. Phys.* **1943**, *11*, 512.
- [213] H. Tobita, A. Hamielec, *Makromol. Chem., Macromol. Symp.* **1988**, *20–21*, 501.
- [214] a) F. Teymour, J. D. Campbell, *Macromolecules* **1994**, *27*, 2460; b) S. Kizilel, V. H. Pérez-Luna, F. Teymour, *Macromol. React. Eng.* **2009**, *3*, 271; c) L. G. Aguiar, E. F. Souza, R. Giudici, *Eur. Polym. J.* **2016**, *74*, 264.
- [215] a) V. Schamboeck, I. Kryven, P. D. Iedema, *Macromol. Theory Simul.* **2017**, *26*, 1700047; b) I. Kryven, P. D. Iedema, *Chem. Eng. Sci.* **2015**, *126*, 296.
- [216] a) M. Wen, L. E. Scriven, A. V. McCormick, *Macromolecules* **2003**, *36*, 4151; b) M. Wen, L. E. Scriven, A. V. McCormick, *Macromolecules* **2003**, *36*, 4140; c) M. Lattuada, E. Del Gado, T. Abete, L. de Arcangelis, S. Lazzari, V. Diederich, G. Storti, M. Morbidelli, *Macromolecules* **2013**, *46*, 5831.
- [217] a) D. M. Kroll, S. G. Croll, *Polymer* **2017**, *116*, 113; b) D. M. Kroll, S. G. Croll, *Polymer* **2017**, *115*, 154.
- [218] a) P. J. Flory, *J. Am. Chem. Soc.* **1941**, *63*, 3083; b) W. H. Stockmayer, *J. Chem. Phys.* **1943**, *11*, 45.
- [219] a) M. Gordon, G. N. Malcolm, *Proc. R. Soc. London, Ser. A* **1966**, *295*, 29; b) I. J. Good, *Math. Proc. Cambridge Philos. Soc.* **1955**, *51*, 240.
- [220] C. W. Macosko, D. R. Miller, *Macromolecules* **1976**, *9*, 199.
- [221] a) H. Tobita, A. E. Hamielec, *Macromolecules* **1989**, *22*, 3098; b) H. Tobita, *Macromol. Theory Simul.* **1997**, *6*, 641.
- [222] Y.-N. Zhou, Z.-H. Luo, *Macromol. React. Eng.* **2016**, *10*, 516.
- [223] a) S. Kizilel, G. Papavasiliou, J. Gossage, F. Teymour, *Macromol. React. Eng.* **2007**, *1*, 587; b) R. Kizilel, S. Kizilel, *Macromol. React. Eng.* **2012**, *6*, 160; c) L. G. Aguiar, *Macromol. React. Eng.* **2016**, *10*, 588.
- [224] a) V. N. Santos, L. G. Aguiar, R. Giudici, *Macromol. React. Eng.* **2017**, *11*, 1600021; b) L. G. Aguiar, *Macromol. Theory Simul.* **2015**, *24*, 176; c) L. G. Aguiar, M. A. Gonçalves, V. D. Pinto, R. Dias, M. R. P. Costa, R. Giudici, *Macromol. React. Eng.* **2014**, *8*, 295; d) L. G. Aguiar, M. A. Gonçalves, V. D. Pinto, R. Dias, M. R. P. Costa, R. Giudici, *Macromol. React. Eng.* **2014**, *8*, 282.

- [225] a) P. D. Iedema, *Polymer* **2011**, 52, 3537; b) I. Kryven, P. D. Iedema, *Macromol. Theory Simul.* **2013**, 22, 89.
- [226] a) D. T. Gillespie, *J. Phys. Chem.* **1977**, 81, 2340; b) H. Tobita, *Acta Polym.* **1995**, 46, 185.
- [227] M. Wen, L. E. Scriven, A. V. McCormick, in *Protective Coatings: Film Formation and Properties* (Eds: M. Wen, K. Dušek), Springer International Publishing, Cham **2017**, p. 67.
- [228] a) R. Wang, J. A. Johnson, B. D. Olsen, *Macromolecules* **2017**, 50, 2556; b) R. Wang, T.-S. Lin, J. A. Johnson, B. D. Olsen, *ACS Macro Lett.* **2017**, 6, 1414; c) R. Wang, A. Alexander-Katz, J. A. Johnson, B. D. Olsen, *Phys. Rev. Lett.* **2016**, 116, 188302.
- [229] Z. G. Qu, X. C. He, M. Lin, B. Y. Sha, X. H. Shi, T. J. Lu, F. Xu, *Nanomedicine* **2013**, 8, 995.
- [230] D. Meimaroglou, C. Kiparissides, *Ind. Eng. Chem. Res.* **2014**, 53, 8963.
- [231] a) N. Hosono, Y. Masubuchi, H. Furukawa, T. Watanabe, *J. Chem. Phys.* **2007**, 127, 164905; b) D. M. Kroll, S. G. Croll, *Polymer* **2015**, 79, 82; c) M. Zee, A. J. Feickert, D. M. Kroll, S. G. Croll, *Prog. Org. Coat.* **2015**, 83, 55; d) S. Zhang, L. Xi, *Polymer* **2017**, 116, 143.
- [232] E. Wang, F. A. Escobedo, *Macromolecules* **2016**, 49, 2375.
- [233] K. Nishi, K. Fujii, U.-i. Chung, M. Shibayama, T. Sakai, *Phys. Rev. Lett.* **2017**, 119, 267801.
- [234] J. Wu, Z. Zhao, C. M. Hamel, X. Mu, X. Kuang, Z. Guo, H. J. Qi, *J. Mech. Phys. Solids* **2018**, 112, 25.
- [235] H. Zhu, X. Yang, G. M. Genin, T. J. Lu, F. Xu, M. Lin, *J. Mech. Behav. Biomed. Mater.* **2018**, 88, 160.
- [236] a) M. W. Tibbitt, A. M. Kloxin, L. A. Sawicki, K. S. Anseth, *Macromolecules* **2013**, 46, 2785; b) K. Peng, I. Tomatsu, B. van den Broek, C. Cui, A. V. Korobko, J. van Noort, A. H. Meijer, H. P. Spaink, A. Kros, *Soft Matter* **2011**, 7, 4881.
- [237] a) D. R. Griffin, A. M. Kasko, *J. Am. Chem. Soc.* **2012**, 134, 13103; b) D. R. Griffin, A. M. Kasko, *ACS Macro Lett.* **2012**, 1, 1330.
- [238] M. W. Tibbitt, A. M. Kloxin, K. S. Anseth, *J. Polym. Sci., Part A: Polym. Chem.* **2013**, 51, 1899.
- [239] S. C. P. Norris, T. Chou, A. M. Kasko, *Macromol. Theory Simul.* **2017**, 26, 1700007.
- [240] a) V. Birman, L. W. Byrd, *Appl. Mech. Rev.* **2007**, 60, 195; b) G. W. Milton, *The Theory of Composites*, Cambridge University Press, Cambridge **2002**.
- [241] S. Zhang, M. L. Minus, L. Zhu, C.-P. Wong, S. Kumar, *Polymer* **2008**, 49, 1356.
- [242] J. J. Gilman, *J. Appl. Phys.* **1960**, 31, 2208.
- [243] A. Verma, A. Parashar, M. Packirisamy, *Wires. Comput. Mol. Sci.* **2017**, 8, e1346.
- [244] Q. H. Zeng, A. B. Yu, G. Q. Lu, *Prog. Polym. Sci.* **2008**, 33, 191.
- [245] a) C. M. Hadden, D. R. Klimek-McDonald, E. J. Pineda, J. A. King, A. M. Reichanadter, I. Miskioglu, S. Gowtham, G. M. Odegard, *Carbon* **2015**, 95, 100; b) M. S. Radue, G. M. Odegard, *Compos. Sci. Technol.* **2018**, 166, 20; c) B. Demir, K. M. Beggs, B. L. Fox, L. Servinis, L. C. Henderson, T. R. Walsh, *Compos. Sci. Technol.* **2018**, 159, 127; d) Y. Li, G. D. Seidel, *Comput. Mater. Sci.* **2015**, 107, 216; e) Y. Li, G. D. Seidel, *Comput. Mater. Sci.* **2018**, 153, 363; f) J. M. Wernik, S. A. Meguid, *Int. J. Solids Struct.* **2014**, 51, 2575; g) S. Yang, H. Shin, M. Cho, *J. Mech. Sci. Technol.* **2019**, 33, 307; h) G. Marom, H. Daniel Wagner, *J. Mater. Sci.* **2017**, 52, 8357; i) L. Y. Jiang, Y. Huang, H. Jiang, G. Ravichandran, H. Gao, K. C. Hwang, B. Liu, *J. Mech. Phys. Solids* **2006**, 54, 2436.
- [246] J. Zhao, L. Wu, C. Zhan, Q. Shao, Z. Guo, L. Zhang, *Polymer* **2017**, 133, 272.
- [247] B. Demir, L. C. Henderson, T. R. Walsh, *ACS Appl. Mater. Interfaces* **2017**, 9, 11846.
- [248] R. Rahman, J. T. Foster, *Comput. Mater. Sci.* **2014**, 87, 232.
- [249] S. Torquato, *Random Heterogeneous Materials: Microstructure and Macroscopic Properties*, Springer Science & Business Media, New York **2005**.
- [250] a) Z. Hashin, S. Shtrikman, *J. Mech. Phys. Solids* **1962**, 10, 335; b) Z. Hashin, S. Shtrikman, *J. Mech. Phys. Solids* **1963**, 11, 127.
- [251] a) S. Nobakhti, S. J. Shefelbine, *Curr. Osteoporosis Rep.* **2018**, 16, 404; b) G. M. Genin, V. Birman, *Int. J. Solids Struct.* **2009**, 46, 2136; c) Y. Liu, S. Thomopoulos, C. Chen, V. Birman, M. J. Buehler, G. M. Genin, *J. R. Soc., Interface* **2014**, 11, 20130835.
- [252] D. Eshelby John, E. Peierls Rudolf, *Proc. R. Soc. London, Ser. A* **1957**, 241, 376.
- [253] T. Mori, K. Tanaka, *Acta Metall.* **1973**, 21, 571.
- [254] A. L. R. Bug, S. A. Safran, I. Webman, *Phys. Rev. Lett.* **1985**, 54, 1412.
- [255] a) Y. Kantor, I. Webman, *Phys. Rev. Lett.* **1984**, 52, 1891; b) J. P. Marquez, G. M. Genin, E. L. Elson, *J. Biomech.* **2006**, 39, 2145; c) J. P. Marquez, G. M. Genin, G. I. Zahalak, E. L. Elson, *Biophys. J.* **2005**, 88, 765; d) J. P. Marquez, G. M. Genin, G. I. Zahalak, E. L. Elson, *Biophys. J.* **2005**, 88, 778.
- [256] S. C. Baxter, C. T. Robinson, *Compos. Sci. Technol.* **2011**, 71, 1273.
- [257] J. L. Kardos, J. Raison, *Polym. Eng. Sci.* **1975**, 15, 183.
- [258] J. Diani, P. Gilormini, Y. Merckel, F. Vion-Loisel, *Mech. Mater.* **2013**, 59, 65.
- [259] Z. Liu, J. A. Moore, W. K. Liu, *J. Mech. Phys. Solids* **2016**, 95, 663.
- [260] a) S. K. Kanaun, D. Jeulin, *J. Mech. Phys. Solids* **2001**, 49, 2339; b) F. Saadat, V. Birman, S. Thomopoulos, G. M. Genin, *J. Mech. Phys. Solids* **2015**, 82, 367.
- [261] a) H. L. Cox, *Br. J. Appl. Phys.* **1952**, 3, 72; b) X. L. Gao, K. Li, *Int. J. Solids Struct.* **2005**, 42, 1649; c) J. Rosenthal, *Polym. Compos.* **1992**, 13, 462.
- [262] a) J. N. Coleman, M. Cadek, K. P. Ryan, A. Fonseca, J. B. Nagy, W. J. Blau, M. S. Ferreira, *Polymer* **2006**, 47, 8556; b) J. N. Coleman, M. Cadek, R. Blake, V. Nicolosi, K. P. Ryan, C. Belton, A. Fonseca, J. B. Nagy, Y. K. Gun'ko, W. J. Blau, *Adv. Funct. Mater.* **2004**, 14, 791.
- [263] J. C. H. Afdl, J. L. Kardos, *Polym. Eng. Sci.* **1976**, 16, 344.
- [264] R. F. Landel, L. E. Nielsen, *Mechanical Properties of Polymers and Composites*, CRC Press, Boca Raton, FL **1993**.
- [265] S. Ramakrishna, T. C. Lim, R. Inai, K. Fujihara, *Mech. Adv. Mater. Struct.* **2006**, 13, 77.
- [266] K. Hbaieb, Q. X. Wang, Y. H. J. Chia, B. Cotterell, *Polymer* **2007**, 48, 901.
- [267] A. Hussein, B. Kim, *Compos. Struct.* **2018**, 202, 170.
- [268] a) Z. Guo, L. Song, C. G. Boay, Z. Li, Y. Li, Z. Wang, *Compos. Struct.* **2018**, 199, 1; b) K. N. Spanos, S. K. Georgantzinos, N. K. Anifantis, *Compos. Struct.* **2015**, 132, 536.
- [269] Y. Han, W. Yang, W. Cui, K. Yang, X. Wang, Y. Chen, L. Deng, Y. Zhao, W. Jin, *J. Mater. Chem. B* **2019**, 7, 1563.
- [270] a) M. M. Chelsea, L. A. Daniel, S. A. Kristi, *Biomed. Mater.* **2016**, 11, 022001; b) H. K. Lau, K. L. Kiick, *Biomacromolecules* **2015**, 16, 28; c) V. Delplace, J. Nicolas, *Nat. Chem.* **2015**, 7, 771.
- [271] W. Li, Z. Yan, J. Ren, X. Qu, *Chem. Soc. Rev.* **2018**, 47, 8639.
- [272] a) B. D. Cosgrove, K. L. Mui, T. P. Driscoll, S. R. Caliar, K. D. Mehta, R. K. Assoian, J. A. Burdick, R. L. Mauck, *Nat. Mater.* **2016**, 15, 1297; b) Z. Gong, S. E. Szczesny, S. R. Caliar, E. E. Charrier, O. Chaudhuri, X. Cao, Y. Lin, R. L. Mauck, P. A. Janmey, J. A. Burdick, V. B. Shenoy, *Proc. Natl. Acad. Sci. USA* **2018**, 115, E2686; c) W. Wan, B. Cheng, C. Zhang, Y. Ma, A. Li, F. Xu, M. Lin, *Biophys. J.* **2019**, 117, 129.
- [273] a) S. Gobaa, S. Hoehnel, M. Rocco, A. Negro, S. Kobel, M. P. Lutolf, *Nat. Methods* **2011**, 8, 949; b) H. D. Kim, E. A. Lee, Y. H. Choi, Y. H. An, R. H. Koh, S. L. Kim, N. S. Hwang, *Acta Biomater.* **2016**, 34, 21; c) S. L. Vega, M. Y. Kwon, K. H. Song, C. Wang, R. L. Mauck, L. Han, J. A. Burdick, *Nat. Commun.* **2018**, 9, 614; d) D. G. Anderson, S. Levenberg, R. Langer, *Nat. Biotechnol.* **2004**, 22, 863.
- [274] B. D. Hoffman, C. Grashoff, M. A. Schwartz, *Nature* **2011**, 475, 316.
- [275] a) A. M. Hilderbrand, E. M. Ovadia, M. S. Rehmann, P. M. Kharkar, C. Guo, A. M. Kloxin, *Curr. Opin. Solid State Mater.*

- Sci.* **2016**, *20*, 212; b) K. Vats, D. S. W. Benoit, *Tissue Eng., Part B* **2013**, *19*, 455; c) M. S. Rehmann, A. M. Kloxin, *Soft Matter* **2013**, *9*, 6737; d) C. M. Kirschner, K. S. Anseth, *Acta Mater.* **2013**, *61*, 931; e) N. P. Murphy, K. J. Lampe, *J. Mater. Chem. B* **2015**, *3*, 7867; f) J. A. Burdick, W. L. Murphy, *Nat. Commun.* **2012**, *3*, 1269.
- [276] J. L. Young, A. J. Engler, *Biomaterials* **2011**, *32*, 1002.
- [277] K. R. Levental, H. Yu, L. Kass, J. N. Lakins, M. Egeblad, J. T. Erler, S. F. T. Fong, K. Csiszar, A. Giaccia, W. Weninger, M. Yamauchi, D. L. Gasser, V. M. Weaver, *Cell* **2009**, *139*, 891.
- [278] M. Guvendiren, J. A. Burdick, *Nat. Commun.* **2012**, *3*, 792.
- [279] S. R. Caliar, M. Perelpyuk, B. D. Cosgrove, S. J. Tsai, G. Y. Lee, R. L. Mauck, R. G. Wells, J. A. Burdick, *Sci. Rep.* **2016**, *6*, 21387.
- [280] H. E. Kim, S. S. Dalal, E. Young, M. J. Legato, M. L. Weisfeldt, J. D'Armiento, *J. Clin. Invest.* **2000**, *106*, 857.
- [281] J. Bondeson, S. Wainwright, C. Hughes, B. Caterson, *Clin. Exp. Rheumatol.* **2008**, *26*, 139.
- [282] A. McGarry Houghton, *Matrix Biol.* **2015**, *44–46*, 167.
- [283] a) D. D. McKinnon, T. E. Brown, K. A. Kyburz, E. Kiyotake, K. S. Anseth, *Biomacromolecules* **2014**, *15*, 2808; b) C. Yang, M. W. Tibbitt, L. Basta, K. S. Anseth, *Nat. Mater.* **2014**, *13*, 645.
- [284] A. M. Rosales, S. L. Vega, F. W. DelRio, J. A. Burdick, K. S. Anseth, *Angew. Chem., Int. Ed.* **2017**, *56*, 12132.
- [285] L. C. Bahlmann, A. Fokina, M. S. Shoichet, *MRS Commun.* **2017**, *7*, 472.
- [286] a) L. Rossetti, L. A. Kuntz, E. Kunold, J. Schock, K. W. Müller, H. Grabmayr, J. Stolberg-Stolberg, F. Pfeiffer, S. A. Sieber, R. Burgkart, A. R. Bausch, *Nat. Mater.* **2017**, *16*, 664; b) A. Di Luca, I. Lorenzo-Moldero, C. Mota, A. Lepedda, D. Auhl, C. Van Blitterswijk, L. Moroni, *Adv. Healthcare Mater.* **2016**, *5*, 1753.
- [287] Y. J. Blinder, D. J. Mooney, S. Levenberg, *Curr. Opin. Chem. Eng.* **2014**, *3*, 56.
- [288] a) L. Wang, Y. Li, G. Huang, X. Zhang, B. Pingguan-Murphy, B. Gao, T. J. Lu, F. Xu, *Crit. Rev. Biotechnol.* **2016**, *36*, 553; b) M. Singh, C. Berkland, M. S. Detamore, *Tissue Eng., Part B* **2008**, *14*, 341.
- [289] a) R. F. Pereira, P. J. Bártolo, *J. Appl. Polym. Sci.* **2015**, *132*, 4258; b) M. Guvendiren, J. Molde, R. M. D. Soares, J. Kohn, *ACS Biomater. Sci. Eng.* **2016**, *2*, 1679; c) Y. S. Zhang, K. Yue, J. Aleman, K. Mollazadeh-Moghaddam, S. M. Bakht, J. Yang, W. Jia, V. Dell'Erba, P. Assawes, S. R. Shin, M. R. Dokmeci, R. Oklu, A. Khademhosseini, *Ann. Biomed. Eng.* **2017**, *45*, 148; d) J. C. Rose, L. De Laporte, *Adv. Healthcare Mater.* **2018**, *7*, 1701067.
- [290] a) K. C. Hribar, Y. S. Choi, M. Ondeck, A. J. Engler, S. Chen, *Adv. Funct. Mater.* **2014**, *24*, 4922; b) G. Vincent Ludovic, S. Choi Yu, B. Alonso-Latorre, C. del Álamo Juan, J. Engler Adam, *Biotechnol. J.* **2013**, *8*, 472; c) R. Sunyer, V. Conte, J. Escribano, A. Elosegui-Artola, A. Labernadie, L. Valon, D. Navajas, J. M. García-Aznar, J. J. Muñoz, P. Roca-Cusachs, X. Trepat, *Science* **2016**, *353*, 1157.
- [291] a) R. A. Marklein, J. A. Burdick, *Soft Matter* **2010**, *6*, 136; b) M. Guvendiren, M. Perelpyuk, R. G. Wells, J. A. Burdick, *J. Mech. Behav. Biomed. Mater.* **2014**, *38*, 198.
- [292] M. C. Lampi, M. Guvendiren, J. A. Burdick, C. A. Reinhart-King, *ACS Biomater. Sci. Eng.* **2017**, *3*, 3007.
- [293] W. J. Hadden, J. L. Young, A. W. Holle, M. L. McFetridge, D. Y. Kim, P. Wijesinghe, H. Taylor-Weiner, J. H. Wen, A. R. Lee, K. Bieback, B.-N. Vo, D. D. Sampson, B. F. Kennedy, J. P. Spatz, A. J. Engler, Y. S. Choi, *Proc. Natl. Acad. Sci. USA* **2017**, *114*, 5647.
- [294] a) B. Babaei, A. Davarian, S.-L. Lee, K. M. Pryse, W. B. McConnaughey, E. L. Elson, G. M. Genin, *Acta Biomater.* **2016**, *37*, 28; b) J. P. Marquez, E. L. Elson, G. M. Genin, *Philos. Trans. R. Soc., A* **2010**, *368*, 635.
- [295] O. Chaudhuri, *Biomater. Sci.* **2017**, *5*, 1480.
- [296] M. Weinhart, A. Hocke, S. Hippenstiel, J. Kurreck, S. Hedtrich, *Pharmacol. Res.* **2019**, *139*, 446.
- [297] B. Duan, E. Kapetanovic, L. A. Hockaday, J. T. Butcher, *Acta Biomater.* **2014**, *10*, 1836.
- [298] H. Cui, W. Zhu, M. Nowicki, X. Zhou, A. Khademhosseini, L. G. Zhang, *Adv. Healthcare Mater.* **2016**, *5*, 2174.
- [299] E. A. Aisenbrey, A. Tomaschke, E. Kleinjan, A. Muralidharan, C. Pascual-Garrido, R. R. McLeod, V. L. Ferguson, S. J. Bryant, *Macromol. Biosci.* **2018**, *18*, 1700267.
- [300] a) A. Schmocker, A. Khoushabi, D. A. Frauchiger, B. Gantenbein, C. Schizas, C. Moser, P.-E. Bourban, D. P. Pioletti, *Biomaterials* **2016**, *88*, 110; b) Y. Gan, P. Li, L. Wang, X. Mo, L. Song, Y. Xu, C. Zhao, B. Ouyang, B. Tu, L. Luo, L. Zhu, S. Dong, F. Li, Q. Zhou, *Biomaterials* **2017**, *136*, 12.
- [301] R. Raman, T. Hua, D. Gwynne, J. Collins, S. Tamang, J. Zhou, T. Esfandiary, V. Soares, S. Pajovic, A. Hayward, R. Langer, G. Traverso, *Sci. Adv.* **2020**, *6*, eaay0065.
- [302] C. D. DiDomenico, M. Lintz, L. J. Bonassar, *Nat. Rev. Rheumatol.* **2018**, *14*, 393.
- [303] A. C. Daly, F. E. Freeman, T. Gonzalez-Fernandez, S. E. Critchley, J. Nulty, D. J. Kelly, *Adv. Healthcare Mater.* **2017**, *6*, 1700298.
- [304] N. Eslahi, M. Abdorahim, A. Simchi, *Biomacromolecules* **2016**, *17*, 3441.
- [305] I. Van Nieuwenhove, L. Tytgat, M. Ryx, P. Blondeel, F. Stillaert, H. Thienpont, H. Ottevaere, P. Dubruel, S. Van Vlierberghe, *Acta Biomater.* **2017**, *63*, 37.
- [306] a) O. S. Fenton, K. N. Olafson, P. S. Pillai, M. J. Mitchell, R. Langer, *Adv. Mater.* **2018**, *30*, 1705328; b) Q. Zhang, Y. Li, Z. Y. Lin, K. K. Y. Wong, M. Lin, L. Yildirimer, X. Zhao, *Drug Discovery Today* **2017**, *22*, 1351.
- [307] E. R. Ruskowitz, C. A. DeForest, *Nat. Rev. Mater.* **2018**, *3*, 17087.
- [308] J. M. Silva, E. Silva, R. L. Reis, *J. Controlled Release* **2019**, *298*, 154.
- [309] S. H. Lim, H. Kathuria, J. J. Y. Tan, L. Kang, *Adv. Drug Delivery Rev.* **2018**, *132*, 139.
- [310] Z. Ning, B. Tan, B. Chen, D. S. A. Lau, T. M. Wong, T. Sun, S. Peng, Z. Li, W. W. Lu, *Macromol. Biosci.* **2019**, *19*, 1900020.
- [311] K. Modaresifar, A. Hadjizadeh, H. Niknejad, *Artif. Cells, Nanomed., Biotechnol.* **2018**, *46*, 1799.
- [312] W. S. Lim, K. Chen, T. W. Chong, G. M. Xiong, W. R. Birch, J. Pan, B. H. Lee, P. S. Er, A. V. Salvekar, S. S. Venkatraman, Y. Huang, *Biomaterials* **2018**, *165*, 25.
- [313] D. Aycan, N. Alemdar, *Carbohydr. Polym.* **2018**, *184*, 401.
- [314] M. K. Schesny, M. Monaghan, A. H. Bindermann, D. Freund, M. Seifert, J. A. Eble, S. Vogel, M. P. Gawaz, S. Hinderer, K. Schenke-Layland, *Biomaterials* **2014**, *35*, 7180.
- [315] Y. Ding, Z. Song, Q. Liu, S. Wei, L. Zhou, J. Zhou, J. Shen, *Dalton Trans.* **2017**, *46*, 11875.
- [316] J. Yu, Y. Zhang, W. Sun, C. Wang, D. Ranson, Y. Ye, Y. Weng, Z. Gu, *Nanoscale* **2016**, *8*, 9178.
- [317] a) J. Wang, A. Goyanes, S. Gaisford, A. W. Basit, *Int. J. Pharm.* **2016**, *503*, 207; b) E. A. Clark, M. R. Alexander, D. J. Irvine, C. J. Roberts, M. J. Wallace, S. Sharpe, J. Yoo, R. J. M. Hague, C. J. Tuck, R. D. Wildman, *Int. J. Pharm.* **2017**, *529*, 523.
- [318] Q. Liu, H. Wang, G. Li, M. Liu, J. Ding, X. Huang, W. Gao, W. Huayue, *Chin. Chem. Lett.* **2019**, *30*, 485.
- [319] D. Zhao, Q. Tang, Q. Zhou, K. Peng, H. Yang, X. Zhang, *Soft Matter* **2018**, *14*, 7420.
- [320] E. R. Ruskowitz, M. P. Comerford, B. A. Badeau, C. A. DeForest, *Biomater. Sci.* **2019**, *7*, 542.
- [321] a) T. Li, G. Li, Y. Liang, T. Cheng, J. Dai, X. Yang, B. Liu, Z. Zeng, Z. Huang, Y. Luo, T. Xie, W. Yang, *Sci. Adv.* **2017**, *3*, e1602045; b) D. J. Preston, P. Rothemund, H. J. Jiang, M. P. Nemitz, J. Rawson, Z. Suo, G. M. Whitesides, *Proc. Natl. Acad. Sci. USA* **2019**, *116*, 7750.
- [322] a) C. Yang, Z. Suo, *Nat. Rev. Mater.* **2018**, *3*, 125; b) H. Yuk, B. Lu, X. Zhao, *Chem. Soc. Rev.* **2019**, *48*, 1642.
- [323] a) C. Wang, C. Wang, Z. Huang, S. Xu, *Adv. Mater.* **2018**, *30*, 1801368; b) J. Odent, T. J. Wallin, W. Pan, K. Kruempelstaedter, R. F. Shepherd, E. P. Giannelis, *Adv. Funct. Mater.* **2017**, *27*, 1701807;

- c) S. Lin, H. Yuk, T. Zhang, A. Parada German, H. Koo, C. Yu, X. Zhao, *Adv. Mater.* **2016**, *28*, 4497.
- [324] C. Keplinger, J.-Y. Sun, C. C. Foo, P. Rothmund, G. M. Whitesides, Z. Suo, *Science* **2013**, *341*, 984.
- [325] a) J.-Y. Sun, C. Keplinger, G. M. Whitesides, Z. Suo, *Adv. Mater.* **2014**, *26*, 7608; b) M. S. Sarwar, Y. Dobashi, C. Preston, J. K. M. Wyss, S. Mirabbasi, J. D. W. Madden, *Sci. Adv.* **2017**, *3*, e1602200; c) M.-j. Yin, Y. Zhang, Z. Yin, Q. Zheng, A. P. Zhang, *Adv. Mater. Technol.* **2018**, *3*, 1800051; d) L. M. Zhang, Y. He, S. Cheng, H. Sheng, K. Dai, W. J. Zheng, M. X. Wang, Z. S. Chen, Y. M. Chen, Z. Suo, *Small* **2019**, *15*, 1804651; e) C.-C. Kim, H.-H. Lee, K. H. Oh, J.-Y. Sun, *Science* **2016**, *353*, 682.
- [326] a) L. Han, X. Lu, M. Wang, D. Gan, W. Deng, K. Wang, L. Fang, K. Liu, C. W. Chan, Y. Tang, L.-T. Weng, H. Yuan, *Small* **2017**, *13*, 1601916; b) S. Zhao, P. Tseng, J. Grasman, Y. Wang, W. Li, B. Napier, B. Yavuz, Y. Chen, L. Howell, J. Rincon, F. G. Omenetto, D. L. Kaplan, *Adv. Mater.* **2018**, *30*, 1800598.
- [327] C. H. Yang, B. Chen, J. J. Lu, J. H. Yang, J. Zhou, Y. M. Chen, Z. Suo, *Extreme Mech. Lett.* **2015**, *3*, 59.
- [328] J. Tavakoli, Y. Tang, *Polymers* **2017**, *9*, 364.
- [329] a) H. Banerjee, M. Suhail, H. Ren, *Biomimetics* **2018**, *3*, 15; b) L. Liu, L. Li, Y. Qing, N. Yan, Y. Wu, X. Li, C. Tian, *Polym. Chem.* **2016**, *7*, 7142; c) C. Zhang, G. G. Cano, P. V. Braun, *Adv. Mater.* **2014**, *26*, 5678; d) A. Richter, G. Paschew, S. Klatt, J. Lienig, K.-F. Arndt, H.-J. P. Adler, *Sensors* **2008**, *8*, 561.
- [330] M. A. Lee, F. T. Nguyen, K. Scott, N. Y. L. Chan, N. A. Bakh, K. K. Jones, C. Pham, P. Garcia-Salinas, D. Garcia-Parraga, A. Fahlman, V. Marco, V. B. Koman, R. J. Oliver, L. W. Hopkins, C. Rubio, R. P. Wilson, M. G. Meekan, C. M. Duarte, M. S. Strano, *ACS Sens.* **2019**, *4*, 32.
- [331] M. Fernandez-Villamarin, L. Brooks, P. M. Mendes, *Adv. Opt. Mater.* **2019**, *7*, 1900215.
- [332] A. Lendlein, O. E. C. Gould, *Nat. Rev. Mater.* **2019**, *4*, 116.
- [333] C. Lv, H. Xia, Q. Shi, G. Wang, Y.-S. Wang, Q.-D. Chen, Y.-L. Zhang, L.-Q. Liu, H.-B. Sun, *Adv. Mater. Interfaces* **2017**, *4*, 1601002.
- [334] H. Yuk, S. Lin, C. Ma, M. Takaffoli, N. X. Fang, X. Zhao, *Nat. Commun.* **2017**, *8*, 14230.
- [335] T. M. Valentin, E. M. DuBois, C. E. Machnicki, D. Bhaskar, F. R. Cui, I. Y. Wong, *Polym. Chem.* **2019**, *10*, 2015.
- [336] a) J. Shintake, V. Cacucciolo, D. Floreano, H. Shea, *Adv. Mater.* **2018**, *30*, 1707035; b) M. Sitti, *Nat. Rev. Mater.* **2018**, *3*, 74; c) J. Paik, *Nat. Rev. Mater.* **2018**, *3*, 81.
- [337] H.-W. Huang, M. S. Sakar, A. J. Petruska, S. Pané, B. J. Nelson, *Nat. Commun.* **2016**, *7*, 12263.
- [338] S. R. Shin, B. Migliori, B. Miccoli, Y.-C. Li, P. Mostafalu, J. Seo, S. Mandla, A. Enrico, S. Antona, R. Sabarish, T. Zheng, L. Pirrami, K. Zhang, Y. S. Zhang, K.-t. Wan, D. Demarchi, M. R. Dokmeci, A. Khademhosseini, *Adv. Mater.* **2018**, *30*, 1704189.
- [339] a) S. Ahadian, R. B. Sadeghian, S. Salehi, S. Ostrovidov, H. Bae, M. Ramalingam, A. Khademhosseini, *Bioconjugate Chem.* **2015**, *26*, 1984; b) A. Vedadghavami, F. Minooei, M. H. Mohammadi, S. Khetani, A. Rezaei Kolahchi, S. Mashayekhan, A. Sanati-Nezhad, *Acta Biomater.* **2017**, *62*, 42.